Contract No:

This document was prepared in conjunction with work accomplished under Contract No. DE-AC09-08SR22470 with the U.S. Department of Energy (DOE) Office of Environmental Management (EM).

Disclaimer:

Interim Glycol Flowsheet REDuction/OXidation (REDOX) Model for the Defense Waste Processing Facility (DWPF)

C.M. Jantzen
M.S. Williams
J.R. Zamecnik
D.M. Missimer
March 2016

SRNL-STI-2015-00702, Revision 0

DISCLAIMER

Printed in the United States of America

Prepared for
U.S. Department of Energy

SRNL-STI-2015-00702
Revision 0

Keywords: *Glycol, Alternate Reductant DWPF, Oxidation/Reduction, REDOX*

Retention: *Permanent*

Interim Glycol Flowsheet REDuction/OXidation (REDOX) Model for the Defense Waste Processing Facility (DWPF)

C.M. Jantzen
M.S. Williams
J.R. Zamecnik
D.M. Missimer

March 2016

Prepared for the U.S. Department of Energy under contract number DE-AC09-08SR22470.

Savannah River National Laboratory™
OPERATED BY SAVANNAH RIVER NUCLEAR SOLUTIONS

REVIEWS AND APPROVALS

AUTHORS:

C.M. Jantzen, Engineering Process Development Date

M.S. Williams, Oak Ridge Associated Universities Date

J.R. Zamecnik, Process Technology Programs Date

D.M. Missimer, Analytic Development Date

TECHNICAL REVIEW:

C.J. Martino, Process Technology Programs Date

T.B. Edwards, Engineering Process Development, Reviewed per E7 2.60 Date

APPROVAL:

E.N. Hoffman, Manager Date
Process Technology Programs

D. E. Dooley, Director Date
Environmental & Chemical Process Technology Research Programs

E. J. Freed, Manager Date
DWPF Engineering

ACKNOWLEDGEMENTS

The authors would like to thank fellow researchers in the SRNL Engineering Process Development and , Process Technology Programs of the Savannah River National Laboratory (SRNL) who performed the various REDOX procedures: Fabienne Johnson, Dan Lambert, David Newell, Jake Amoroso, Phyllis Workman, and Holly Hall. The authors would also like to thank Ronnie Rutherford of SRNL's Analytical Development (AD) for assistance with the X-ray Diffraction (XRD) analyses and Tom White of AD for the development of a caustic quench glycolate analysis method. Special thanks are due to David Best, Whitney Riley, and Kimberly Wyszynski of SRNL's Process Science Analytical Laboratory (PSAL) for $Fe^{2+}/\Sigma Fe$, formate, oxalate, nitrate, nitrite, and weight percent solids measurements.

The special talents of James G. Dobos of the SRNL glass shop and Ken J. Imrich of the Material Science & Technology Section of SRNL in developing the geometry of the bubbled crucible experiments in conjunction with the lead author are noted. Special thanks are also due to Sherry Vissage for her dedication and performing the bubbled crucible experiments.

This paper was prepared in connection with work done under Contract Nos. DE-AC09-76SR00001, DE-AC09-96SR18500, DE-AC09-08SR22470 with the U.S. Department of Energy.

EXECUTIVE SUMMARY

Control of the REDuction/OXidation (REDOX) state of glasses containing high concentrations of transition metals, such as High Level Waste (HLW) glasses, is critical in order to eliminate processing difficulties caused by overly reduced or overly oxidized melts. Operation of a HLW melter at $Fe^{+2}/\Sigma Fe$ ratios of between 0.09 and 0.33, a range which is not overly oxidizing or overly reducing, helps retain radionuclides in the melt, i.e. long-lived radioactive ^{99}Tc species in the less volatile reduced Tc^{4+} state, ^{104}Ru in the melt as reduced Ru^{+4} state as insoluble RuO_2, and hazardous volatile Cr^{6+} in the less soluble and less volatile Cr^{+3} state in the glass. The melter REDOX control balances the oxidants and reductants from the feed and from processing additives such as antifoam.

An electron exchange (EE) REDOX model was developed at the Savannah River National Laboratory (SRNL) to balance reductants (e.g., oxalate, coal, sugar, formate, antifoam) and oxidants (e.g., nitrates, nitrites, and manganic species) for any melter feed. The model is represented by the number of electrons gained during reduction or lost during oxidation of various species. The overall relationship between the REDOX ratio of the final glass and the melter feed chemistry is given in terms of the transfer of molar Electron Equivalents, ξ_A, where the A represents the overall EE including antifoam to distinguish it from earlier versions of the EE model that did not include an EE term for antifoam. The addition of Ar bubbling, to improve melt rate during radioactive melting operations, sparges free oxygen from the melt. The Ar effect was quantified in the 2012 DWPF EE REDOX model.

Currently, the Defense Waste Processing Facility (DWPF) is running a formic acid-nitric acid (FN) flowsheet where formic acid is the main reductant and nitric acid is the main oxidant. During decomposition formate and formic acid releases H_2 gas which requires close control of the melter vapor space flammability. A switch to a nitric acid-glycolic acid (GN) flowsheet is desired as the glycolic acid flowsheet releases considerably less H_2 gas upon decomposition. This would greatly simplify DWPF processing.

Development of an EE term for glycolic acid in the GN flowsheet is documented in this study. The development of this term has been problematic due to variability in the glycolate measurement in the feed and variability in the determined $Fe^{+2}/\Sigma Fe$ which was found to be highly dependent on the type of closed (sealed) crucible (CC) method utilized to produce glass for REDOX measurement. In this document, the CC_{ramp}, CC_{Ar} and CCOG variants of the CC method are shown to be unsuitable for REDOX modeling. The CC_{hot}, for an 1150°C hot insertion of the CC into the furnace, has been and continues to be the most reliable method for $Fe^{+2}/\Sigma Fe$ determination. The CC_{hot} methodology was supplemented by Melt Rate Furnace (MRF) tests of the same feeds. The MRF tests gave comparable $Fe^{+2}/\Sigma Fe$ ratios to the CC_{hot} tests.

For some simulated SB6 feeds, when coupled with a refractory frit like Frit 418, the CC_{hot} methodology was found to give irreproducible $Fe^{+2}/\Sigma Fe$ ratio determinations. This had been observed previously during SB4 REDOX testing with Frit 418: the glass in the CC test was at too high a viscosity and thus inhibited convection in the crucible, producing an inhomogeneous glass. Inhomogeneous glass gives non-uniform $Fe^{+2}/\Sigma Fe$ measurement results. To ensure that the glass viscosity variable was controlled the SRNL REDOX procedure was adjusted to require that the sludge-frit mixture being tested in CC_{hot} have a calculated viscosity of 50-60 poise at 1150°C. This was the viscosity found to provide a homogeneous glass during SB4 testing. If the sludge-frit mixture is calculated to have a viscosity of >60 poise, $LiBO_2$ is now required to be added as a flux that does not impact the overall REDOX of the mixture.

Based on the combined CC_{hot} and MRF analyses provided in this study, it is recommended that the DWPF use the 2012 REDOX model slope and intercept with a glycol EE of 6 and a Mn EE of 0 as an *interim* REDOX model for the GN flowsheet at 100-125% acid stoichiometry as indicated below:

$$\xi_{A\text{-}gly} = \left[\left(2[F] + 4[C] + 4[O_T] + 3.39 * eff\,[C_A] + 6[Gly] - 5[N] - 0[Mn] \right) \frac{45}{T} \right]$$

where [F] = formate (mol/kg feed)
[C] = coal (carbon) (mol/kg feed)
$[O_T]$ = $oxalate_{Total}$ (soluble and insoluble) (mol/kg feed)
$[C_A]$ = carbon from antifoam (mol/kg feed)
eff = effective antifoam impact = 0.85
[gly] = glycolate (mol/kg feed)
[N] = nitrate + nitrite (mol/kg feed)
[Mn] = manganese (mol/kg feed)
T = total solids (wt%)
$\xi_{A\text{-}gly}$ = EE term with antifoam and glycolate

and

$$\frac{Fe^{2+}}{\Sigma Fe} = 0.2358 + 0.1999\xi_{A-gly}$$

An EE of 6 for glycolate is the theoretical number of electrons transferred when a mole of glycol in the feed converts to CO_2 in the off-gas in the DWPF melter. A deminimus of 800 mg/kg essentially reduces the antifoam term in the above equation to zero. If lower acid stoichiometries are used, the Mn EE=0 will have to be re-evaluated.

While some bias was found in the CC_{hot} samples toward the upper 95% confidence limit of the 2012 REDOX model, there is corresponding MRF data for the same feeds that fall within the 2012 REDOX model confidence bands. Likewise, there is a high bias in both the MRF and the CC_{hot} for the CEF-2 feeds. Since the "predicted REDOX" for the CEF-2 (Cold-cap Evaluation Furnace) feeds is calculated as a negative $Fe^{+2}/\Sigma Fe$ ratio, which is impossible to achieve experimentally, it is recommended that in the future, the feed concentrations of the exact samples used for REDOX be analyzed. This is because the CEF-2 feeds analyzed in this study were taken intermittently during the CEF-2 melter campaigns there is not an exact 1:1 correspondence of the feed chemistry to the feed samples used for the CC_{hot} and MRF experiments.

Since only 27 CC_{hot} and 7 MRF samples were used to develop the interim REDOX model, it is suggested that more glasses be tested in CC_{hot} and MRF to build a better $Fe^{+2}/\Sigma Fe$ measurement data pool. The existing glycolic flowsheet data is too poor to be refit alone until more CC_{hot} and MRF data are generated. Adding more CC_{hot} and MRF data will allow the 2012 model to be refit with more accuracy. Using the 2012 slope and intercept is conservative compared to a model refit by combining the 34 glycol flowsheet data points with the existing historic REDOX model data, i.e. the 2012 model predicts a more reducing $Fe^{+2}/\Sigma Fe$ than a refit model.

TABLE OF CONTENTS

EXECUTIVE SUMMARY vi
TABLE OF CONTENTS viii
LIST OF TABLES x
LIST OF FIGURES xi
LIST OF ABBREVIATIONS xiii
1.0 Introduction 1
1.1 The Role of Reductants and Oxidants in DWPF Processing 1
1.2 DWPF Formic/Nitric Flowsheet 2
1.3 The Role of Reductants and Oxidants in the REDOX Model 4
1.4 DWPF Formic/Nitric Flowsheet with Oxalate, Coal, and Manganese 5
1.5 DWPF Formic/Nitric Flowsheet with Oxalate, Coal and Higher Manganese 9
1.6 DWPF Formic/Nitric Flowsheet with Oxalate, Coal, Higher Manganese, Antifoam, and Ar Bubbling 10
1.7 Theoretical DWPF Formic/Nitric Flowsheet with Glycolic and Nitric Acid 12
2.0 Experimental Procedure 13
2.1 Closed Crucible Hot Insertion (CC_{hot}) 13
2.2 Closed Crucible Ramped Heat Treatment (CC_{ramp}) 14
2.3 Closed Crucible with Ar bubbling (CC_{Ar}) 15
2.4 Closed Crucible with Off-gas Analysis (CCOG) 16
2.5 Melt Rate Furnace (MRF) 18
2.6 Quality Assurance 20
3.0 Results and Discussion 20
3.1 Variability of REDOX Replicate Measurements 20
3.2 Homogeneity of Closed Crucible Ramped Heat Treatment (CC_{ramp}) 22
3.3 Homogeneity of Closed Crucible Hot Insertion (CC_{hot}) 24
3.4 Homogeneity of Closed Crucible with Off-gas Analysis (CCOG) 24
3.5 Homogeneity of Closed Crucible with Ar bubbling (CC_{Ar}) 27
3.6 Homogeneity of Melt Rate Furnace (MRF) 28
3.7 Selection of Terms for the GN Interim DWPF REDOX Model 29
3.8 Selection of GN Data for Interim DWPF REDOX Model 31
3.8.1 Glasses Unacceptable for Modeling (GN Flowsheet) 32
3.8.1.1 CC_{ramp} Dataset 32

3.8.1.2 CCOG Dataset 34
3.8.1.3 CC_{Ar} Dataset 35
3.8.2 Glasses Acceptable for Modeling (GN Flowsheet) 36
3.8.2.1 CC_{hot} Dataset 36
3.8.2.2 MRF Dataset 39
3.8.2.3 Combined CC_{hot} and MRF Datasets 39
4. Conclusions 40
5. Recommendations, Path Forward or Future Work 40
6. References 42
Appendix A . Historic REDOX Database as Used in This Document A-1
Appendix B . GLYCOL REDOX DATABASE B-1

LIST OF TABLES

Table 1. Identified Phases for the Nitric-glycolic Flowsheet Samples (Dried at 40^0 C).[36] 30

Table 2. Identified Phases for the Nitric-glycolic Flowsheet Samples (Heat and Stop Runs).[36] 31

Table 3. HTXRD Identified Phases for Nitric-glycolic Flowsheet Runs.[34] 31

Table 4. CCOG Off-gas Species Observed 35

LIST OF FIGURES

Figure 1-1. Relationship between the Measured REDOX ratio (y axis) and the Difference Between the Feed Reductants (formate) and Oxidants (nitrate). The "S" Shaped curvature of the Relationship is Demonstrated Along with the Linear Portion used for Modeling. 3

Figure 1-2. (a) Historic Data Reductants (formic acid only) vs. Oxidizers (nitrates only) weighted by 45/T where T is the weight percent solids. The DWPF REDOX model is developed by fitting a slope and intercept to the data in figure "b". 4

Figure 2-1. Experimental setup to bubble Ar through DWPF simulated feeds in a sealed crucible during the feed-to-glass conversion. Furnace chamber can be simultaneously purged with argon if desired. 16

Figure 2-2. Cross-sectional view of Closed Crucible with Off-gas (CCOG) Measurement. 16

Figure 2-3. CCOG Gas Flow System 17

Figure 2-4. Cross-sectional view of Melt Rate Furnace (MRF). 19

Figure 3-1. Non-homogeneous Glasses from FN flowsheet (SB4) made with Frit 418 that gave poor REDOX replicate reproducibility.[29] 21

Figure 3-2. Variation in Measurement of Fe^{+2} and Total Fe for Inhomogeneous CC_{ramp} and both Inhomogeneous and Homogeneous CC_{hot} Experiments. 22

Figure 3-3. CC_{ramp} REDOX Ratios are generally higher than CC_{hot} REDOX Ratios. 22

Figure 3-4. Crystallization of REDOX Samples GN74, GN75, and GN76 on the surface (a,c,e) and inhomogneities in the interior as shown in the cross section photographs (b,d,f). 23

Figure 3-5. Cross Sections of CC_{hot} Samples GN78, GN77, GN76 and GN71 (1 hour residence time at temperature (a-e) and GN78 (4 hour residence time, figure f) 25

Figure 3-6. Cross Sections of CCOG Samples GN79, GN71 and CEF-2. 26

Figure 3-7. Cross Sections of CCOG Samples SB8-D3 with and without antifoam spikes. Glasses are a distinct reddish color compared to SB8-D3 tested with CC_{ramp}. 27

Figure 3-8. Cross Sections of CC_{Ar} Samples in cross section. Most are homogeneous except where metallic nodules and precipitates were formed due to either the reducing nature of the feeds (GN71) or the Ar bubbling. 28

Figure 3-9. Cross Sections of MRF Samples in cross section. 29

Figure 3-10. Comparison of CC_{ramp} measured and predicted REDOX using different versions of the historic REDOX model and different EE values for Mn as discussed in the text. 33

Figure 3-11. Comparison of the CCOG data to the DWPF Historic REDOX Model. 34

Figure 3-12. Comparison of the CC_{Ar} data (points labelled with the letter A) to the DWPF Historic REDOX Model. 36

Figure 3-13. Comparison of CC_{hot} measured and predicted REDOX using different versions of the historic REDOX model and different electron equivalents for Mn as discussed in the text. 38

Figure 3-14. Interim REDOX model with CC_{hot} and MRF experimental measurements..... 39

Figure 5-1. Reductants vs. Oxidants showing the balance (equilibrium) achieved with the DWPF pour spout (PS) samples and showing where the glycol flowsheet samples (GN's and H values) are on the 1:1 equilibrium line. 41

LIST OF ABBREVIATIONS

AD	Analytic Development
CC	Closed (sealed) crucible
CC_{Ar}	Closed (Sealed) Crucible with Ar bubbling
CC_{hot}	Closed (Sealed) Crucible with Hot insertion
CC_{ramp}	Closed (Sealed) Crucible with Ramped heat treatment
CCOG	Closed Crucible with Off-Gas Measurement
CEF	Cold-cap Evaluation Furnace
CWAO	Catalytic Wet Air Oxidation
DSC	Differential Scanning Calorimetry
DWPF	Defense Waste Processing Facility
EE	Electron Equivalents
FN	Nitric Formic Flowsheet
FTIR	Fourier Transform Infrared Spectroscopy
GC	Gas Chromatograph
GN	Nitric Glycolic Flowsheet
H&S	Heat & Stop Experiments
HTXRD	High Temperature X-Ray Diffraction
ICDD	International Centre for Diffraction Data
LHS	Left Hand Side
MFT	Melter Feed Tank
MRF	Melt Rate Furnace
MS	Mass Spectrometer
MTS	Methyl Tri Siloxane
OLS	Ordinary Least Squares
PEO	Poly Ethylene Oxide
PS	Pour Spout
PSAL	Process Science Analytical Laboratory
REDOX	REDuction/OXidation
RHS	Right Hand Side
SB	Sludge Batch
SME	Slurry Mix Evaporator
SMRF	Slurry Melt Rate Furnace
SRAT	Sludge Receipt and Adjustment Tank
SRNL	Savannah River National Laboratory
SRTC	Savannah River Technology Center
TOC	Total Organic Carbon
XRD	X-ray Diffraction

1.0 Introduction

The HLW sludge is being immobilized at the Savannah River Site (SRS) by vitrification into borosilicate glass at the Defense Waste Processing Facility (DWPF). During melting of HLW glass, the REDOX of the melt pool cannot be measured. Therefore, the $Fe^{2+}/\Sigma Fe$ REDOX ratio in the glass poured from the melter must be related to melter feed organic and oxidant concentrations to ensure production of a high quality glass without impacting production rate (e.g., foaming) or melter life (e.g., metal and/or metal sulfide formation and accumulation on the melter floor).

The DWPF REDOX model is used to control the ratio of melter feed reductants and oxidants between a $0.09 > Fe^{2+}/\Sigma Fe < 0.33$ production range as glasses >0.09 $Fe^{2+}/\Sigma Fe$ will not foam due to deoxygenation of higher valent manganese oxides. Controlling the HLW melters at a REDOX equilibrium of $Fe^{2+}/\Sigma Fe \leq 0.33$ [1,2] prevents the formation of Ni°, Ru° , and S^{-2} which can form undesired Ni° or Ni_3S_2 deposits on the floor of the melter during vitrification. Control of foaming due to deoxygenation of manganic species is achieved at the lower REDOX limit of $Fe^{2+}/\Sigma Fe \geq 0.09$ where about 99% of the manganic species are converted to Mn^{2+} [1,2]. Therefore, the lower REDOX limit eliminates melter foaming from deoxygenation of manganic oxides.

In summary, the REDOX equilibrium in Joule heated HLW melters are controlled to prevent the following:

- reduction of metallic species such as $NiO \rightarrow Ni° + ½\ O_2$ and $RuO_2 \rightarrow Ru° + O_2$ which can fall to the melter floor and cause shorting of electrical pathways in the melt and accumulations which may hinder glass pouring
- reduction of sulfate ($SO_4^{=}$) to sulfide ($S^{=}$) and Ni^{2+} to Ni°, and Cu^{2+} to Cu° causes Ni_2S_3 and Cu_2S metal sulfides and/or Ni°-Cu° alloys to form (Figure 1-1) which can fall to the melter floor and cause shorting of electrical pathways and/or hinder glass pouring
- overly reduced glasses which can be less durable than oxidized equivalents [3]
- reduced corrosion rates of the reduced K-3 refractory used to line the melters at SRS, WVNS, and WTP [4]

The target REDOX for the world's largest operating HLW melter, the DWPF, has been a $Fe^{2+}/\Sigma Fe$ ratio of 0.2 which is in the middle of the $0.09 > Fe^{2+}/\Sigma Fe < 0.33$ production range. This ratio minimizes release of ^{99}Tc, ^{104}Ru., and Cr^{6+}.

Recently, the DWPF implemented bubbling to increase the melt rate of the incoming feeds and improve melt pool convection.[5] A decision was made not to bubble air as this would create an oxidized melt pool but to bubble argon (Ar) gas instead due to the advantages discussed above for volatilization of ^{99}Tc, ^{104}Ru, and Cr^{6+}. Argon sparges or degasses excess oxygen from the melt and creates a more reduced melt. [6,7,8] Therefore, the Ar impact was quantified so that the overall REDOX, including the impact of Ar, could continue to be targeted at $Fe^{2+}/\Sigma Fe=0.2$ in the middle of the $0.09 > Fe^{2+}/\Sigma Fe < 0.33$ production range.

1.1 The Role of Reductants and Oxidants in DWPF Processing

The REDOX model is used to control the balance of feed reductants and oxidants in the pre-melt processing tank known as the Sludge Receipt and Adjustment Tank (SRAT). While some oxidants and reductants are present in the waste, additional oxidants and reductants are added to facilitate processing such as formic acid and nitric acid. These acids are refluxed in the SRAT and analysis of dried SRAT product indicates that alkali/alkaline earth salts such as $NaNO_3$ and NaCOOH, are formed.[9,10,11] The chemical balance of oxidants and reductants that is set by the end of the SME cycle can only be altered by

the addition of additional oxidants or reductants to the SME. Alteration of the REDOX in the melter can also be accomplished by sparging with an oxidizing (air) or reducing (Ar) gas.
In the DWPF SRAT, oxidizing and reducing acids are added to the waste sludge [12] for the following reasons:

- control potential melt foaming which adversely impacts melt rate by:
  -
  - destroying nitrites
  - converting carbonates in the feed to CO_2 which vaporizes in the SRAT off-gas rather than in the melter and
  - converting a large fraction [13] of the oxidized Mn^{4+} or Mn^{3+} present as MnO_2, Mn_2O_3, Mn_3O_4, or $NaMn^{7+}O_4$ and/or hydrous complexes in the feed to $Mn^{2+}O$ or $Mn^{2+}(COOH)_2$, so that oxygen from the +4 to +2 conversion is liberated in the SRAT to the solution rather than liberated as O_2 gas in the melter;
- reduce and steam strip mercury for subsequent removal, $HgO \rightarrow Hg°$; and
- improve slurry rheology by neutralizing excess hydroxide (OH^-) in the feed by converting species such as NaOH to NaCOOH (sodium formate) salt.

The NaCOOH and $NaNO_3$ salts react in the melter cold cap at elevated temperatures: the reaction of these salts in the cold cap controls the melter REDOX.
The SRAT product is then fed to the DWPF SME, where borosilicate glass frit slurry is added to produce the melter feed slurry. The melter feed slurry is nominally concentrated to 30-50 wt% total solids in the SME and then fed to the Melter Feed Tank (MFT) which is just a holding tank for transfer into the DWPF Joule-heated melter where it is vitrified at 1150°C.

1.2 DWPF Formic/Nitric Flowsheet

The first REDOX model developed for DWPF balanced formic acid [F] and nitric acid [N] with a 1:1 stoichiometry [14,15,16,17] which implied that the oxidizing power of nitric acid was equivalent to the reducing power of formic acid on a molar basis. During this initial crucible study, it was shown that the relationship between the REDOX ratio and the {[F]-[N]} was "S" shaped: all {[F]-[N]}<0.9 were on a REDOX plateau of $Fe^{2+}/\Sigma Fe<0.05$ (the bottom of the "S" shape; Figure 1-1). For overly reduced glasses ($Fe^{2+}/\Sigma Fe\geq0.6$ and {[F]-[N]}>1.7), the absolute concentrations of formate and nitrate had no appreciable effect on glass REDOX either and a second plateau formed at a $Fe^{2+}/\Sigma Fe$ of ~0.65 (the top of the "S" shape). In this overly reduced regime, excess reductant reduced >60% of the ferric iron to ferrous and then began conversion of $NiO \rightarrow Ni°$ and $1.5SO_4^{=} \rightarrow 1.5S^{2-} + 3O_2$ causing Ni_3S_2 and/or Ni° to form (Figure 1-1). In the range between the two plateaus, the $Fe^{2+}/\Sigma Fe$ response was linear with respect to {[F]-[N]} and a model was was fit to the data.

In 1997, the data used to develop the {[F]-[N]} relationship was revisited because inclusion of any data from the two plateau regions can highly leverage the Ordinary Least Squares (OLS) fit to the data. Hence, glass quality and REDOX measurement criteria were developed to screen the data used for modeling. This redefined the population of glasses by excluding those below one half the $Fe^{2+}/\Sigma Fe$ measurement detection limit of 0.03 or 0.015 (the bottom of the "S") and those that precipitated metallic and/or sulfide species (the top of the "S") [18]. Averaging of formate, nitrate and measured REDOX ratios was used to minimize model error. Regression of the redefined data demonstrated that the {[F]-[N]} parameter was a less accurate predictor ($R^2=0.68$) of waste glass REDOX than had previously been calculated. The regression of the redefined data [18] showed that there was an {[F]-3[N]} relationship between the feed reductants, oxidants, and the glass REDOX ratio,

Equation 1 $Fe^{2+}/\Sigma Fe = 0.217 + 0.253[F]-0.739[N]$, $R^2=0.89$

where the F and N concentrations are normalized to a feed that is 45 wt% solids as the concentrations of F and N are dependent on the solid and liquid concentrations in the feed.[t] This equation was used during DWPF initial operations (Sludge Batch 1 and 2; SB1 and SB2) when off-gas surges were common. The surges were studied by neural net modeling of thirty-nine DWPF melter parameters. This modeling indicated that melter feed flow and melter level (which includes any contributions from foam generation) had a direct impact on the melter pour surges [19] and a more reducing flowsheet was adhered to from SB2 on.

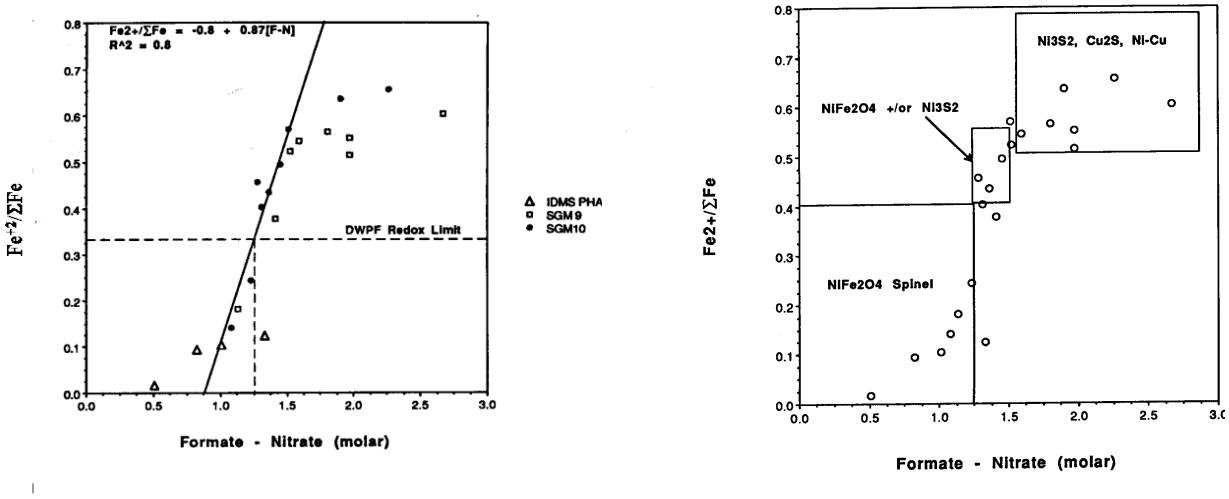

Figure 1-1. Relationship between the Measured REDOX ratio (y axis) and the Difference Between the Feed Reductants (formate) and Oxidants (nitrate). The "S" Shaped curvature of the Relationship is Demonstrated Along with the Linear Portion used for Modeling.

Both the {[F]-[N]} and the {[F]-3[N]} REDOX models assumed that the melter feeds were properly formated and refluxed to ensure that 66-100% of the Mn^{3+} and Mn^{4+} were converted to Mn^{2+} as $Mn(COOH)_2$ during preprocessing in the SRAT, e.g., before the melter feed entered the melter. The goal of reducing 66-100% of manganese to avoid oxygen foaming in the melter is based on work performed by Hrma in the 1980's specifically for the DWPF [summarized by Plodinec in 20,21]. Hrma's experiments, which were performed in the absence of nitrates, indicated that melter foaming from oxygen liberation would not be extensive with the DWPF formic acid flow sheet if a minimum of 66% of the oxidized Mn^{+4} present in a waste feed were reduced to Mn^{+2} prior to vitrification. Hrma [20,21] developed the following equation to demonstrate how oxygen liberation due to the reduction of Mn_3O_4 ($1MnO_2 \bullet 2MnO$) to a mixture more rich in MnO could cause foaming in DWPF type glasses.

Equation 2 $$(p)MnO_{\frac{4}{3}} + (1-p)MnO \xrightarrow{\substack{Melt \\ Dissolution}} (1-q)MnO + (q)MnO_{\frac{3}{2}} + \frac{1}{12}(2p-3q)O_2$$

[t] The water content of a melter feed alters the species concentrations of the [reductants] and [oxidants] and can influence the equilibrium oxygen fugacity (f_{O_2}) in a melter during vitrification. Since the effects of water on oxygen fugacity are small relative to the impact of dilution on feed concentrations, the molar concentrations were transformed to a 45% solids basis.

Where p = molar fraction of MnO in a mixture of calcined MnO + Mn_3O_4 before melting
q = equilibrium molar fraction of Mn_2O_3 in the MnO + Mn_3O_4 mixture dissolved in the melt which is independent of pressure, dependent on temperature, dependent on partial pressure of oxygen, p_{O_2}, and dependent on the composition the melt.

Both the {[F]-[N]} and the {[F]-3[N]} REDOX models demonstrated that the REDOX model balances the reductants and the oxidants so that the slope of an x-y plot of oxidants vs reductants has a slope of ~1 and an intercept of ~0 (Figure 1-2a) for the historic REDOX data (Appendix A) only, i.e. the formic/nitric flowsheet. Figure 1-2a demonstrates that when the oxidants and reductants are balanced exactly they are on the 1:1 line shown and that the 1:1 line in Figure 1-2a corresponds to the zero line in Figure 1-2b, where the oxidants are subtracted from the reductants and plotted against the measured REDOX. Excess oxidants are below the 1:1 line in Figure 1-2a and to the left of zero in Figure 1-2b. Excess reductants are above the 1:1 line in Figure 1-2a and to the right of zero in Figure 1-2b.

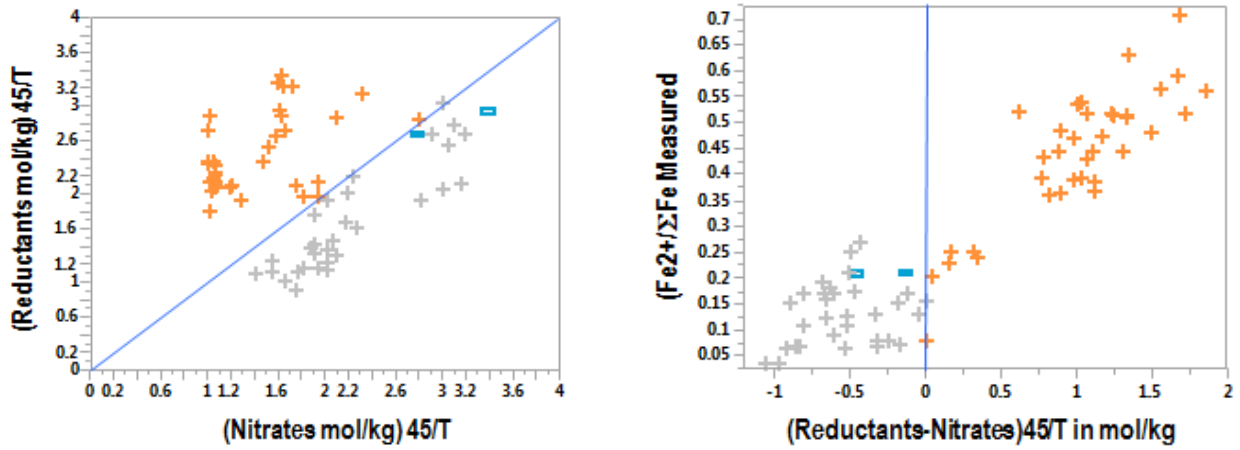

(a) (b)

Figure 1-2. (a) Historic Data Reductants (formic acid only) vs. Oxidizers (nitrates only) weighted by 45/T where T is the weight percent solids. The DWPF REDOX model is developed by fitting a slope and intercept to the data in figure "b".

The two horizontal rectangles represent DWPF SME and SRAT 224 from Sludge Batch 2(SB2).

1.3 The Role of Reductants and Oxidants in the REDOX Model

During feed-to-glass conversion, the REDOX reactions occur primarily in the cold cap along with feed decomposition and calcination. In the melt pool, further degassing and homogenization occur primarily by additional REDOX reactions. The gaseous products from the cold cap and the volatile feed components further react with air in the melter vapor space. In order to represent the gradual nature of the feed-to-glass conversion, a 4-stage cold cap model was developed by Choi [22] which approximates the melting of feed solids as a continuous, 4-stage counter-current process [23]. In Stage 1 formate salts formed in the SRAT, such as NaCOOH[f], are decomposed to CO, CO_2 and H_2 or steam. The Na forms oxides or otherwise interacts with any silicate, borate, or aluminate species available in the cold cap. The CO subsequently gets oxidized by the air diffusing into the cold cap from the top and by the oxygen being

[f] While the example equations are written as the sodium salts, i.e. NaCOOH, it should be noted that such species as $Ca(COOH)_2$, $Ni(COOH)_2$, $Mn(COOH)_2$ form and undergo similar reaction.

liberated during the Stage 2 denitration reactions (at further depth in the cold cap). Thus, a generalized set of decomposition and calcination reactions occurring in Stages 1 and 2 can be represented [22,23] by the combined equation:

Equation 3

$$\underbrace{2NaCOOH + 2NaNO_3}_{melter\ feed} \rightarrow \underbrace{CO\uparrow + CO_2\uparrow + H_2\uparrow}_{Stage\ 1} + \underbrace{N_2O\uparrow + 2O_2\uparrow}_{Stage\ 2} + \underbrace{2Na_2O}_{Stage\ 1\ and\ 2} \rightarrow$$

$$\underbrace{2CO_2\uparrow + H_2O\uparrow + N_2\uparrow + 1.5O_2\uparrow}_{plenum} + \underbrace{2Na_2O}_{glass}$$

recognizing that other species such as NO could also likely exist as intermediate species.

Multiple oxides begin to form during Stage 3. These oxides are assumed to form solid solutions such as spinels which coexist with the REDOX species in the same phase. Stage 4 represents the final fusion where the oxides formed in Stage 3 form aluminate, borate, or silicate groups in the melt, e.g., Fe_2SiO_4 and Na_2SiO_3.

In order to represent all four stages of cold cap reaction simultaneously (omitting the intermediate CO, N_2O and NO species produced in Stage 1 and Stage 2 in the cold cap reactions) and include terms for reduced and oxidized iron and silica one can assume a generalized or equilibrium form of the cold cap reactions as follows:

Equation 4 $$Fe_2O_3 + 5SiO_2 + 6NaCOOH + 2NaNO_3 \rightarrow Fe_2SiO_4 + 6CO_2\uparrow + N_2\uparrow + 4Na_2SiO_3 + 3H_2O\uparrow$$

Equation 4 assumes that Fe^{3+} enters the melter as Fe_2O_3 and that the reductant $COOH^-$ and the oxidizer NO_3^- enter as sodium formate and sodium nitrate salts, respectively. The formated and nitrated salts react with glass formers such as SiO_2 to form Fe^{+2} and Na^+ silicate components in the glass and liberate CO_2, N_2, and H_2O vapors to the melter plenum (Equation 4). If oxidants are undersupplied in the melter, CO instead of CO_2 may dominate the off-gas. If reductants are undersupplied in the melter, NO or N_2O may dominate the off-gas.

For simplicity and consistency in prediction, a mechanistic REDOX model was developed using a *generalized form* of the cold cap reactions (Equation 4). This equation can be rewritten in terms of $2Fe^{2+}$ and $2Fe^{3+}$ instead of the iron oxides, and the SiO_2 term can be omitted as it is not involved in the REDOX reactions, e.g. it does not change oxidation state. In addition, the product phases on the right-hand-side (RHS) of the REDOX equilibrium do not consider the intermediate gaseous species generated in Stage 1 and Stage 2 of the cold cap (see Equation 4).. The left-hand-side (LHS) of the REDOX equilibrium (Equation 4) represents the SRAT/SME reductant and oxidant salts that react in the cold cap.

1.4 DWPF Formic/Nitric Flowsheet with Oxalate, Coal, and Manganese

DWPF Sludge Batch 3 (SB3) was purported to contain high concentrations of reductants that were not in the simple formate vs. nitrate REDOX correlations used for SB1 and SB2: species such as oxalate and coal. After SB2 but before SB3 it was recognized that the 1:3 relationship between formic acid and nitric acid in Equation 1 was related to the number of electrons transferred by the carbon in the sodium formate as it was oxidized to CO_2 in the melter and the sodium nitrate as it was reduced to N_2 in the melter.

Thus a REDOX model using Electron Equivalents (EE) transferred during the REDOX reactions was developed with terms for the additional reductants [24,25] based on the cold cap interactions discussed in the previous section. In addition, a manganese term was added to the EE model to account for potential differences in the oxidation state of Mn in the feed (+4) and in the glass (+2) as it could not be guaranteed that 66-100% of the manganese was reduced to $Mn(COOH)_2$ in the SRAT. When coal and oxalate were absent, the EE model reverted to an [F]-2.5[N] stoichiometry plus the term for manganese.

Using the EE approach generates Equation 5 below as the controlling REDOX reaction between reducing formate salts and oxidizing nitrated salts, in the melter cold cap:

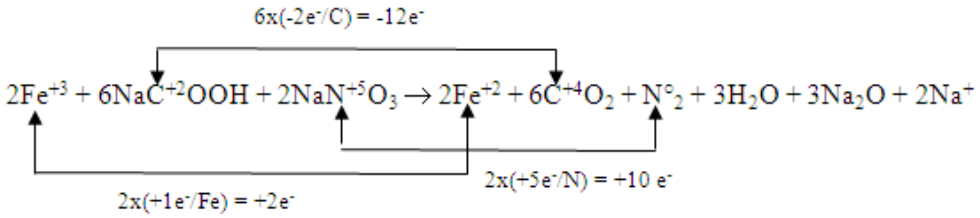

Equation 5

The oxidation/reduction equilibrium shown in the Equation 5 between nitrate and formate indicates that one mole of nitrate gains 5 electrons when it is reduced to N_2 while one mole of carbon in formate loses 2 electrons during oxidation to CO_2. This is an oxidant:reductant ratio of 5:2 which indicates that nitrate is approximately 2½ times as effective an oxidizing agent as formate is a reducing agent (when nitrogen gas is the reaction product). So if the formate exchanges 2 EE's per mole of carbon, the nitrate exchanges 5EE's per mole of nitrate.

The oxidation/reduction equilibrium shown in Equation 6 between coal and the oxidized nitrated salts indicates that one mole of nitrate gains 5 electrons when it is reduced to N_2 while one mole of carbon in coal loses 4 electrons during oxidation to CO_2. This is an oxidant:reductant ratio of 5:4 which indicates that nitrate is only 1¼ times as effective an oxidizing agent as coal is a reducing agent (when nitrogen gas is the reaction product). So if the coal exchanges 4 EE's per mole of carbon, the nitrate exchanges 5EE's per mole of nitrate.

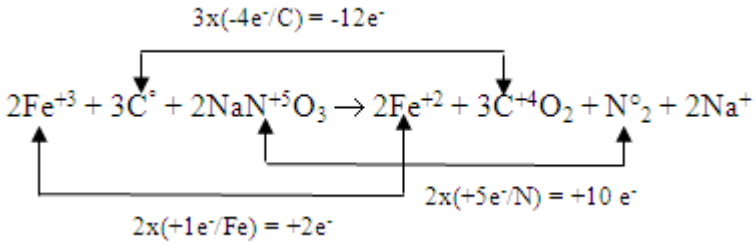

Equation 6

The oxidation/reduction equilibrium between the oxalate and nitrate salts is given in Equation 7.

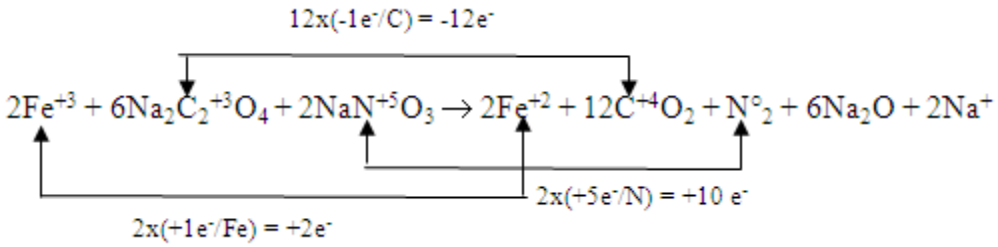

Equation 7

This reaction, written in the format of the preceding cold cap reactions, indicates that one mole of nitrate should gain 5 electrons when it is reduced to N_2 while one mole of carbon in oxalate should lose 1 electron during oxidation to CO_2. This is an oxidant:reductant ratio of 5:2 (since there are 2 moles of carbon in a mole of oxalate). This indicates that nitrate is 2.5 times as effective an oxidizing agent as the two carbons in oxalate are a reducing agent (when nitrogen gas is the reaction product).

However, the REDOX modeling data indicated that oxalate was twice as strong a reductant as would be indicated by a 2.5:1 ratio. During further investigation of the apparent increase in the reducing power of oxalate, data became available that demonstrated that oxalate salts convert to oxalic acid, which then forms formic acid and CO_2 during SRAT processing [26]. The process was later identified by Koopman, et.al. [27] as spontaneous catalytic wet air oxidation (CWAO) of the oxalate which proceeds with a formate as as an intermediate product. If CWAO also occurs in the cold cap then six moles of oxalate become 12 moles of formate and 4 EE's are exchanged per oxalate overall (see Equation **8**).

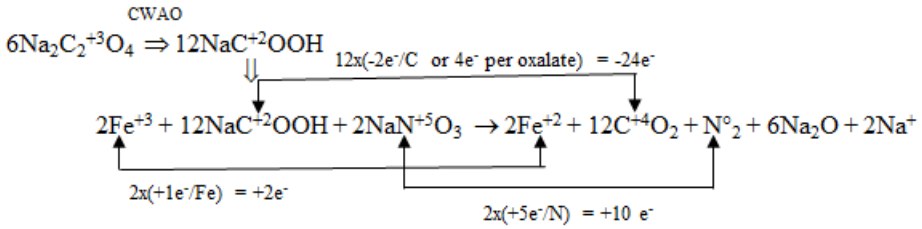

Equation 8

An electron transfer equation was written for the reduction of manganese by any carbon containing reductant. The equation assumed that the manganese entered the melter as Mn^{+4} either from the sludge where it has can be present as $Mn^{+3}OOH$, Mn_3O_4 (mixed Mn^{+4} and Mn^{+2}), $Mn^{+4}O_2$, jacobsite (Fe_2MnO_4), mixed unidentified Fe-Mn oxides/hydroxides [28] or from SRAT processing. During DWPF SB3 SRAT processing the distribution of the soluble manganese, that is Mn^{+2}, showed no relation to any combination of feed oxidizers or reductants. This is because manganese can complex with formate as soluble $Mn(COOH)_2$ in the SRAT supernate, as insoluble MnO_2 in the SRAT insoluble solids, or as insoluble manganous oxalate in the SRAT insoluble solids . The role as $Mn(COOH)_2$ is pH dependent, e.g. $Mn(COOH)_2$ is stable at-near neutral pH while aqueous Mn^{+2} is soluble at lower SRAT pH values. Therefore, a measurement of the soluble Mn in the SRAT supernate is insufficient to determine if 66% of the Mn^{+4} has been reduced to Mn^{+2} when the SRAT/SME pH values fluctuate and oxalate is present.

In addition, manganese oxalate was found during the Differential Scanning Calorimetry (DSC) analysis of Tank 7 sludge.[‡] X-ray diffraction (XRD) analysis of the dried SRAT solids also showed the presence of manganous oxalate $C_2MnO_4 \bullet 2H_2O$ and ferrous oxalate which is isostructural ($C_2FeO_4 \bullet 2H_2O$) and indistinguishable from manganous oxalate during XRD analysis. Subsequent Scanning Electron

[‡] Fernando Fondeur, personal communication February 28, 2003

Microscopy (SEM) analyses of the dried SRAT product also indicated the presence of $MnSO_4$, manganous sulfate. Since the distribution of $Mn^{+2}/Mn^{+3}/Mn^{+4}$ in the DWPF SRAT product was inconclusive and the REDOX ratio was found to be highly dependent on the molar concentration of MnO in a glass during SB3 testing [24,25], a manganese term was included in the DWPF EE REDOX model. The manganese was conservatively assumed to be all Mn^{+4} and Equation 9 was used to determine the electron transfers between Mn^{+4} conversion to Mn^{+2} in the cold cap.

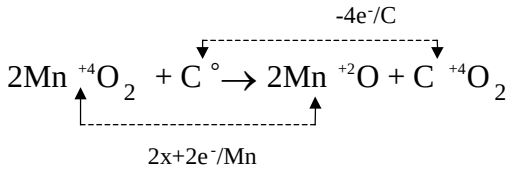

Equation 9

Therefore, the number of electrons gained during reduction or lost during oxidation are the following:

- $[NO_3]$ = +5
- [Mn] = +2
- $[C]_{formate}$ = -2
- $[C]_{coal}$ = -4
- $[C]_{oxalate}$ = -4

The water content of a melter feed alters the species concentrations of the [reductants] and [oxidants] and can influence the equilibrium oxygen fugacity (f_{O_2}) in a melter during vitrification. Since the effects of water on oxygen fugacity are small relative to the impact of dilution on feed concentrations, the molar concentrations were transformed to a 45% solids basis as was done in previous REDOX modeling.

The overall relationship between the REDOX ratio and the Electron Equivalents, ξ, can then be expressed as:

Equation 10
$$\frac{Fe^{2+}}{\Sigma Fe} = f\left[\left(2[F]+4[C]+4[\mathrm{O_T}]-5[N]-2[Mn]\right)\frac{45}{T}\right] = f[\xi]$$

where f = indicates a function
[F] = formate (mol/kg feed)
[C] = coal (carbon) (mol/kg feed)
$[O_T]$ = $oxalate_{Total}$ (soluble and insoluble) (mol/kg feed)
[N] = nitrate + nitrite (mol/kg feed)
[Mn] = manganese (mol/kg feed)
T = total solids (wt%)

$$\xi = \left(2[F]+4[C]+4[\mathrm{O_T}]-5[N]-2[Mn]\right)\frac{45}{T}$$

When the REDOX data generated from SB3 and the historic REDOX data [18] are then fit as a linear function of ξ:

Equation 11
$$\frac{Fe^{2+}}{\Sigma Fe} = 0.1942 + 0.1910\xi$$

the DWPF Electron Equivalents REDOX model was generated with an adjusted R^2 of 0.8037 and a Root Mean Square Error of 0.0690 for 120 data observations (53 from the SB study and 67 from the historic study).

During validation of the DWPF EE model [24,25] against production melter data from West Valley Nuclear Fuel Services, a melter that used sugar as a reductant, a term for sugar was added to Equation 10. The sugar electron transfers were calculated as:

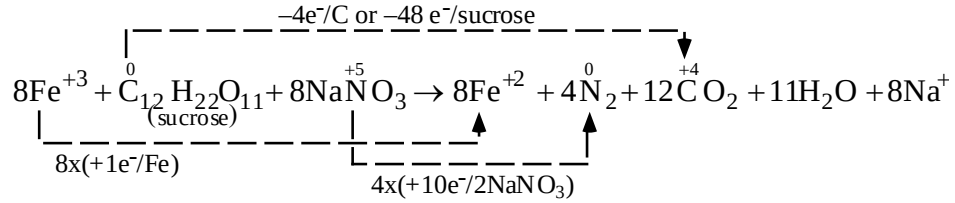

Equation 12

The Electron Equivalents term in Equation 10 becomes

$$\xi = \left(2[F] + 4[C] + 4[S] + 4[O_T] - 5[N] - 2[Mn]\right)\frac{45}{T}$$

where [S] = sugar carbon (mol/kg feed).

1.5 DWPF Formic/Nitric Flowsheet with Oxalate, Coal and Higher Manganese

At the time the EE model was developed for SB3 [24,25], further investigation into the role of oxidized Mn species (+4, +5, +6, and +7) in the feed was suggested. Higher manganese concentrations had been experienced in the early projections of DWPF Sludge Batch 4 (SB4) compositions. During non-radioactive melt rate testing of SB4 feed simulants, Equation 10 and Equation 11 predicted a REDOX target of $Fe^{2+}/\Sigma Fe$ of 0.2 but produced glasses that were overly oxidized, $Fe^{2+}/\Sigma Fe \sim 0$. These overly oxidized feeds foamed and the copious amounts of foam adversely impacted melt rate. At this point the EE model parameters were reinvestigated and it was determined the high nitrate in DWPF SB4 feeds was reoxidizing divalent manganese in the melter feeds during the denitration reactions in the cold cap. Therefore, the manganese in the cold cap is likely Mn^{+7} and not Mn^{+4} as assumed in Equation 10 and Equation 11.

Therefore, the 2003 DWPF EE REDOX model was refit in 2007 [29] with a factor of 5 for the manganese EE transfer in order to avoid foaming in high manganese containing feeds:

Equation 13
$$\frac{Fe^{2+}}{\Sigma Fe} = f\left[\left(2[F] + 4[C] + 4[O_T] - 5[N] - 5[Mn]\right)\frac{45}{T}\right] = f[\xi]$$

where
f	=	indicates a function
[F]	=	formate (mol/kg feed)
[C]	=	coal (carbon) (mol/kg feed)
$[O_T]$	=	$oxalate_{Total}$ (soluble and insoluble) (mol/kg feed)
[N]	=	nitrate + nitrite (mol/kg feed)
[Mn]	=	manganese (mol/kg feed)
T	=	total solids (wt%)

$$\xi = \left(2[F] + 4[C] + 4[O_T] - 5[N] - 5[Mn]\right)\frac{45}{T}$$

and

Equation 14 $$\frac{Fe^{+2}}{\sum Fe} = 0.2358 + 0.1999\xi$$

The $\frac{Fe^{2+}}{\Sigma Fe}$ predictions from the Electron Equivalents model given above were fitted to measured REDOX data generated from the DWPF melter from SME Batch 224, to data generated by the Savannah River Technology Center (SRTC) now SRNL mini-melter, and to data from the SRTC Slurry-fed Melt Rate Furnace (SMRF). Since only 19 data points were available for the development of the revised manganese term and many of the glasses were inhomogeneous due to the high viscosity of the feeds, the five EE transfer for manganese should be further verified for higher manganese containing feeds.

1.6 DWPF Formic/Nitric Flowsheet with Oxalate, Coal, Higher Manganese, Antifoam, and Ar Bubbling

In 2012, an EE was needed for the antifoam feed additive.[30] Antifoam is an organic chain structure composed of methyltrisiloxane (MTS) end groups and a center polymer chain of varying length (8 to 12 polyethyleneoxide or PEO groups), and the EE term must be based on the number of carbons in each part of the organic group and their relative EE term. This is the same strategy used to fit a carbon term for coal in the EE model but the antifoam molecule contains carbons of different oxidation states so it is more complex.

The MTS end groups of the antifoam molecule have 7-8 carbons of -4 charge and the 8 chain PEO groups have 16 carbons of -1 charge while the 12 chain polymers have 24 carbons of -1 charge. Since the ratio of the 8:12 polymer chains is 90%:10%, there are 16.8 carbons of -1 charge in the weighted polymer chain and 8 carbons in the MTS if the MTS groups are assumed to be octa-MTS instead of hepta-MTS for a total of 24.8 carbons in the antifoam organic molecule (sum of 0.9*16 + 0.1*24). The -1 carbons of the PEO exchange 5EE's per carbon to oxidize to CO_2 in the melter. The -4 carbons of the octa-MTS exchange 8EE's per carbon to oxidize to CO_2 in the melter. Experimentation and modeling have shown that the MTS cleave off the antifoam during processing and do not participate in reduction of the melt pool. Therefore, the EE of the PEO are 16.8/24.8 carbons * 5 EE per carbon for a total EE transfer term of +3.39 per mole/kg of carbon once the following conversions are made so that

mg/kg of antifoam→mg/kg of total carbon in antifoam→mol/kg of total carbon in antifoam.

This method of conversion from antifoam to mol/kg of carbon was chosen because the DWPF data available was in mg/kg of antifoam calculated from how many gallons of antifoam had been measured per SME batch and sealed crucible studies that had been performed after known amounts of antifoam had been added were available in mg./kg of antifoam. The DWPF data was also available as the measured Total Organic Carbon (TOC) in mg/kg of carbon. The mg/kg of carbon from the antifoam was determined by subtracting the carbon contribution from formic acid, oxalate/oxalic acid, and coal. Modeling was performed using mol/kg carbon derived from gallons of antifoam used and from TOC measurements.

Experimentation and modeling has shown that the antifoam PEO's are 80-100% effective in melt pool reduction. The modeling performed for the REDOX model for antifoam suggests that the efficiency is 85%. Therefore, 85% of +3.39 EE yields an overall EE transfer of +2.88 per mol/kg of carbon from antifoam compared to +2 for formic acid and +4 for oxalate and coal. Having an antifoam term in the DWPF REDOX model may allow antifoam to be used as a reductant source while also controlling feed

foaming. More information has been obtained on how antifoam degrades [31,32] and the antifoam term may be revised in the future. This would alter the antifoam term slightly but then also alter the efficiency factor that was fit to experimental data so the impact of the overall term on REDOX would remain the same.

In addition, the DWPF had begun to sparge the melt pool with Ar bubblers and the impact of the Ar bubbling on REDOX was needed. There is an additive impact on the melt pool REDOX from the argon bubbling. Argon (Ar) degasses or sparges the oxygen from the melt. Thus, REDOX is a function of both the oxidants and reductants in the melt pool and the Ar sparging. While Ar is an inert gas, Ar replaces the free oxygen in a glass. This process also occurs when inert gasses are used to sparge the oxygen or other gasses out of solutions, molten metals, or glasses. The REDOX equilibrium in a glass melt can be represented by

Equation 15

$$Fe^{3+}_{melt} + \frac{n}{2} O^{2-}_{melt} \leftrightarrow Fe^{2+}_{melt} + \frac{n}{4} O_{2\ melt}$$

where n = the number of electrons transferred
O^{2-} = the oxygen ion activity or basicity of the melt
O_2 is the physically dissolved oxygen in the holes of the network structure.

The REDOX-oxygen balance equation is written as reversible as going from the right hand side (RHS) to the left hand side (LHS) is the reduction of ferric to ferrous iron and going from LHS to RHS is the oxidation of ferrous to ferric iron. Since the DWPF melt pool reductants shift the equilibrium to the RHS where dissolved oxygen exists in the glass, it is the dissolved oxygen on the RHS of this equation that is being displaced by the Ar in the melt pool. This is because the free oxygen on the RHS of the equation is being sparged out and the equilibrium between the RHS and the LHS no longer exists, driving the equilibrium to the RHS. Therefore, O_2 must be provided by either (1) additional melt pool oxidants (the theory of targeting a more oxidizing REDOX target to compensate for the Ar sparging) or (2) using a mixing valve to admix small amounts of air into the argon while sparging. Reference 30 provides the calculations of Ar-air mixtures that would be acceptable if the latter route is desired.

Measurement of the REDOX of DWPF pour stream (PS) samples (with and without Ar bubbling) and measurement of a simulated SB6 feed that was Ar bubbled during the feed-to-glass transformation in a sealed crucible inside an Ar bubbled oven demonstrated that the argon bubbling impact is a linear constant of $Fe^{+2}/\Sigma Fe$ of ~0.1. Therefore, it is recommended that targeting a chemical REDOX of 0.1 should yield a realized $Fe^{+2}/\Sigma Fe$ of ~0.2. While there is no EE term that can be developed for Ar sparging, an "effective offset" term has been added to the REDOX model to account for Ar degassing.

The DWPF REDOX model then takes the form

Equation 16

$$\frac{Fe^{2+}}{\Sigma Fe} = f\left[\left(2[F] + 4[C] + 4[O_T] + 3.39 * eff\,[C_A] - 5[N] - 5[Mn]\right)\frac{45}{T}\right] = f\left[\xi_A\right]$$

where f = indicates a function
[F] = formate (mol/kg feed)
[C] = coal (carbon) (mol/kg feed)
$[O_T]$ = $oxalate_{Total}$ (soluble and insoluble) (mol/kg feed)
$[C_A]$ =carbon from antifoam (mol/kg feed)
eff = effective antifoam impact = 0.85
[N] = nitrate + nitrite (mol/kg feed)
[Mn] = manganese (mol/kg feed)
T = total solids (wt%)

$$\xi_A = \left[\left(2[F]+4[C]+4[O_T]+3.39*eff[C_A]-5[N]-5[Mn]\right)\frac{45}{T}\right]$$

When the REDOX data generated were fit as a linear function of ξ_A they fell within the confidence bands of the 2007 EE model (Equation 13 and Equation 14) and so the slope and intercept were not refit. This gives the form of the DWPF REDOX model with an antifoam term (the 2012 model) as:

Equation 17
$$\frac{Fe^{2+}}{\Sigma Fe} = 0.2358 + 0.1999\xi_A$$

The impact of Ar sparging on REDOX was quantified and the Ar adjusted DWPF model takes on the form:

Equation 18
$$\frac{Fe^{2+}}{\Sigma Fe} = 0.2358 + 0.1999\xi_A + 0.1_{Ar}$$

1.7 Theoretical DWPF Formic/Nitric Flowsheet with Glycolic and Nitric Acid

It is assumed that the glycolic acid forms a sodium glycolate salt during reflux in the SRAT similar to the manner in which formic acid forms a sodium formate salt during reflux in the SRAT. The glycolic acid flowsheet is similar to the formic acid flowsheet in that it buffers around a pH of 4 and the amount of free acid is a function of the final pH of the SRAT, i.e. a portion of the glycolate may exist as glycolic acid. Whether glycolate exists as a salt or as the acid does not affect the REDOX balance calculation. The simplest reaction for sodium glycolate being oxidized by sodium nitrate is given as Equation 19, assuming that all of the carbon oxidizes to CO_2 as do all the other reductants in the DWPF REDOX model.[30]

Equation 19

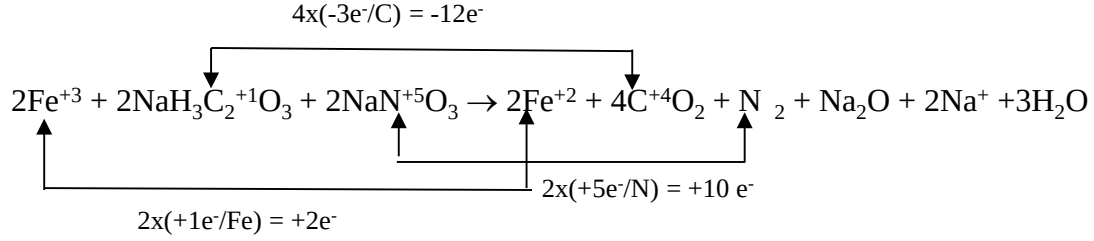

Equation 19 demonstrates that 3 electron equivalents (EE) are lost per carbon for a total of 6 EE per mole of glycolate oxidized. In reality the carbons in glycolate are approximately +2 and a 0 for an average of +1 per carbon as indicated in Equation 19. Therefore, if the equation were written with the zero carbon losing 4 electrons to oxidize to +4 carbon and the +2 carbon losing 2 electrons to oxidize to +4 carbon it would still give an EE of (4+2) = 6 EE per mole of glycolate.

2.0 Experimental Procedure

Glycolate measurements in SRAT and SME feeds have been problematic until SRNL Analytic Din (AD) developed a caustic quench method [33] to improve glycolate analysis. Until accurate glycolate measurements were available it was difficult to develop a glycolate term for the REDOX model.

All of the Closed (sealed) Crucible (CC) studies described below used Frit 418. Frit 418 had been shown to be problematic during SB4 REDOX [29] modeling and many of the closed crucible tests below yielded inhomogeneous glasses because this frit is very viscous. During SB4 testing alternate frits (F320, F503 and FP2-2) were developed for REDOX testing.[29]

Analyses by X-Ray Diffraction (XRD) were performed on air dried SRAT and SME products. High Temperature X-Ray Diffraction (HTXRD) was performed [34] on the nitric-glycolic (GN) flowsheet for comparison to HTXRD's performed on the nitric-formic (FN) flowsheet.[10,35] In addition, Heat and Stop (H&S) crucible studies were performed where the SME product is heated to a given temperature for 1 hour and the reaction stopped at that temperature so that the SME product phases could be identified by XRD. Heat and stop samples were heat treated to 40°C, 300°C, 500°C, and 775°C and then the phases were identified by XRD.[36] The details of the HTXRD and H&S are given elsewhere [34,36] and the results summarized in this report.

In order to facilitate REDOX measurements for the GN flowsheet, several different permutations of the closed crucible (sealed crucible) method were tried. The four major variations to the CC method are:

1. Closed (sealed) Crucible hot insertion method (CC_{hot})
2. Closed (sealed) Crucible ramped method (CC_{ramp})
3. Closed Crucible with Argon bubbling method (CC_{Ar})
4. Closed Crucible with Off-gas Analysis method (CCOG).

In addition, Melt Rate Furnace (MRF) tests were performed. Each of these methods were compared to each other and to the historic REDOX database from 1997 to 2012. The various methods are described below.

2.1 Closed Crucible Hot Insertion (CC_{hot})

The procedure for CC_{hot}, which has been used since 1997, begins with measuring out enough SME product to fill the chosen crucible (typically a 100mL alumina crucible) to approximately 2/3 full (between 60 and 70mL). The exact amount is calculated by a formula given in the revised REDOX procedure.[37] The sludge/frit mixture in the crucible is then dried in a 40 - 50°C oven until it reaches a consistency similar to "thick peanut butter". The dried sludge is then stirred to homogeneity and the lid is sealed onto the crucible using nepheline gel. The gel is dried and the crucible is preheated at 70°C for at least one hour to prevent thermal shock. The preheated crucible is placed directly into a hot furnace at 1100-1150°C. Once the oven recovers temperature from the process of inserting crucibles, the samples are held for one hour and then removed to a pan of sand or a refractory brick to quench cool in air. When the samples have cooled, the glass is cut out of the crucible and pieces isolated in the interior of the glass, away from the surface exposed to the atmosphere or the surface in contact with the alumina crucible, are sampled for REDOX measurements.[37] The surface and cut faces of the glass are also available for microscopic and SEM analysis to examine glass homogeneity. Often a different top layer, which looks

like a cold cap, can be observed in the CC_{hot} experiments. A cold cap type reaction layer was also noted in SB4 testing.[29]

A known issue with the REDOX procedure includes failing to dry the SRAT or SME product sufficiently to reduce the amount of steam escaping when the hot furnace insertion is performed. Large amounts of steam from the insufficiently dried sample can cause the lid to pop off, exposing the material to the oxygen in the air and releasing reactive off-gas species before they were able to react and yield a valid REDOX measurement. The procedure has been revised to dry to an almost dry consistency rather than to a thick peanut butter consistency. An additional issue which has been observed is loading of too many samples at one time into an oven such that the recovery of the oven temperature is delayed. Overloading furnaces also reduced the insertion temperature that the later crucibles experience as the furnace has significantly cooled by the time they are inserted. Ideally only one sample or a few samples (1-3) should be loaded at a time.

For some of the SB6 feeds, when coupled with the refractory frit Frit 418, the CC_{hot} methodology was found to give irreproducible $Fe^{+2}/\Sigma Fe$ ratio determinations. This had been observed previously during SB4 REDOX testing with Frit 418: the glass in the CC test was at too high a viscosity and thus inhibited convection in the crucible and produced an inhomogeneous glass. Inhomogeneous glass gives non-uniform $Fe^{+2}/\Sigma Fe$ measurement results. To ensure that the glass viscosity variable was controlled the SRNL REDOX procedure was adjusted to require that the sludge-frit mixture being tested in CC_{hot} had a viscosity of 50-60 poise at 1150°C. This was the viscosity found to provide a homogeneous glass during SB4 testing. If the sludge-frit mixture is calculated to have a viscosity of >60 poise, $LiBO_2$ is now required to be added as a flux that does not impact the overall REDOX of the mixture. A method to calculate the viscosity had been added to the REDOX procedure

The ITS-00520 procedure requires that the REDOX procedure be repeated 3 times on different REDOX samples. The REDOX ratio is then determined by the Baumann methodology [38] which is the same as the Process Science Analytic Laboratory (PSAL) REDOX procedure.[39] Each glass is dissolved once and the Fe^{2+} and total Fe are read twice colorimetrically so that the $Fe^{2+}/\Sigma Fe$ ratio can be calculated.

2.2 Closed Crucible Ramped Heat Treatment (CC_{ramp})

The CC_{ramp} method was used in the SRNL shielded cells when the REDOX of DWPF SME samples was being tested. For these samples, the crucible lids were popping off due to excessive steam release. As described above the procedure has been changed to dry to an almost dry consistency rather than a thick peanut butter consistency.

Initially, it appeared that the CC_{ramp} gave the same results as the CC_{hot} for the formic acid flowsheet. However, the CC_{ramp} method, which is not a part of the REDOX procedure, has a heating profile that is ramped up from room temperature to 1150°C. The samples are prepared and sealed the same way as CC_{hot} up until the preheating step. At this point, the samples are placed in a cold oven. The oven is then programmed to heat up to 1100 - 1150°C over approximately 1 – 1.5 hours. The samples are held at temperature for one hour and quench cooled, sampled, and analyzed in the same manner.

The CC_{ramp} differs from the CC_{hot} procedure partially because of the response of the nepheline gel and the crystallization of the sample. When the crucible is placed directly into a hot furnace (CC_{hot}), the alumina crucible and sample are preheated at 40°C. The alumina crucible heats up faster than the SME contents in the crucible and the gel sets before a significant amount of off-gas is produced by chemical reactions. When the crucible is ramped up to temperature, the material inside undergoes the chemical reactions necessary to produce off-gas before the furnace reaches a sufficient temperature to set the nepheline gel (the gel curing temperature is ~400-600°C per the manufacturer ZYP Coatings). This may allow more

off-gas to escape from the crucible, altering the glass-gas equilibrium that controls the REDOX behavior of the overall system.

The main problem with the CC_{ramp} procedure is that the glass goes through the maximum crystallization temperature during the ramp up more slowly than in the CC_{hot} insertion, which causes spinel crystals to form on the glass surface and causes the glasses to be more inhomogeneous. Since spinel (nominally $NiFe_2O_4$) sequesters iron from the glass it can alter the glass REDOX results. For the past several years the REDOX procedure [37] has cautioned that ramping a crucible up can alter the final measured REDOX. Samples from the GN flowsheet that have been subjected to the CC_{ramp} method have shown higher (more reduced) REDOX values than those from the CC_{hot} method. While it is not clear why the REDOX is consistently higher in CC_{ramp}, it may be due to the fact that the formation of the $NiFe_2O_4$ spinel phases observed during microscopic examination coats the upper surface of the sample blocking the reaction between the glass underneath and the vapors in the "atmosphere in the vapor space" (plenum) of the crucible.

2.3 Closed Crucible with Ar bubbling (CC_{Ar})

For the CC_{Ar} method, the loading and drying procedure are the same as for CC_{hot}, but the atmosphere control is very different. Once the samples are sufficiently dried, a lid is sealed with nepheline gel on to the top of the crucible, but this lid has a hole in the middle. Through this hole, an Inconel® 690 bubbler is inserted that is long enough to enter the SME product during the feed-to-glass conversion, but not long enough to touch the bottom of the crucible.

Through this bubbler, argon gas is sparged slowly through the product during the melting process. The rate at which the argon is bubbled is set using a needle valve. The flowrate used was determined by flowing argon through 5000 centistoke silicone oil which has a similar viscosity to molten glass at 1150°C and examining the bubble generation rate (Figure 2-1). The desired rate is one bubble every two to three seconds. Once the needle valve is set, this provides the correct argon flow through molten waste glass. The oven chamber is also swept with Ar so no air can flow around the bubbler through the hole in the crucible lid.

The lid with the hole is sealed around the edge with nepheline gel and set in a 70°C oven for at least one hour. Then the bubbler is inserted and flow is started. Over-pressurization of the crucible is not an issue because there is sufficient room around the bubbler in its hole in the lid to vent. The bubbler is attached to an argon supply manifold through the back of the furnace. To be able to safely attach the manifold, the oven is cold when the crucible with bubbler is inserted. Once the bubbler is attached to the manifold and argon is flowing in the crucible and into the rear of the furnace cavity, the oven is set to ramp to temperature (1100-1150°C) over 1-1.5 hours. The sample is held at temperature with bubbling for one hour. The glasses do not crystallize because of the agitation caused by the bubbling and the samples are found to be homogeneous.

After one hour, the oven is turned off and the sample is allowed to cool in the furnace with argon still flowing in the chamber but no longer flowing through the bubbler. Once the sample is cooled, the bubbler is removed, typically with minimal force, and the glass is sampled and analyzed as previous. Typically the effect of the argon sparging on the REDOX of the material is very reducing. The argon is able to both displace dissolved oxygen from the melt and sweep away any produced off-gas before it has the ability to interact with the material as discussed above. This reducing environment, or at least less oxidizing environment, raises the REDOX values of samples processed with the CC_{Ar} method.

(a) (b)

Figure 2-1. Experimental setup to bubble Ar through DWPF simulated feeds in a sealed crucible during the feed-to-glass conversion. Furnace chamber can be simultaneously purged with argon if desired.

2.4 Closed Crucible with Off-gas Analysis (CCOG)

For the CCOG method, the nature of the experiment is similar to the CC_{Ar} method, but fundamentally different from all of the other CC tests. The sample in this method is loaded as wet sludge (approx. 20g) into a quartz crucible designed with a conical reservoir below two ball-and-socket joints as shown in Figure **2-2**. An inlet tube extends from the bottom of the smaller of the two ball-and-socket joints down into the vessel to just above the liquid level of the sludge. This tube allows argon or any gas mixture to be directed into the chamber and across the surface of the slurry but not sparged through the slurry as in the CC_{Ar} method. This sweep gas carries any off-gas species produced into the analysis train for sampling by the Gas Chromatograph (GC), Mass Spectrometer (MS), and Fourier Transform Infrared Spectroscopy (FTIR). More details of the experimental setup can be found in reference [40].

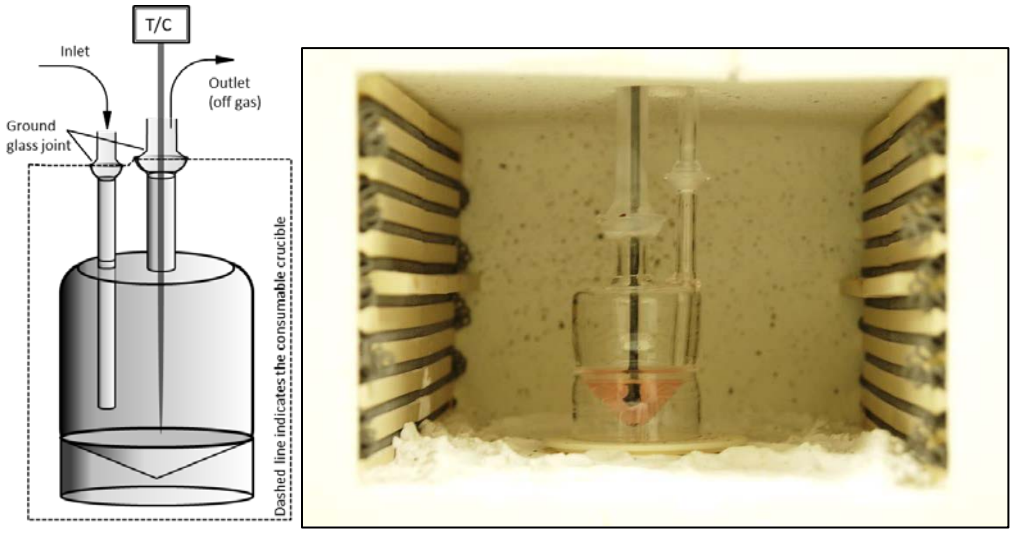

Figure 2-2. Cross-sectional view of Closed Crucible with Off-gas (CCOG) Measurement.

The CCOG experiment is set up in a cold furnace. The crucible with wet sludge is connected to the argon inlet and off-gas outlet line through the hole in the roof of the furnace. Once the inlet and outlet are in place, argon is used to purge the crucible at approximately 1.5 L/min. It has been determined that changing the argon flowrate changes the REDOX response. A diagram of the gas system is shown in Figure **2-3**. Once the setup is complete and the off-gas analysis train has begun to sample the purge gas, the oven is ramped to just over 100°C to begin drying the sample.

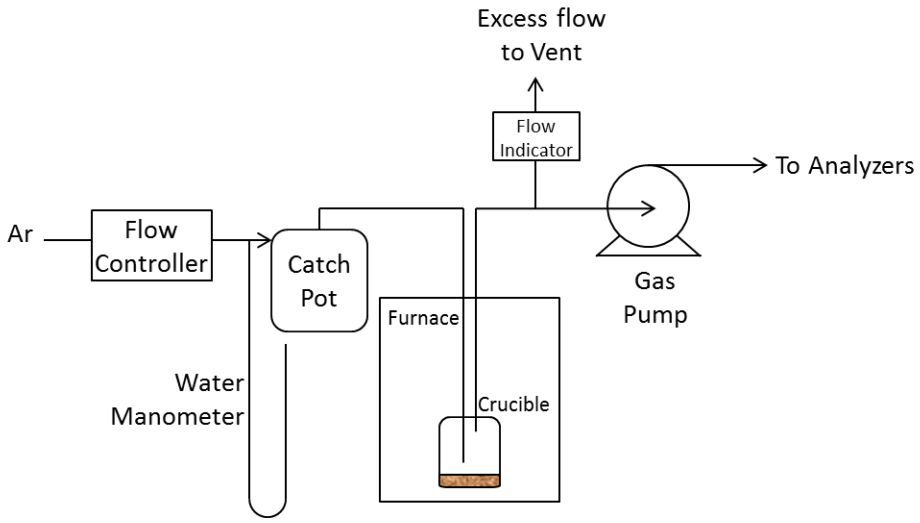

Figure 2-3. CCOG Gas Flow System

An external thermocouple monitors the oven to verify the temperature of the chamber to the program temperature. An internal thermocouple tracks the temperature of the sludge as it dries. A combination of visual observation of the sludge and monitoring of the internal thermocouple is used to determine when the sample is considered dry relative to the other CC methods' definition. The sludge visibly contracts and begins to change color as it dries. At this point, with the sludge sufficiently dry, the oven is set to ramp to 550°C at 10°C/min and from there to 1150°C at 15°C/min. The difference between the external temperature of the oven and the internal temperature of the material in the crucible can be tracked by the two thermocouples.

Once the oven reaches 1150°C, the sample is held for one hour with flowing argon. Then the oven is turned off and the sample is allowed to cool. The argon is allowed to continue flowing until the sample registers a temperature of about 600°C. The off-gas analysis train samples and monitors the progress of the reaction as a function of time from before the start of drying to just after the one hour hold. The sweeping action of the purging argon gas has a similar effect on the REDOX behavior of the system as to that of the sparging argon in the CC_{Ar} method. However, since the argon in the CCOG method is only sweeping and not sparging, the effect on REDOX is not quite as dramatic. The REDOX values are increased less than in the CC_{Ar} method.

In this method, the resulting glass sample is very thin which makes sampling for the REDOX measurement difficult. In addition, the purge rate of the Ar appears to impact the REDOX of the glass, and this effect is not well understood. In addition, sweeping of Ar across the slurry during the feed-to-glass transition does not allow the gases released in Stage 1 and 2 of the cold cap reactions to interact, i.e., equilibrium may or may not be achieved at sufficiently high purge rates.

2.5 Melt Rate Furnace (MRF)

In the MRF method, a region of partially melted slurry is formed above the glass that resembles the cold cap of larger melters such as the Cold Cap Evaluation Furnace (CEF) and DWPF melters. This procedure most closely matches that of CC_{hot} in both operation and REDOX results, except that the vessel used for the MRF is not sealed from the atmosphere. The MRF vessel is a stainless steel beaker.[41]

The MRF beakers are larger than the CC crucibles or CCOG crucible, so more material is used. Also, all of the material is not melted in the MRF, so more material has to be used so that enough is converted to glass for analysis. Each voxel of material remaining in the MRF beaker was categorized into one of four zones in the order from the most to least dense:

Melt:	Fully melted glass with little or no gas bubbles.
Froth:	Melted material interspersed among gas bubbles.
Un-melted:	Feed material which may have begun to soften but is still fundamentally in its original, loose granular form.
Below:	Material of very low but non-zero density arising from voids of gas.[42]

For the MRF, approximately 125 mL of sludge is measured out and placed in a 40°C oven to dry. Once the same or slightly drier moisture level as for the other CC methods is achieved, the material is transferred to the stainless steel beaker. If the material is too wet when processed with the MRF method, too much of the material will be forced above the void space and reduce the amount of glass that is formed or the cold cap will rupture venting too much of the off-gas before it has time to interact with the glass. This behavior is very similar to what is observed in the CC_{hot} method if the material is too wet.

The beakers are placed in ceramic collars that prevent heat from reaching the sides of the beaker, so that heating only occurs from the bottom. This arrangement approximates the melter cold cap with hot glass underneath a cold cap of unreacted or partially reacted feed (Figure 2-4). As the material under the surface begins to melt and react to produce off-gas species, if the top dry surface is sufficiently intact, then the gases will be trapped against the surface of the molten glass. If the layer on the top is not properly sealing, the off-gas will escape before interacting with the glass and result in different glass REDOX.

Secondly, the dried feed must be free of voids open through the sample so as to create the most intact cold cap surface. As the material under the surface begins to melt and react producing off-gas species, if the top, dry surface is sufficiently intact, then the gases will be trapped against the surface of the molten glass. This is observed when the samples are cooled as void spaces between a molten glass layer on the bottom and a porous dry powder layer on top. If the layer on the top is not properly sealing, the off-gas will escape before interacting with the glass and cause the REDOX behavior of the glass to change.

Once the sufficiently dried feed is lightly packed into the stainless steel beakers and the beakers placed inside of the ceramic collars, the collars are loaded into the preheated MRF furnace. Here, timing is essential. The time frame must be such that a sufficient amount of glass is formed, but not all of the material is converted to glass. To achieve this, the heating profile and time at temperature of the sample is rigorously tracked. As soon as the collar containing the sample is inserted, a timer is started. The first measurement made is to mark the lowest observed temperature of the furnace after the sample was inserted. There is a natural drop in the temperature of the furnace due to the removal of the lid and insertion of a room temperature object. Once the lowest temperature has been recorded, three points in time during the reheating process are recorded: the time it takes for the oven to recover to 1125°C, the time to recover to 1145°C and the time to recover to 1150°C. These three points are observed and compared between samples to verify that each sample is receiving similar heat treatment by the furnace.

After these points are recorded, the sample is allowed to remain in the furnace for either 20 minutes (the standard time) or 25 minutes (an extended time). At the end of the hold time, the sample collar is promptly removed from the furnace and placed on a refractory brick to cool and the lid is replaced on the MRF furnace to allow the furnace to maintain temperature.

The sample beaker is left in the collar to cool naturally. The MRF furnace is allowed to recover for at least 20 minutes between samples to ensure consistent heating environments. Once cooled, the samples are removed from the stainless steel beakers in two steps. First, the cold cap is removed by gently striking the side of the inverted beaker with a hammer. Due to the reduced contact with the glass and beaker from the presence of the void space, the cold cap typically separates seamlessly from the glass. Once the cold cap is removed, the glass is separated from the beaker by striking the bottom of the inverted beaker with a hammer.

One must be careful when sampling glass from the MRF for a number of reasons. To prevent overly reduced or oxidized glass, glass must be selected that was neither in contact with the stainless steel beaker or a pocket of gas in the void space. This can get difficult as the glass does splinter fairly easily coming out of the beaker, but it is not impossible. Also, one must wear gloves when handling the glass from the MRF beaker due to the splintered nature of the glass. This glass has a much higher tendency to form sharp shards than glass from the CC methods that typically come out of their containers as pucks that must be cut or smashed to sample. Samples for REDOX measurement were taken from the melt zone rather than the other three zones noted above. Samples from other regions were taken for comparative purposes and shown to give different REDOX values. So care has to be exercised as to where a sample is taken in the MRF in order to get reproducible results.

The typical observed effect of the MRF method are similar to that of the CC_{hot} method. Even with the sample open to the air the entire time it is heated, due to the presence of a self-forming cold cap, the sample is protected from the atmosphere and is able to undergo the necessary reactions between the molten glass and off-gas species to produce accurate REDOX values.

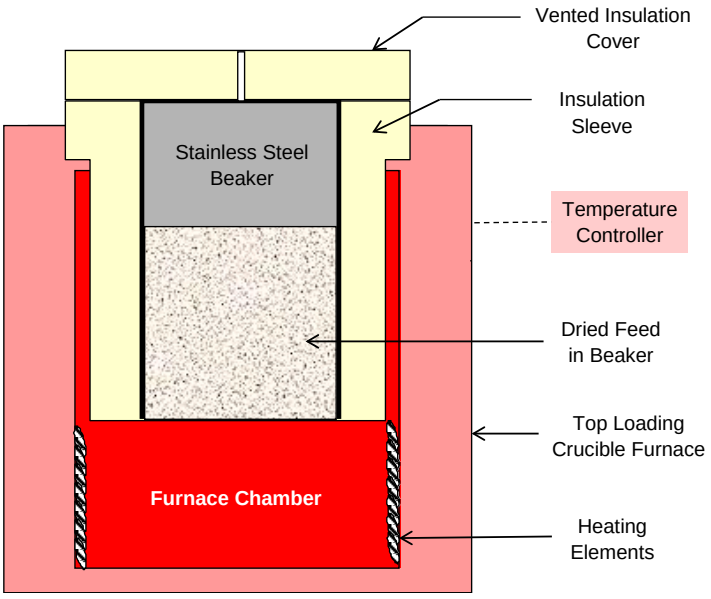

Figure 2-4. Cross-sectional view of Melt Rate Furnace (MRF).

2.6 Quality Assurance

Requirements for performing reviews of technical reports and the extent of review are established in manual E7 2.60. SRNL documents the extent and type of review using the SRNL Technical Report Design Checklist contained in WSRC-IM-2002-00011, Rev. 2. The historic REDOX database is given in Appendix A and the glycol REDOX database is given in Appendix B.

3.0 Results and Discussion

3.1 Variability of REDOX Replicate Measurements

For CC_{hot}, CC_{ramp}, and CC_{Ar}, triplicate REDOX experiments are preferred. If the agreement between these replicates is poor then the glasses are usually not homogeneous. This was observed in SB4 REDOX experiments when glasses were found to be inhomogeneous on a microscopic scale due to the use of Frit 418 (Figure **3-1**). Frit 418 was coupled with a high Al_2O_3 waste and the calculated viscosity was over 300 poise: much too stiff a glass to melt homogeneously in a static crucible environment.

Examples of poor REDOX reproducibility in terms of both the Fe^{+2} measurement and total Fe measurement are shown in Figure **3-2**. The variability in the Fe^{+2} and total Fe measurements for CC_{ramp} are shown in Figure **3-2**a and for CC_{hot} in Figure **3-2**b. Note that the variability in each measured parameter is usually wider for CC_{ramp} than for CC_{hot} using the same sludge and frit. This can be interpreted as CC_{ramp} samples being more inhomogeneous than CC_{hot}. In addition, the CC_{ramp} REDOX ratios are biased higher in most cases to the CC_{hot} for the same sludge and frit combinations (Figure **3-3**).

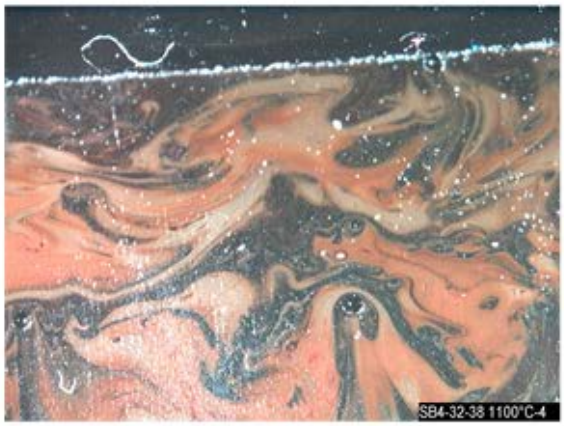

SB4-32 at 35 wt% Waste Loading – Frit 418

SB4-49 at 35% Waste Loading – Frit 418

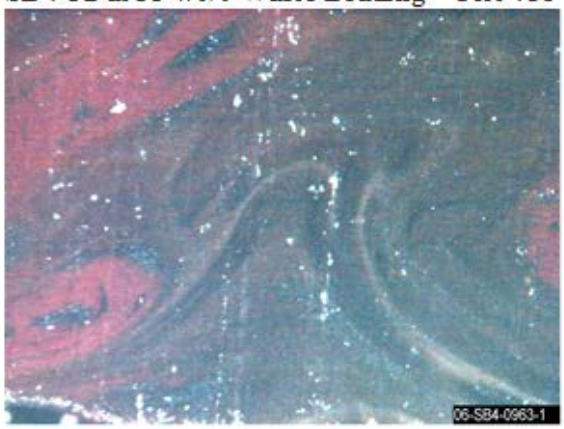

SB4-51 at 35% Waste Loading – Frit 425

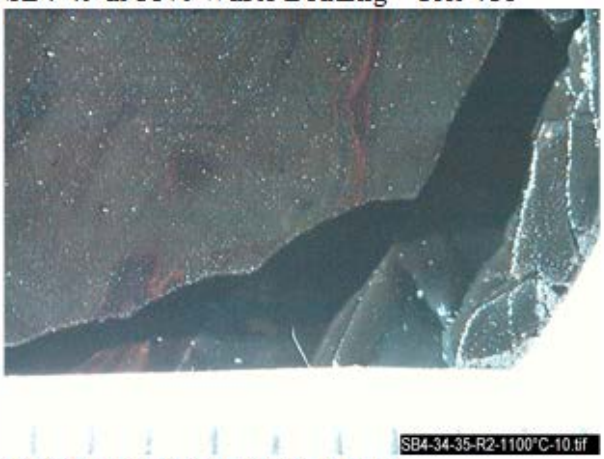

SB4-34 at 35% Waste Loading – Formic Acid Only

Figure 3-1. Non-homogeneous Glasses from FN flowsheet (SB4) made with Frit 418 that gave poor REDOX replicate reproducibility.[29]

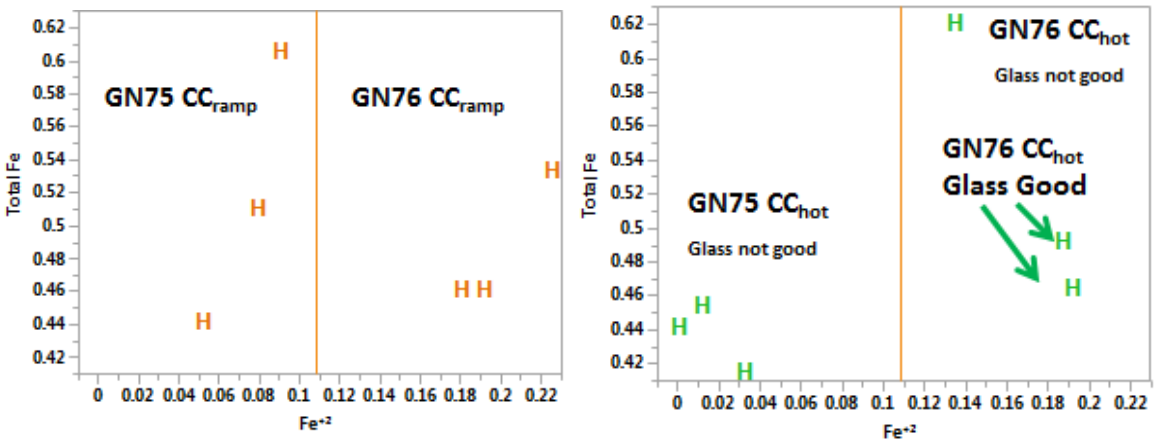

(a) CC_{ramp} Experiments (b) CC_{hot} Experiments

Figure 3-2. Variation in Measurement of Fe^{+2} and Total Fe for Inhomogeneous CC_{ramp} and both Inhomogeneous and Homogeneous CC_{hot} Experiments.

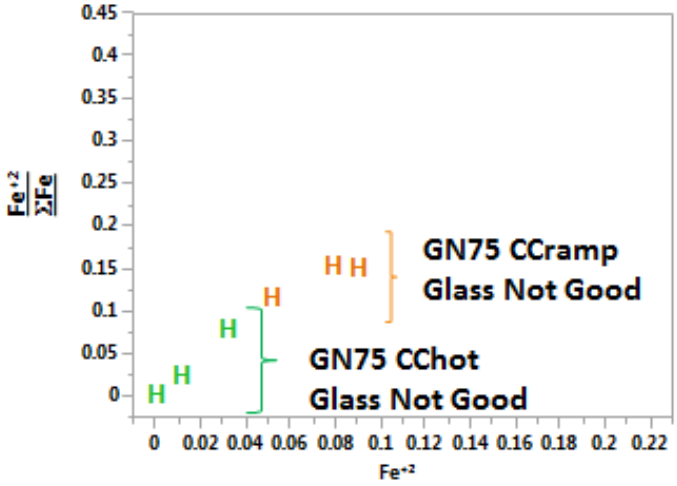

Figure 3-3. CC_{ramp} REDOX Ratios are generally higher than CC_{hot} REDOX Ratios.

3.2 Homogeneity of Closed Crucible Ramped Heat Treatment (CC_{ramp})

Typically, a glass that was subjected to CC_{ramp} was inhomogeneous on the surface having crystallized various phases including $NiFe_2O_4$ spinel which then alters the remaining iron in the glass (Figure **3-4**). This is due to the fact that the glass spends considerable time in-between 400-900°C where the maximum amount of crystallization is known to occur.[43,44]

Both the crystallization and inhomogeneity shown in Figure **3-4** contribute to the poor reproducibility of the Fe^{+2} measurement and total Fe measurement as shown in Figure **3-2**. Crystallization and inhomogeneity also impact that poor reproducibility of the REDOX ratio ($Fe^{2+}/\Sigma Fe$) and the bias in the ratio, i.e. CC_{ramp} $Fe^{2+}/\Sigma Fe$ is biased higher than CC_{hot} as was shown in Figure **3-3** and will be shown below when compared to the DWPF historic REDOX model.

(a) GN75 CC_{ramp} top surface

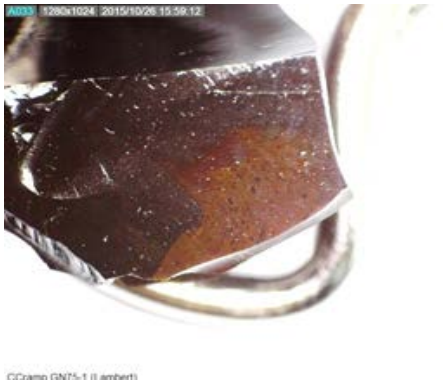

(b) GN75 CC_{ramp} cross section

(c) GN76 CC_{ramp} top surface

(d) GN76 CC_{ramp} cross section

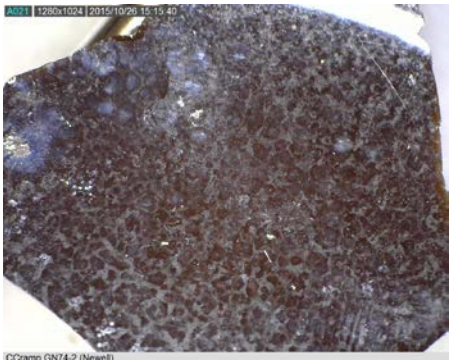

(e) GN74 CC_{ramp} top surface

(f) GN74 CC_{ramp} cross section

Figure 3-4. Crystallization of REDOX Samples GN74, GN75, and GN76 on the surface (a,c,e) and inhomogneities in the interior as shown in the cross section photographs (b,d,f).

3.3 Homogeneity of Closed Crucible Hot Insertion (CC_{hot})

In general, the CC_{hot} samples were more homogeneous internally and had little to no crystallization on the surfaces due to the rapidity of the feed-to-glass conversion during the hot furnace insertion. However, due to the use of the more refractory Frit 418, there were still some CC_{hot} samples that were inhomogeneous in cross section (Figure **3-5**). Some of the replicates of the same glass (Figure **3-5**a and b) were inhomogeneous while others were homogeneous demonstrating that Frit 418 viscosity is close to making an acceptable glass but not quite fluid enough. This was noted in SB4 when Frit 418 was coupled with a high Al_2O_3 waste [29] as shown in Figure **3-1** for the formic acid flowsheet. Holding the sample at 1150°C for 4 hours ((Figure **3-5**f) did not make the glass any more homogeneous than the required 1 hour residence time at 1150°C.

3.4 Homogeneity of Closed Crucible with Off-gas Analysis (CCOG)

In general, the CCOG samples were more inhomogeneous internally than the CC_{hot} but had little to no crystallization on the surfaces. Again the use of the more refractory Frit 418 was partially responsible for the inhomogeneities in cross section (Figure **3-6**). More problematic is the fact that even with the formic acid flowsheet (SB8) campaigns, the CCOG glasses appear poorly reacted (red coloration) compared to SB8 CC_{ramp} and CC_{Ar} samples (compare Figure **3-7**a to b and Figure **3-7**c to d) that were black and shiny. This indicates that the feed to glass reactions may not always be going to completion.

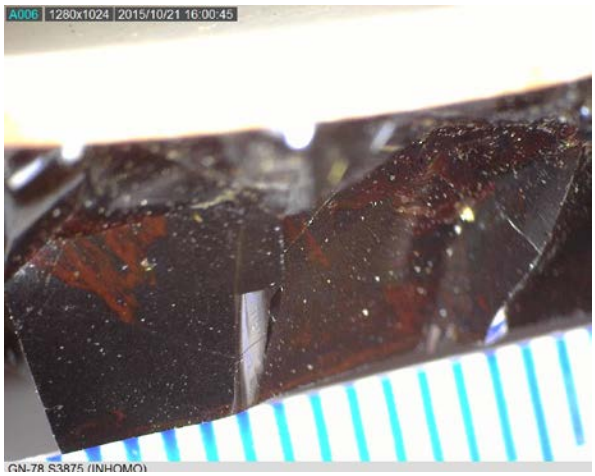

(a) GN78 CC_{hot} cross section (inhomogeneous)

(b) GN78 CC_{hot} cross section (homogeneous)

(c) GN77 CC_{hot} cross section (inhomogeneous)

(d) GN71 CC_{hot} cross section (inhomogeneous with metallic inclusions)

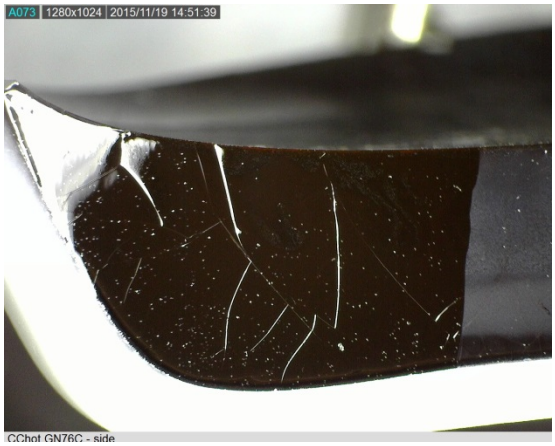

(e) GN76 CC_{hot} cross section (homogeneous)

(f) GN78 CC_{hot} cross section – 4 hour residence time (inhomogeneous)

Figure 3-5. Cross Sections of CC_{hot} Samples GN78, GN77, GN76 and GN71 (1 hour residence time at temperature (a-e) and GN78 (4 hour residence time, figure f).

(a) GN79 in CCOG cross section (inhomogeneous)

(b) GN71 in CCOG cross section (inhomogeneous)

(c) CEF-2 CCOG cross section (inhomogeneous)

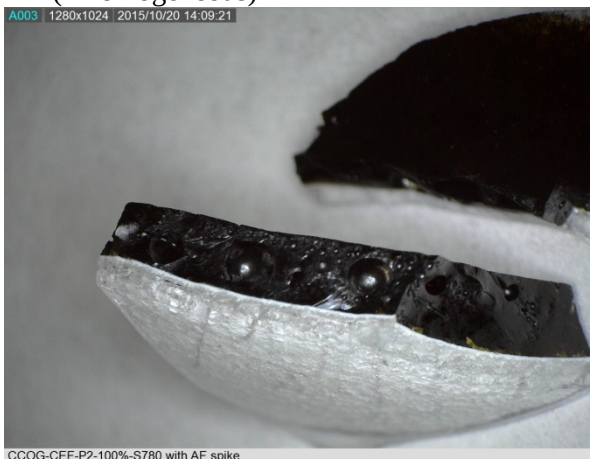

CEF-2 CCOG cross section (homogeneous)

Figure 3-6. Cross Sections of CCOG Samples GN79, GN71 and CEF-2.

Different replicates of the same sample (CEF-2) can be homogeneous or inhomogeneous depending on run conditions (Ar purge and depth of sample in the crucible).

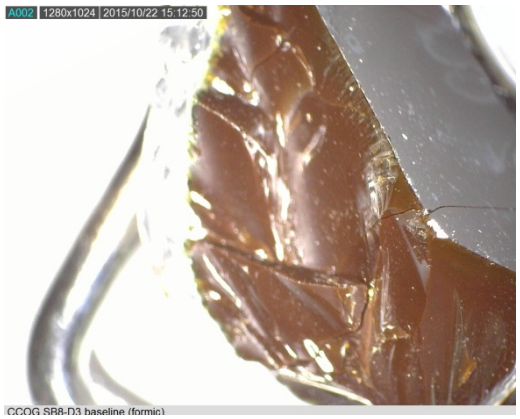

(a) CCOG SB8-D3 Baseline cross section.

(b) CC_{Ar} SB8-D3 Baseline cross section.

(c) CCOG SB8-D3 with Antifoam spike cross section.

(d) CCOG SB8-D3 with Antifoam spike cross section.

Figure 3-7. Cross Sections of CCOG Samples SB8-D3 with and without antifoam spikes. Glasses are a distinct reddish color compared to SB8-D3 tested with CC_{ramp}.

3.5 Homogeneity of Closed Crucible with Ar bubbling (CC_{Ar})

The CC_{Ar} samples were the most homogeneous of all the samples due to the Ar bubbler agitating the sample continuously during the feed-to-glass transformation (Figure **3-8**). Samples did have a tendency to precipitate metal nodules due to the reducing nature of the feeds (GN71) and the sparging of the oxygen in the glass by the Ar bubbling. These tests were performed with leaving the Ar bubbler on to purge during the cool down which is not representative of DWPF operations. When it was realized that leaving the Ar bubbling on during cooling gave a REDOX ratio where the offset was greater than the 0.1 experienced in DWPF processing, the Ar sparging was turned off during cooling.

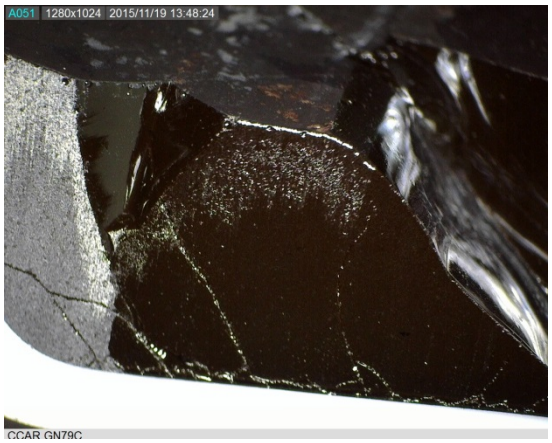

(a) CC_{Ar} on GN79 cross section (homogeneous)

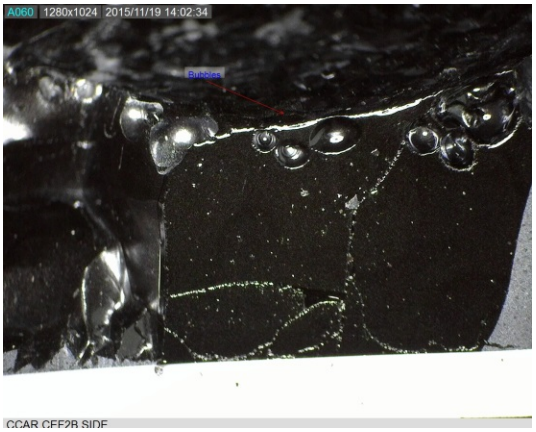

(b) CC_{Ar} on CEF-2 cross section (homogeneous)

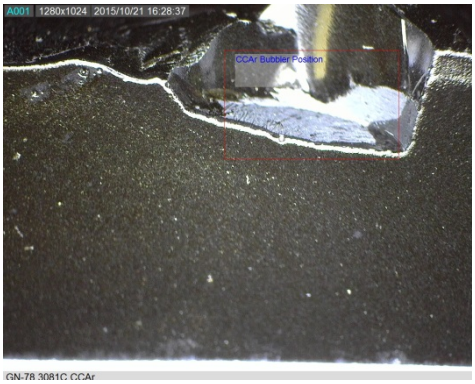

(c) CC_{Ar} on GN78 cross section (homogeneous except in region of Ar bubbler, i.e. dip in surface, where metal was made).

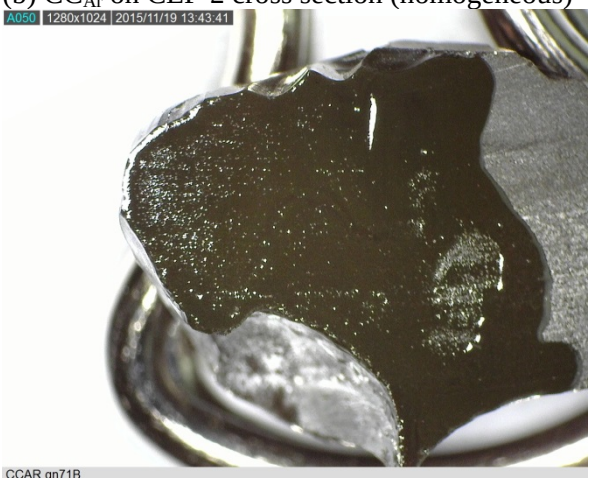

(d) CCAr on GN71 cross section (homogeneous except for a large metal nodule).

Figure 3-8. Cross Sections of CC_{Ar} Samples in cross section. Most are homogeneous except where metallic nodules and precipitates were formed due to either the reducing nature of the feeds (GN71) or the Ar bubbling.

3.6 Homogeneity of Melt Rate Furnace (MRF)

The samples taken from the MRF melt zone appear to be homogeneous. To date not many samples have been run and examined by optical homogeneity but the CEF-2 samples run in the MRF are shown in Figure **3-9**.

(a) MRF CEF-2 (homogeneous-slight red coloration but no swirls)

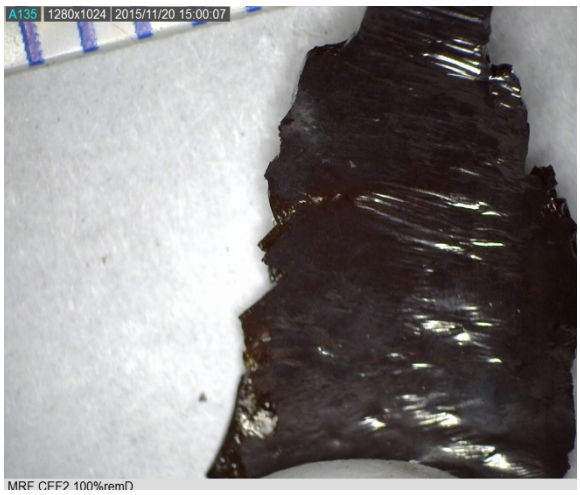

(b) MRF CEF-2 100% remediated (homogeneous).

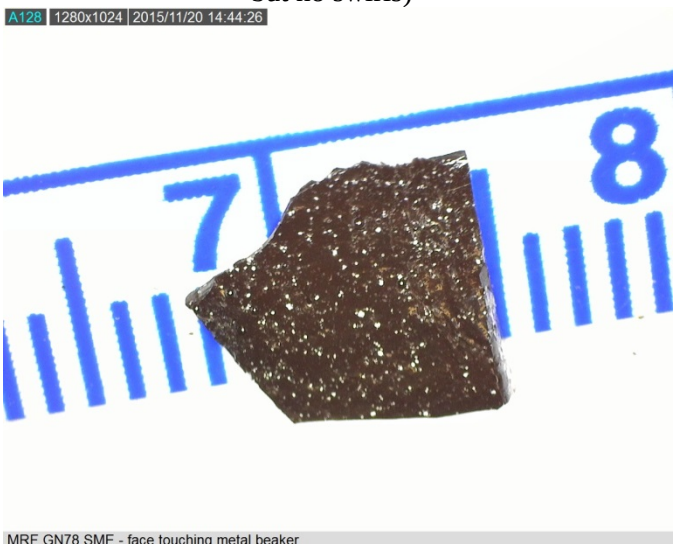

(c) MRF GN78 cross section (homogeneous-slight red coloration but no swirls)

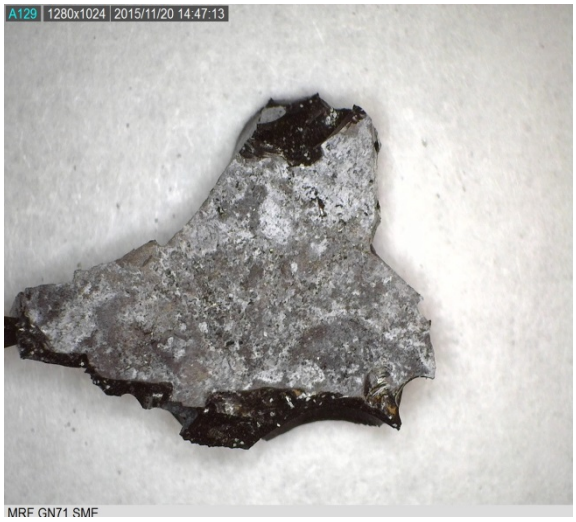

(d) MRF GN71 (inhomogeneous with metallic deposits).

Figure 3-9. Cross Sections of MRF Samples in cross section.

Samples are homogeneous except where metallic nodules and precipitates were formed due to either the reducing nature of the feeds (GN71).

3.7 Selection of Terms for the GN Interim DWPF REDOX Model

All the REDOX data sets measured by the various REDOX methods described above, were evaluated by comparing the data using the following values for the different component terms. For the manganese term, various comparisons were made at Mn = 5, 2, and 0 as given below:

- EE_{glycol} = 6 (Equation 19)
- $EE_{formate}$ = 2, EE_{oxalte} = 4, EE_{coal} = 4, $EE_{nitrate}$ = 5
- EE_{Mn} = 5 (2007 model Equation 16/Equation 17 with 2012 antifoam factor no Ar term)
- EE_{Mn} = 2 (2003 REDOX model Equation 10/Equation 11) with the 2012 antifoam term)
- EE_{Mn} = 0 (modification of the 2003 with the 2012 antifoam term)

The different permutations of the Mn term were examined because the H&S [36] and HTXRD [34] experiments had shown the presence of a Mn^{+2} species in the nitric-glycolic flowsheet samples dried at 40°C (Table 1) and in the "lard" deposits found in the CEF feeds [36,45]. So if the incoming manganese species from the SME is +2 then there is no need for a manganese term in the nitric-glycolic flowsheet acid interim REDOX model.

Likewise, the dried feed species shown in Table 1 and the phases observed in the H&S experiments in Table 2 showed that the only measureable Fe^{+2} species present was an iron formate. Since there is so little formate in the nitric-glycolic acid feeds, there is no need for an Fe^{+2} species in the interim REDOX model. However, this may be something to further investigate for the final glycolic/nitric REDOX model to determine if omitting an Fe^{+2} term is providing bias in the model. The presence of iron formate in the feed may also be the source of the magnetite observed in the HTXRD samples (Table 3).

Table 1. Identified Phases for the Nitric-glycolic Flowsheet Samples (Dried at 40^0 C).[36]

Sample Identification	**Nitratine**	**Quartz**	**Gibbsite**	**Hematite**	**Goethite**	**Diaqua-bis(glycolato)-Manganese(ii) ***	**Iron Formate**	**Calcium Glycolate Trihydrate***	**Other Unidentified Compound(s)**
	$NaNO_3$	**SiO_2**	**$Al(OH)_3$**	**Fe_2O_3**	**$Fe^{+3}O(OH)$**	**$C_4H_{10}MnO_8$**	**$C_2H_2FeO_4 \cdot 2H_2O$**	**$C_4H_6CaO_6 \cdot 3H_2O$**	
GN76 SME	X	X	X	X	X	X			
GN78 SME	X	X	X	X	X	X	X		
GN79 SME	X		X	X		X			
CEF-2 SRAT	X		X			X		X	X
CEF-2 Composite SME	X	X	X			X			X

* Where the divalent glycolate compounds are the closest match in the organic International Centre for Diffraction Data (ICDD)

Table 2. Identified Phases for the Nitric-glycolic Flowsheet Samples (Heat and Stop Runs).[36]

SME Sample Identification	Nitratine	Quartz	Gibbsite	Bohmite	Hematite	Goethite	Sodium Nitrite*	Trevorite	Corundum	Cristobalite
	$NaNO_3$	SiO_2	$Al(OH)_3$	AlO(OH)	Fe_2O_3	$Fe^{+3}O(OH)$	$NaNO_2$	$NiFe_2O_4$	Al_2O_3	SiO_2
GN78-300	X	X	X	X	X	X	X			
GN78-500	X	X			X					
GN78-775								X	X	
GN79-300	X		X	X	X					
GN79-500		X			X					
GN78-775								X		X

* Where the sodium nitrite identification is uncertain.

Table 3. HTXRD Identified Phases for Nitric-glycolic Flowsheet Runs.[34]

		Temperature (ºC) in Ar	
Compound	**Formula**	**GN-78 SME**	**GN-79 SME**
Nitratine	$NaNO_3$	25-250	25-250
Gibbsite	$Al(OH)_3$	25-200	25-200
Hematite	Fe_2O_3	200-350	200-350, 600
Quartz	SiO_2	350-450	600
Magnetite	$Fe^{+2}Fe^{+3}O_4$	400-600	400-600
Platinum	Pt	400-1100 (Sample cup insert)	550, 650-1100 (Sample cup insert)

3.8 Selection of GN Data for Interim DWPF REDOX Model

In order to determine which of the five REDOX methods described in Section 2.0 provided $Fe^{2+}/\Sigma Fe$ ratios that were useful for modeling, the $Fe^{2+}/\Sigma Fe$ ratios measured by each method were compared to the historic REDOX model developed on CC_{hot} samples that were shown repeatedly [18,24,25,29,30] to compare to the REDOX measured from DWPF pour spout samples. During this comparison only data from glasses that (1) had been shown to be homogeneous by microscope examination or (2) were unavailable for microscopic examination were used. That means that there is still some variability in the $Fe^{2+}/\Sigma Fe$ datasets due to the glass samples that could not be located for microscopic examination. That is why the glycol flowsheet REDOX model is being considered as an *Interim Model* until more data can be generated with the methods shown to give the most reproducible results.

3.8.1 Glasses Unacceptable for Modeling (GN Flowsheet)

The glasses that were found to be unacceptable for modeling included all the CC_{ramp} data, all the CCOG data, and all the CC_{Ar} data. The datasets could not be assessed against each other as there was too much scatter in each data set.

3.8.1.1 CC_{ramp} Dataset

The first unacceptable dataset assessed was the CC_{ramp} methodology as there was more of this data available than CC_{hot}, CCOG, CC_{Ar}, or MRF for the nitric-glycolic flowsheet. The CC_{ramp} data was assessed against the 2012 model where Mn=5 for the historic data and Mn=0 for the GN data (Figure **3-10** Column A), against the 2003 model where Mn=2 for the historic data and Mn=0 for the GN data (Figure **3-10** Column B), and against the 2003 model where Mn=0 for the historic data and Mn=0 for the GN data (Figure **3-10** Column C). This assessment used the 2012 antifoam term in the 2003 model variations as well for consistency.

The CC_{ramp} data was composed of 106 measurements of "good glass" based on microscope evaluation and the regressions had R^2 values ranging from 0.31 to 0.37. The H and M values observed in the graphs in Figure **3-10** (all columns) mean High and Medium confidence in the glycolate analyses. The symbol C means CEF-2 crucible studies, and PS indicates DWPF pour spout samples.

It can readily be seen on the graphs in Figure **3-10** (all columns) that the CC_{ramp} data for the GN flowsheet is biased high in measured $Fe^{2+}/\Sigma Fe$ compared to all the historic models, irrespective of what Mn term is used. The sideways triangles are SB8 CC_{ramp} data for the FN flowsheet overlain on the historic data correlation which also appear biased high but not as high as the data for the GN flowsheet. Most of the bias is attributed to the crystallization of the sample during the ramp up in temperature.

Alteration other terms in the REDOX model could be used to make the CC_{ramp} and historic models overlap. However, altering the REDOX model terms does not fix the poor R^2 values of the CC_{ramp} data which precludes using this data for REDOX model predictions. A comparison of the data plots in column A to column B and C in Figure **3-10** demonstrates that adjusting the Mn term in the historic model from an EE of 5 to an EE of 2 makes the fit of the historic model to the CC_{ramp} even worse while adjusting the EE of 5 to an EE of 2 makes the R^2, slope and intercept about the same.

Column A	Column B	Column C
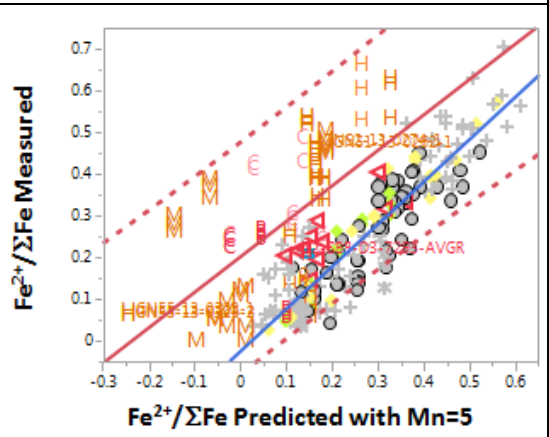	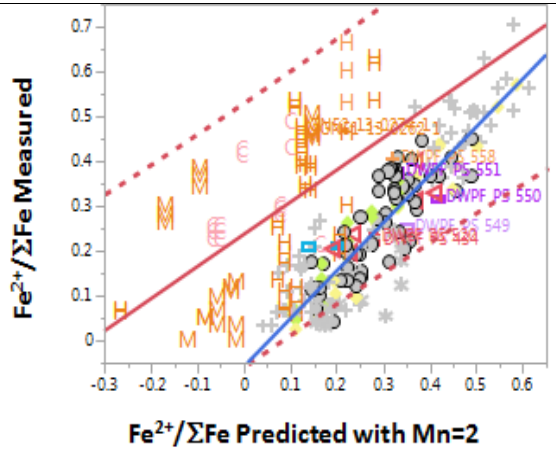	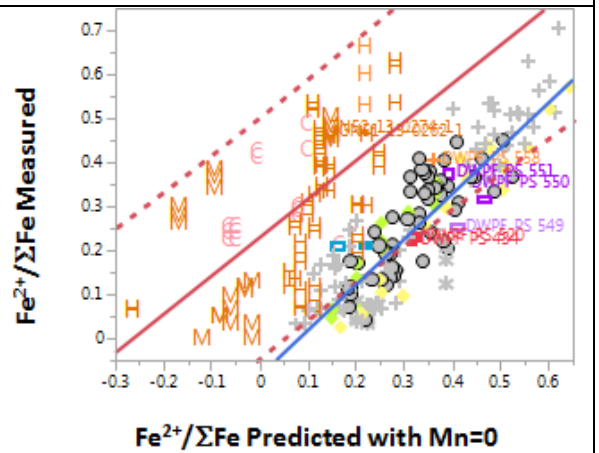
2012 REDOX MODEL Slope = 0.1999 Intercept = 0.2358 Gly EE = 6 N EE = 5 Mn EE = 5 for historic model Mn EE = 0 for GN data	**2003 REDOX MODEL** Slope = 0.1910 Intercept = 0.1942 Gly EE = 6 N EE = 5 Mn EE = 2 for historic model Mn EE = 0 for GN data	**2003 REDOX MODEL** Slope = 0.1910 Intercept = 0.1942 Gly EE = 6 N EE = 5 Mn EE = 0 for historic model Mn EE = 0 for GN data
Fit of CC_{ramp} R^2 = 0.36 106 observations Slope = 0.85 Intercept = 0.20	Fit of CC_{ramp} R^2 = 0.31 106 observations Slope = 0.72 Intercept = 0.24	Fit of CC_{ramp} R^2 = 0.37 106 observations Slope = 0.88 Intercept = 0.23
Fit of $CC_{historic}$ R^2=0.84 178 observations Slope = 1.02 Intercept –0.02	Fit of $CC_{historic}$ R^2=0.82 178 observations Slope = 1.07 Intercept –0.06	Fit of $CC_{historic}$ R^2=0.81 178 observations Slope = 1.03 Intercept –0.08

Figure 3-10. Comparison of CC_{ramp} measured and predicted REDOX using different versions of the historic REDOX model and different EE values for Mn as discussed in the text.

Sample ID's with PS are DWPF Pour Spout samples.

3.8.1.2 CCOG Dataset

The second unacceptable dataset assessed was the CCOG for the nitric-glycolic flowsheet. The CCOG data was assessed against the 2012 model where Mn=5 for the historic data and Mn=0 for the GN data (Figure **3-11**). The CCOG data was composed of 17 measurements of "homogeneous glass" based on microscope evaluation and the regressions had an R^2 value of 0.23. When the additional 9 points for the SB8 formic acid runs performed by CCOG were included in the regression the R^2 value was 0.22 for 26 measurements of "homogeneous glass." The intercept and slope for the 17 "homogeneous" glycol analyses for CCOG were 0.37 and 0.46, respectively, while the 26 glycolic flowsheet (17 homogeneous glasses) and formic (9 homogeneous SB8 glasses) tested by CCOG gave an intercept and slope of 0.39 and 0.46. So whether the 9 formic acid tests were included or not did not change the fit of the CCOG data and only the figure for the 17 measured homogeneous nitric-glycolic glasses are given in Figure **3-11**. The PS values observed in Figure **3-11** indicates DWPF pour spout samples.

It can readily be seen on the graph in Figure **3-11** that the CCOG data for the GN flowsheet is biased high in measured $Fe^{2+}/\Sigma Fe$ compared to all the historic models. This is not surprising as an Ar sweep is used to carry off the off-gas for measurement. However, the bias is not a constant 0.1 offset across all calculated REDOX values as would be expected from the Ar bubbling term in the REDOX model which is based on DWPF pour stream samples.[30]

In addition, Figure **3-11** has some CCOG experiments, i.e. GN78 Purge 1-2881 that fall as low as the historic data correlation. The major gaseous species measured by the CCOG experiments are given in

N_2O and NO are the primary species measured in CCOG [40] and N_2O is a Stage 2 gas predicted in the cold cap model (Equation 3) there are likely issues with whether or not equilibrium has been achieved or achieved in a reproducible manner that contribute to the poor R^2 fit of the data and preclude the CCOG data being used for REDOX modeling.

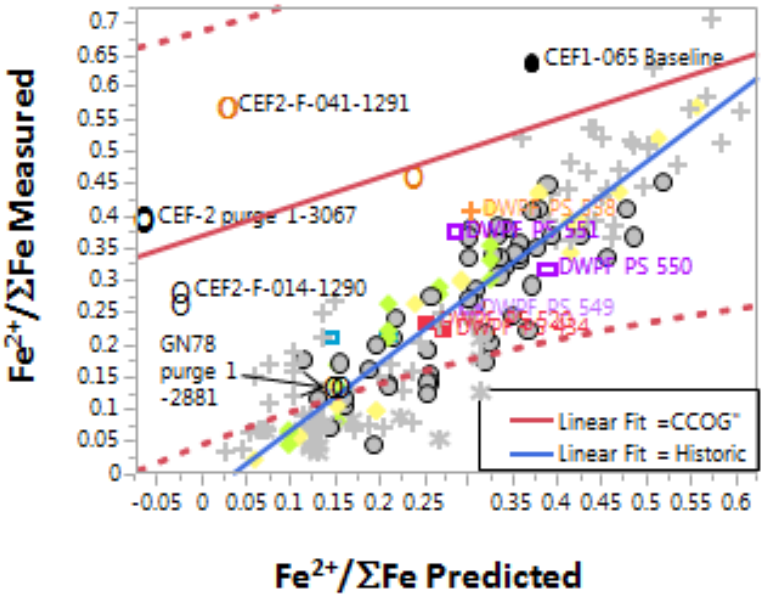

Figure 3-11. Comparison of the CCOG data to the DWPF Historic REDOX Model.

Table 4. CCOG Off-gas Species Observed

Melter Feed	Acid Stoichiometry % (Koopman minimum acid[5])	Acid Ratio (% reducing acid)	Major Off-gas Components Observed, in order of cumulative mmols produced
GN71 SME	125	54.99	CO_2, NO, N_2, H_2, N_2O, O_2, CO, NH_3 and NO_2
GN78 SME	110	52.21	CO_2, NO, N_2, CO, N_2O, O_2, H_2, NO_2, and NH_3
GN79 SME	100	54.54	CO_2, NO, N_2, N_2O, H_2, NO_2, CO, O_2, and NH_3
CEF-2 SME*	100	49.4†	CO_2, NO, N_2, N_2O, H_2, NO_2, O_2, CO, and NH_3,

* Remediated SRAT product; † Acid ratio after remediation.

3.8.1.3 CC_{Ar} Dataset

The third unacceptable dataset assessed was the CC_{Ar} for the nitric-glycolic flowsheet. The CCAr data was assessed against the 2012 model where Mn=5 for the historic data and Mn=0 for the GN data (Figure **3-12**). The CC_{Ar} data was composed of 6 measurements of "homogeneous glass" based on microscope evaluation and the regressions had an R^2 value of 0.48. The intercept and slope for the 6 glycol analyses for CC_{Ar} were 0.35 and 0.49, respectively, not very different from the 0.37 intercept and 0.46 slope of the CCOG measurements. So whether the 9 formic acid tests were included or not did not change the fit of the CCOG data and only the figure for the 17 measured points are given in Figure **3-12**. The PS values observed in Figure **3-12** indicates DWPF pour spout samples and the A's indicate CC_{Ar} samples.

It can readily be seen on the graph in Figure **3-12** that the CC_{Ar} data for the GN flowsheet is biased high in measured $Fe^{2+}/\Sigma Fe$ compared to all the historic models. This is not surprising as the sample is bubbled with Ar. However, the the bias noted in is not a constant 0.1 offset across all calculated REDOX values as would be expected from the Ar bubbling term in the REDOX model which is based on pour stream samples.[30]

While the Figure **3-12** R^2 fit of the CC_{Ar} data is better than that of the CCOG data, it is still low and precludes using the CC_{Ar} data for REDOX modeling.

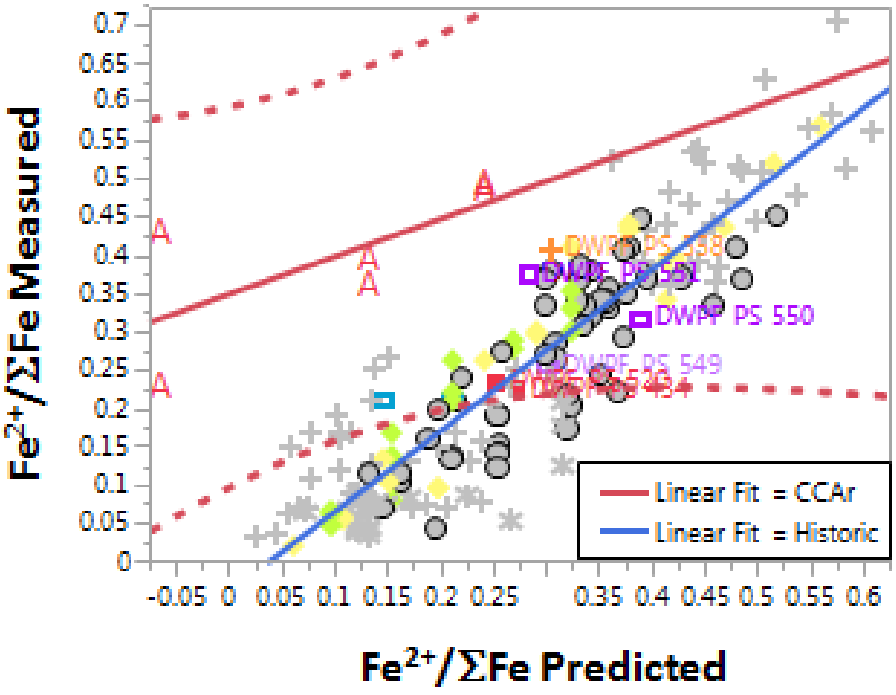

Figure 3-12. Comparison of the CC_{Ar} data (points labelled with the letter A) to the DWPF Historic REDOX Model.

3.8.2 Glasses Acceptable for Modeling (GN Flowsheet)

The glasses that were found to be acceptable for modeling included all the homogeneous CC_{hot} data and all the MRF data. The datasets could not be assessed against each other as there was not much overlap in the glasses analyzed by each method.

3.8.2.1 CC_{hot} Dataset

The first acceptable dataset assessed was the CC_{hot} methodology as there was more of this data available than MRF for the nitric-glycolic flowsheet. The CC_{hot} data was assessed against the 2012 model where Mn=5 for the historic data and Mn=0 for the GN data (Figure **3-13** Column A), against the 2003 model where Mn=2 for the historic data and Mn=0 for the GN data (Figure **3-13** Column B), and against the 2003 model where Mn=0 for the historic data and Mn=0 for the GN data (Figure **3-13** Column C). This assessment used the 2012 antifoam term in the 2003 model variations as well for consistency.

The CC_{hot} data was composed of 27 measurements of "homogeneous glass" based on microscope evaluation and the regressions had R^2 values of 0.37. The H and M values observed in the graphs in Figure **3-13** (all columns) mean High and Medium confidence in the glycolate analyses. The symbol C means CEF-2 crucible studies, and PS indicates DWPF pour spout samples.

For column A, the slope of the CC_{hot} data for the GN and CEF campaigns are parallel and all of the GN and CEF data fall within the 95% confidence bands of the historic data and correlation even though the confidence bands of the 27 data points themselves is broader than that of the historic correlation. The 27 GN and CEF datapoints give a poor R^2 because they are clustered and do not span the range of measured and predicted $Fe^{2+}/\Sigma Fe$ ratios.

It can readily be seen on the graphs in Figure **3-13** (all columns) that some of the CC_{hot} data for the GN flowsheet is biased high in measured $Fe^{2+}/\Sigma Fe$ and some is biased low compared to all the historic models, irrespective of what Mn term is used. All of the "homogeneous glass" CC_{hot} data used Frit 418 and so did most of the "inhomogeneous glasses" and "indeterminate glasses" tested by CC_{hot}. The "indeterminate glasses" were glasses that were not evaluated by microscopy or could not be verified if they had been performed by CC_{hot} or CC_{ramp}.

A comparison of the data plots in column A to column B and C in Figure **3-13** demonstrates that adjusting the Mn term in the historic model from an EE of 5 to an EE of 2 or an EE of 0 makes the overlap of the historic model to the CC_{hot} data even worse, i.e. poorer fit of slope and intercept.

Column A	Column B	Column C
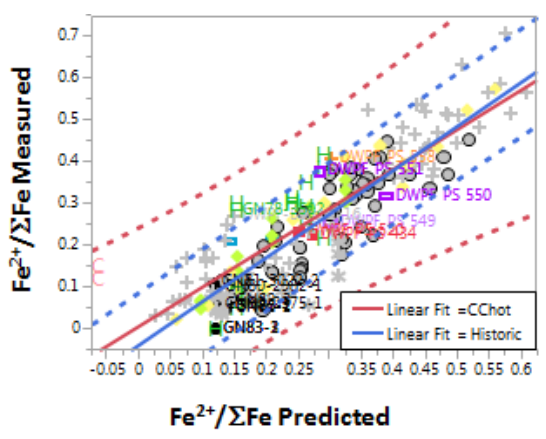	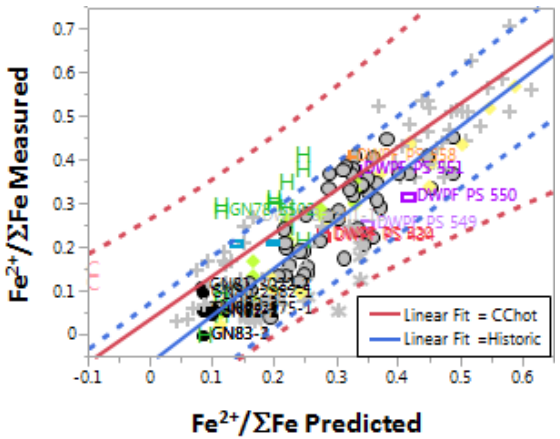	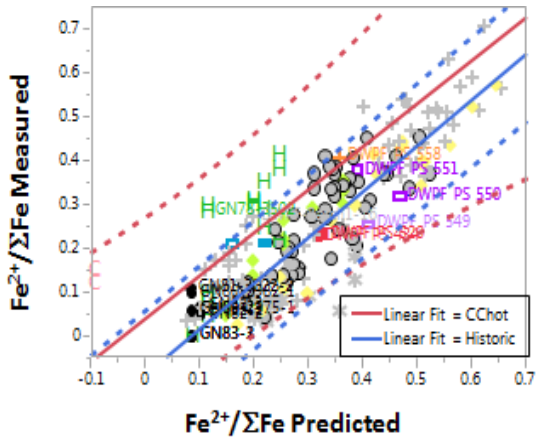
2012 REDOX MODEL Slope = 0.1999 Intercept = 0.2358 Gly EE = 6 N EE = 5 Mn EE = 5 for historic model Mn EE = 0 for GN data	**2003 REDOX MODEL** Slope = 0.1910 Intercept = 0.1942 Gly EE = 6 N EE = 5 Mn EE = 2 for historic model Mn EE = 0 for GN data	**2003 REDOX MODEL** Slope = 0.1910 Intercept = 0.1942 Gly EE = 6 N EE = 5 Mn EE = 0 for historic model Mn EE = 0 for GN data
Fit of CC_{hot} R^2 = 0.37 27 observations Slope = 0.94 Intercept = 0.007	Fit of CC_{hot} R^2 = 0.37 27 observations Slope = 0.98 Intercept = 0.04	Fit of CC_{hot} R^2 = 0.37 27 observations Slope = 0.98 Intercept = 0.04
Fit of $CC_{historic}$ R^2=0.84 178 observations Slope = 1.02 Intercept –0.02	Fit of $CC_{historic}$ R^2=0.82 178 observations Slope = 1.07 Intercept –0.06	Fit of $CC_{historic}$ R^2=0.79 178 observations Slope = 1.04 Intercept –0.09

Figure 3-13. Comparison of CC_{hot} measured and predicted REDOX using different versions of the historic REDOX model and different electron equivalents for Mn as discussed in the text.

Sample ID's with PS are DWPF Pour Spout samples.

3.8.2.2 MRF Dataset

The MRF dataset is composed of seven datasets of which six are replicates of the CEF remediated feed and one experiment with GN78. The one experiment performed with GN71 was inhomogeneous by microscopic examination. The MRF dataset does not have sufficient range in $Fe^{2+}/\Sigma Fe$ to warrant a separate plot.

3.8.2.3 Combined CC_{hot} and MRF Datasets

The MRF dataset for the CEF remediated feeds and the GN78 experiments are very similar. So when the MRF dataset is merged with the CC_{hot} dataset more leverage is given to the REDOX model plot (Figure **3-14**) at the more oxidized range of the CEF remediated feed. Inclusion of the MRF data with the CC_{hot} data gives 34 datapoints and shift the fit of the line slightly from Figure **3-13** Column A. The error bands for the CC_{hot}-MRF data are much wider than the error bands of the historic model in Figure **3-14** and there are no high leverage points in the CC_{hot}-MRF dataset. This causes the R^2 to be particularly poor, i.e. R^2=0.28 for these 34 samples. However, the fact that the CC_{hot}-MRF datasets overlap the historic dataset allows the use of the slope and intercept from the historic model rather than using the slope and intercept that is poorly defined by the 34 points.

However, Figure **3-14** is similar to Figure **3-13** Column A in that the glycolic flowsheet samples, except for the CEF-2 feeds fall within the 95% confidence bands of the 2012 DWPF REDOX model. Some samples like GN-78 are biased high with CC_{hot} but the one GN78 MRF sample is right on the blue line denoting the 2012 REDOX model.

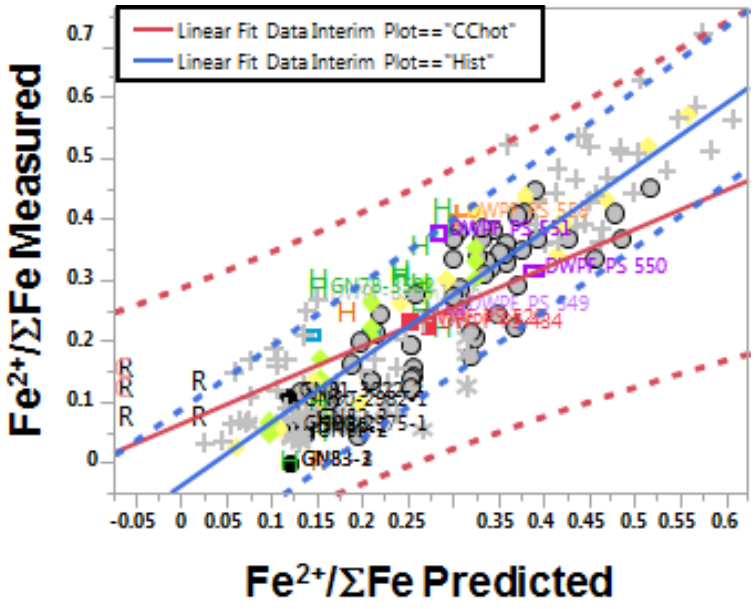

Figure 3-14. Interim REDOX model with CC_{hot} and MRF experimental measurements.

The predicted REDOX for the glycol flowsheet uses the 2012 REDOX model and an EE=6 for glycol and an EE=0 for Mn. The sample ID's with PS are DWPF Pour Spout samples and R are MRF experiments.

4. Conclusions

Based on Figure **3-14** and Figure **3-13** Column A, it is recommended that the DWPF use the 2012 REDOX model slope and intercept (Equation 18) with a glycol EE of 6 and a Mn EE of 0 as shown in Equation 20 as an interim REDOX model for the glycol flowsheet.

Equation 20 $$\xi_{\text{A-gly}} = \left[\left(2[F] + 4[C] + 4[\text{O}_\text{T}] + 3.39 * eff\,[C_A] + 6[Gly] - 5[N] - 0[Mn] \right) \frac{45}{T} \right]$$

While there is some bias in the CC_{hot} samples toward the upper 95% confidence limit of the 2012 model, there is corresponding MRF data for the same feeds that fall within the 2012 model confidence bands. The existing glycolic flowsheet data is too poor to be refit alone until more CC_{hot} and MRF data are generated. Likewise, there is a high bias in both the MRF and the CC_{hot} for the CEF-2 feeds. Since the "predicted REDOX" for the CEF-2 feeds is a negative REDOX, it is recommended that the feed concentrations be double checked. Since the CEF-2 feeds were taken intermittently during the CEF-2 melter campaigns there is not a 1:1 correspondence of the feed chemistry to the feed samples used for the CC_{hot} and MRF experiments.

5. Recommendations, Path Forward or Future Work

Since there are only 27 CC_{hot} and 7 MRF samples to develop the interim correlation it is suggested that more glasses be tested in CC_{hot} and MRF to build a better glass measurement data pool. Of prime importance is that any frit-sludge combination must have a calculated glass viscosity of 60 poise or lower to be fluid enough to make a homogeneous glass in the CC_{hot} method. This may entail adding $LiBO_2$ to the CC_{hot} sample so that there is sufficient convection of the glass in the CC_{hot} crucible. Adding more CC_{hot} and MRF data will allow the 2012 model to be refit with more accuracy.

It is also recommended that the feed concentrations be analyzed for the actual CEF feeds being tested in the CC_{hot} and MRF experiments because the "predicted REDOX" for the CEF-2 feeds is a negative REDOX in Figure **3-13** and Figure **3-14**. This is because the CEF-2 feeds were taken intermittently during the CEF-2 melter campaigns there is not a 1:1 correspondence of the feed chemistry to the feed samples used for the CC_{hot} and MRF experiments.

Another example of why the feed chemistry vs. CC_{hot} or MRF analyses for the CEF-2 feeds are not matched properly in the REDOX database is given in Figure **5-1** by the letter "C" for CEF-2. The CEF-2 feed analyses in the REDOX database are far from the equilibrium balance (1:1) of feed reductants versus oxidants.

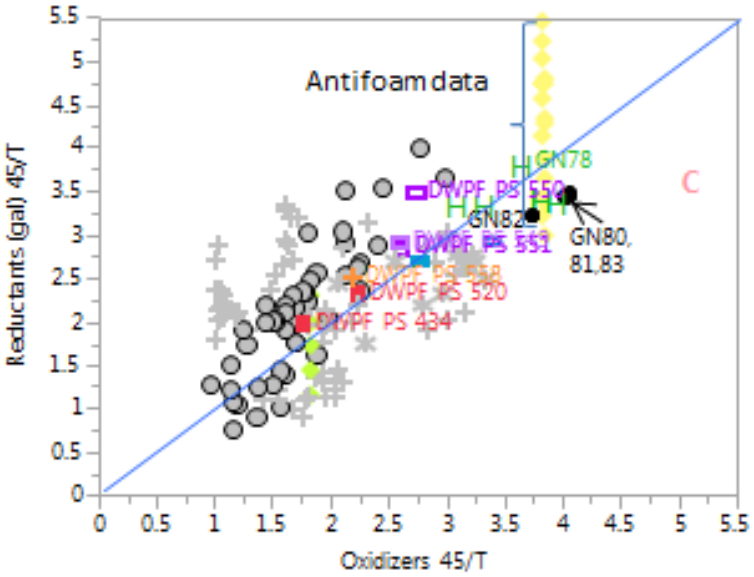

Figure 5-1. Reductants vs. Oxidants showing the balance (equilibrium) achieved with the DWPF pour spout (PS) samples and showing where the glycol flowsheet samples (GN's and H values) are on the 1:1 equilibrium line.

Compare this figure to Figure 1.2 for the simple FN flowsheet. The "C" is the measured CEF-2 feeds for the CC_{hot} and MRF experiments.

6. References

1 H.D. Schreiber, and A.L. Hockman, **"Redox Chemistry in Candidate Glasses for Nuclear Waste Immobilization,"** J. Am. Ceram. Soc., Vol. 70, No. 8, pp. 591-594 (1987).

2 C.M. Jantzen and M.J. Plodinec, **"Composition and Redox Control of Waste Glasses: Recommendation for Process Control Limit,"** U.S. DOE Report DPST-86-773, E.I. duPont deNemours & Co., Savannah River Laboratory, Aiken, SC (November, 1986).

3 C.M. Jantzen, J.B. Pickett, K.G. Brown, T.B. Edwards, D.C. Beam, **"Process/Product Models for the Defense Waste Processing Facility (DWPF): Part I. Predicting Glass Durability from Composition Using a Thermodynamic Hydration Energy Reaction MOdel (THERMO™),"** U.S. DOE Report WSRC-TR-93-0672, Westinghouse Savannah River Co., Aiken, SC, 464p. (Sept. 1995).

4 C.M. Jantzen, K.J. Imrich, K.G. Brown, and J.B. Pickett, "**High Chrome Refractory Characterization and Corrosion: Impact of REDuction/OXidation (REDOX) During Nuclear and Hazardous Waste Vitrification,"** Intl. Jour. Appl. Glass Chem. (in preparation).

5 M.E. Smith and D.C. Iverson, **"Installation of Bubblers in the Savannah River Site Defense Waste Processing Facility Melter,"** U.S. DOE Report SRR-STI-2010-00784 and WM11 Paper # (2010-2011)

6 B.O. Mysen and P. Richet, **"Volatiles II. Noble Gases and Halogens,"** Chapter 16 in **"Silicate Glasses and Melts,"** Vol. 10 in the book series **"Developments in Geochemistry,"** pp.483-502 (2005).

7 G.I. Marziano, A. Paonita, A. Rizzo, B. Scaillet, and F. Gaillard, **"Noble Gas Solubilities in Silicate Melts: New Experimental Results and a Comprehensive Model of the Effects of Liquid Composition, Temperature and Pressure,"** Chemical Geology, 279,145-157 (2010).

8 F.W. Kramer, **"Solubility of Gases in Glass Melts,"** Chapter 13 in "Properties of Glass-Forming Melts," L.D. Pye, A. Montenero, and I. Joseph (Eds.) CRC Press, Boca Raton FL, pp. 405-482 (2005).

9 D.M. Missimer, A.R. Jurgensen and R. Rutherford, "High Temperature X-ray Diffraction Analyses of Simulated DWPF Sludge Batch 2 SRAT Products," SRNL-L4200-2009-00029 (June 2009).

10 D.M. Missimer, A.R. Jurgensen and R. Rutherford, "**High Temperature X-ray Diffraction Analyses of Simulated DWPF Sludge Batch 3 SRAT Products,"** SRNL-L4200-2009-00031 (July 2009).

11 D.M. Missimer, A.R. Jurgensen and R. Rutherford, "High Temperature X-ray Diffraction Analyses of Simulated DWPF Sludge Batch 2 SRAT Products," SRNL-L4200-2009-00033 (July 2009)

12 B.A. Hamm, R.E. Eibling, M.A. Ebra, T. Motyka, and H.D. Martin, **"High-Level Insoluble Waste Preparation for Vitrification,"** Sci. Basis for Nuclear Waste Management, VIII, C.M. Jantzen, M.A. Stone, and R.C. Ewing (Eds.), Materials Research Society, Pittsburgh, PA 793-799 (1985).

13 M.J. Plodinec, **"Foaming During Vitrification of SRP Waste,"** U.S. DOE Report DPST-86-213, E.I. duPont deNemours & Co., Savannah River Laboratory, Aiken, SC (January, 1986).

14 W.G. Ramsey, C.M. Jantzen, and D.F. Bickford, **"Redox Analyses of SRS Melter Feed Slurry; Interactions Between Formate, Nitrate, and Phenol Based Dopants,"** Proceed. of the 5th Intl. Symp. on Ceramics in Nuclear Waste Management, G.G. Wicks, D.F. Bickford, and R. Bunnell (Eds.), American Ceramic Society, Westerville, OH, 259-266 (1991).

15 W.G. Ramsey, T.D. Taylor, K.M. Wiemers, C.M. Jantzen, N.D. Hutson, and D.F. Bickford, **"Effects of Formate and Nitrate Content on Savannah River and Hanford Waste Glass Redox"** Proceed.of the Advances in the Fusion and Processing of Glass, III, New Orleans, LA, D.F. Bickford, et.al. (Eds.) Am. Ceramic Society, Westerville, OH, 535-543 (1993).

16 W.G. Ramsey, N.M. Askew, and R.F. Schumacher, **"Prediction of Copper Precipitation in the DWPF Melter from the Melter Feed Formate and Nitrate Content,"** U.S. DOE Report WSRC-TR-92-385, Westinghouse Savannah River Co., Aiken, SC (Nov.30, 1994).

17 W.G. Ramsey, and R.F. Schumacher, **"Effects of Formate and Nitrate Concentration on Waste Glass Redox at High Copper Concentration."** U.S. DOE Report, WSRC-TR-92-484, Westinghouse Savannah River Co., Aiken, SC (October 23, 1992).

18 K.G. Brown, C.M. Jantzen, and J.B. Pickett, **"The Effects of Formate and Nitrate on REDuction/OXidation (REDOX) Process Control for the Defense Waste Processing Facility,"** U.S. DOE Report WSRC-RP-97-34, Westinghouse Savannah River Co, Aiken, SC (Feb. 1997).

19 T.B. Calloway, C.M. Jantzen, L.M. Medich, and N.R. Spennato, **"Analysis of the DWPF Glass Pouring System Using Neural Networks,"** Waste Management '98 (1998).

20 M.J. Plodinec, **"Foaming During Vitrification of SRP Waste,"** U.S. DOE Report DPST-86-213, E.I. duPont deNemours & Co., Savannah River Laboratory, Aiken, SC (January 10, 1986).

21 M.J. Plodinec, **"Foaming and Dissolution of SRP Waste by Frit,"** U.S. DOE Report DPST-85-419, E.I. duPont deNemours & Co., Savannah River Laboratory, Aiken, SC (April 8, 1985).

22 A.S. Choi, **"Validation of DWPF Melter Off-Gas Combustion Model,"** U.S. DOE Report WSRC-TR-2000-00100, Westinghouse Savannah River Co., Aiken, SC (June 23, 2000).

23 A.S. Choi, **"Prediction of Melter Off-Gas Explosiveness,"** U.S. DOE Report WSRC-TR-90-00346, Westinghouse Savannah River Co., Aiken, SC (January 22, 1992).

24 C.M. Jantzen, J.R. Zamecnik, D.C. Koopman, C.C. Herman, and J.B. Pickett, **"Electron Equivalents Model for Controlling REDuction/OXidation (REDOX) Equilibrium During High Level Waste (HLW) Vitrification,"** U.S. DOE Report WSRC-TR-2003-00126, Rev.0 (May 9, 2003).

25 C.M. Jantzen, D.C. Koopman, C.C. Herman, J.B. Pickett, and J.R. Zamecnik, **"Electron Equivalents REDOX Model for High Level Waste Vitrification,"** Environmental Issues and Waste Management Technologies IX, J.D. Vienna and D.R. Spearing (Eds), Ceramic Transactions 155, 79-91 (2004).

26 D.C. Koopman, C.C. Herman, and N.E. Bibler, **"Sludge Batch 3 Preliminary Acid Requirements Studies with Tank 8 Simulant,"** U.S. DOE Report WSRC-TR-2003-00041, Westinghouse Savannah River Co., Aiken, SC (January 31, 2003).

27 D.C. Koopman, C.C. Herman, J.M. Pareizs, C.J. Bannochie, D.R. Best, N.E.Bibler, and T.L. Fellinger, **"Spontaneous Catalytic Wet Air Oxidation during Pretreatment of High-Level**

Radioactive Waste Sludge," SRNL-STI-2009-00611, International Atomic Energy Agency-International Nuclear Information System (IAEA-INIS) Volume 41[3] Ref.# 41010463 (2009).

28 B.M. Rapko, G.J. Lumetta, **"Status Report on Phase Identification in Hanford Tank Sludges,**" U.S. DOE Report PNNL-13394, Pacific Northwest National Laboratory, Richland, WA (December 2000).

29 C.M. Jantzen and M.E. Stone, **"Role of Manganese Reduction/Oxidation (REDOX) on Foaming and Melt Rate in High Level Waste (HLW) Melters,"** US DOE Report WSRC-STI-2006-00066 (2007).

30 C.M. Jantzen and F.C. Johnson, **"Impacts of Antifoam Additions and Argon Bubbling on Defense Waste Processing Facility (DWPF) REDuction/OXidation (REDOX),"** SRNL-STI-2011-00652 (April 2012).

31 D.P. Lambert, J.R. Zamecnik, J.D. Newell, and M.S. Williams, **"Antifoam Degradation Testing,"** US DOE Report SRNL-STI-2015-00352, Revsision 0 (2015).

32 D.P. Lambert, **"IIT Progress Report and Technical Assistance to Support Antifoam Development,"** Savannah River National Laboratory, Aiken, SC (2016).

33 T.L. White, D.P. Lambert, J.R. Zamecnik, and W.T. Riley, **"Ion Cchromatography (IC) Analyses of Glycolate in Simulated Waste,"** SRNL-STI-2015-0049, Rev. 0 (2015).

34 D.M. Missimer and R. Rutherford, **"High Temperature X-ray Diffraction (HTXRD) Analyses on the Glycol Flowsheet,"** SRNL-L4110-2015-00007 (2016).

35 D.M. Missimer, A.R. Jurgensen and R. Rutherford, "**X-ray Diffraction Analyses of Heat Treated Simulated DWPF Sludge Batch 3 and 4 SME Products,"** SRNL-L4200-2009-00032 (July 2009).

36 D.M. Missimer and R. Rutherford, **"X-ray Diffraction (XRD) Analyses on the Formic/Nitric, Glycolic/Nitric (GN) and Glycolic/Formic (GF) Flowsheet Samples,"** SRNL-L4110-2016-00003 (February 2016).

37 C. M. Jantzen, **"Heat Treatment of Waste Slurries for REDOX ($Fe^{2+}/\Sigma Fe$) And Chemical Composition Measurement,"** Procedure Manual L29, Procedure ITS-0052 Rev. 5 (2016).

38 E.W. Baumann, **"Colorimetric Determination of Iron (II) and Iron (III) in Glass,**" Analyst, 117, 913-916 (1992).

39 **"Determining Fe^{2+}/Fe^{3+} and Fe^{2+}/Fe (total) Using UV Vis Spectrometer,**" Manual L29, Procedure ITS-0042 (latest revision).

40 J.W. Amoroso and J.R. Zamecnik, **"Measurement of Off-gas Species from Thermal Decomposition of Simulated DWPF Melter Feed,"** SRNL-STI-2014-00286, Rev.0 (2014)

41 **"Preparing Batches and Melting in The Dry-Feed Melt Rate Furnace,**" Manual L29, Procedure ITS-0010 (latest revision).

42 A.S. Choi, D.H. Miller and D.M. Immel, **"Determination of HLW Glass Melt Rate Using X-ray Computed Tomography (CT),"** SRNL-STI-2010-00767, Rev.0 (2011).

43 C.M. Jantzen, D.F. Bickford, D.G. Karraker, and G.G. Wicks, **"Time-Temperature-Transformation Kinetics in SRL Waste Glass,"** Adv. in Ceramics, Vol. 8, American Ceramic Society, Westerville, OH, 30-38 (1984).

44 M.K. Andrews, C.A. Cicero, S.L. Marra, D.C. Beam, and C.M. Jantzen, **"Phase Stability Determinations of DWPF Waste Glasses,"** Nucleation and Crystallization in Liquids and Glasses, M.C. Weinberg (Ed.), Ceramic Transactions, v.30, 371-374 (1993).

45 C.J. Martino, **"Analysis of Precipitated White Solids from Nitric-Glycolic Flowsheet Chemical Processing Cell Products,"** SRNL-L3100-2016-00004 (February 2016).

DISTRIBTUION

Appendix A. **Historic REDOX Database as Used in This Document**

Sample ID	Data Type	Data Subtype	Good Glass?	Any Formate mol/kg	Any Nitrate mol/kg	Any Oxalate mol/kg	Any Coal mol/kg	Any Mn mol/kg	Frit	Target Waste Loading	Total Antifoam (mg/kg)	Alt Total Antifoam Carbon from gal and mg/kg (mol/kg)
SB3-1-25-320A	SB3	Hist	Y	0.32	0.15	0.00	0.00	0.07	320	25	800	0.03
SB3-1-30-320A	SB3	Hist	Y	0.34	0.16	0.00	0.00	0.07	320	30	800	0.03
SB3-5-30-320A	SB3	Hist	Y	0.39	0.19	0.26	0.00	0.06	320	30	800	0.03
SB3-5-35-320A	SB3	Hist	Y	0.41	0.20	0.28	0.00	0.06	320	35	800	0.03
SB3-6-25-320A	SB3	Hist	Y	0.36	0.14	0.13	0.00	0.06	320	25	800	0.03
SB3-6-30-320A	SB3	Hist	Y	0.39	0.15	0.14	0.00	0.07	320	30	800	0.03
SB3-7-25-320A	SB3	Hist	Y	0.30	0.27	0.24	0.00	0.05	320	25	800	0.03
SB3-7-30-320A	SB3	Hist	Y	0.32	0.28	0.25	0.00	0.05	320	30	800	0.03
SB3-7-35-320A	SB3	Hist	Y	0.34	0.30	0.27	0.00	0.05	320	35	800	0.03
SB3-15-30-320A	SB3	Hist	Y	0.57	0.25	0.20	0.01	0.06	320	30	800	0.03
SB3-1-25-202A	SB3	Hist	Y	0.32	0.15	0.00	0.00	0.07	202	25	800	0.03
SB3-1-35-202A	SB3	Hist	Y	0.36	0.17	0.00	0.00	0.07	202	35	800	0.03
SB3-2-25-200A	SB3	Hist	Y	0.31	0.16	0.00	0.08	0.06	200	25	800	0.03
SB3-2-30-200A	SB3	Hist	Y	0.33	0.17	0.00	0.08	0.07	200	30	800	0.03
SB3-2-35-200A	SB3	Hist	Y	0.35	0.18	0.00	0.09	0.07	200	35	800	0.03
SB3-3-25-200A	SB3	Hist	Y	0.40	0.16	0.00	0.08	0.06	200	25	800	0.03
SB3-4-25-202A	SB3	Hist	Y	0.30	0.16	0.00	0.08	0.06	202	25	800	0.03
SB3-6-25-202A	SB3	Hist	Y	0.36	0.14	0.13	0.00	0.06	202	25	800	0.03
SB3-6-30-202A	SB3	Hist	Y	0.39	0.15	0.14	0.00	0.07	202	30	800	0.03
SB3-7-25-202A	SB3	Hist	Y	0.30	0.27	0.24	0.00	0.05	202	25	800	0.03
SB3-7-30-202A	SB3	Hist	Y	0.32	0.28	0.25	0.00	0.05	202	30	800	0.03
SB3-7-35-202A	SB3	Hist	Y	0.34	0.30	0.27	0.00	0.05	202	35	800	0.03
SB3-8-25-202A	SB3	Hist	Y	0.30	0.27	0.23	0.06	0.05	202	25	800	0.03
SB3-8-35-202A	SB3	Hist	Y	0.33	0.30	0.26	0.07	0.05	202	35	800	0.03

Sample ID	Data Type	Data Subtype	Good Glass?	Any Formate mol/kg	Any Nitrate mol/kg	Any Oxalate mol/kg	Any Coal mol/kg	Any Mn mol/kg	Frit	Target Waste Loading	Total Antifoam (mg/kg)	Alt Total Antifoam Carbon from gal and mg/kg (mol/kg)
SB3-9-25-202A	SB3	Hist	Y	0.33	0.22	0.23	0.06	0.05	202	25	800	0.03
SB3-9-30-202A	SB3	Hist	Y	0.35	0.23	0.24	0.06	0.05	202	30	800	0.03
SB3-10-35-202A	SB3	Hist	Y	0.41	0.23	0.21	0.01	0.06	202	35	800	0.03
SB3-11-25-202A	SB3	Hist	Y	0.41	0.19	0.18	0.01	0.05	202	25	800	0.03
SB3-12-25-202A	SB3	Hist	Y	0.42	0.24	0.19	0.06	0.05	202	25	800	0.03
SB3-12-30-202A	SB3	Hist	Y	0.45	0.25	0.20	0.06	0.05	202	30	800	0.03
SB3-13-25-202A	SB3	Hist	Y	0.49	0.25	0.20	0.06	0.05	202	25	800	0.03
SB3-13-30-202A	SB3	Hist	Y	0.52	0.27	0.22	0.06	0.06	202	30	800	0.03
SB3-14-30-202A	SB3	Hist	Y?	0.44	0.24	0.22	0.01	0.06	202	30	800	0.03
SB3-15-25-202A	SB3	Hist	Y	0.54	0.23	0.19	0.01	0.05	202	25	800	0.03
SB3-15-30-202A	SB3	Hist	Y	0.57	0.25	0.20	0.01	0.06	202	30	800	0.03
SB3-16-25-202A	SB3	Hist	Y	0.41	0.25	0.21	0.06	0.05	202	25	800	0.03
SB3-18-25-202A	SB3	Hist	Y	0.41	0.22	0.00	0.08	0.07	202	25	800	0.03
SB3-22-30-320 SME	SB3	Hist	Y	1.17	0.65	0.31	0.08	0.00	320	30	800	0.03
SB3-23-30-320 SME	SB3	Hist	Y	0.77	0.47	0.20	0.09	0.00	320	30	800	0.03
SB3-24-25-202	SB3	Hist	Y	0.25	0.31	0.50	0.06	0.03	202	25	800	0.03
SB3-24-30-202	SB3	Hist	Y	0.26	0.33	0.53	0.07	0.04	202	30	800	0.03
SB3-A1-25-202	SB3	Hist	Y	0.49	0.32	0.37	0.06	0.07	202	25	800	0.03
SB3-A1-30-202	SB3	Hist	Y	0.53	0.34	0.39	0.06	0.07	202	30	800	0.03
SB3-A1-35-202	SB3	Hist	Y	0.55	0.35	0.41	0.06	0.07	202	35	800	0.03
SB3-A2-25-202	SB3	Hist	Y	0.41	0.24	0.20	0.07	0.09	202	25	800	0.03
SB3-A2-30-202	SB3	Hist	Y	0.47	0.27	0.23	0.08	0.10	202	30	800	0.03
SB3-A2-35-202	SB3	Hist	Y	0.49	0.29	0.24	0.08	0.11	202	35	800	0.03
SB3-A3-25-202	SB3	Hist	Y	0.51	0.26	0.24	0.07	0.08	202	25	800	0.03
SB3-A3-30-202	SB3	Hist	Y	0.54	0.28	0.25	0.08	0.08	202	30	800	0.03
SB3-A4-25-202	SB3	Hist	Y	0.43	0.20	0.00	0.10	0.11	202	25	800	0.03
SB3-A4-30-202	SB3	Hist	Y	0.46	0.22	0.01	0.10	0.12	202	30	800	0.03

Sample ID	Data Type	Data Subtype	Good Glass?	Any Formate mol/kg	Any Nitrate mol/kg	Any Oxalate mol/kg	Any Coal mol/kg	Any Mn mol/kg	Frit	Target Waste Loading	Total Antifoam (mg/kg)	Alt Total Antifoam Carbon from gal and mg/kg (mol/kg)
DWPF SME 224 melter	SB3	Hist	Y	1.37	0.54	0.00	0.00	0.05	200		800	0.03
DWPF SRAT 224 SRAT	SB3	Hist	Y	1.42	0.62	0.00	0.00	0.05	200		800	0.03
SB4-20-418 (coppt)	SB4	Hist		1.00	0.45	0.00	0.00	0.10	418	35	800	0.03
SB4RE-32-418-35 (#886-7)	SB4	Hist		0.78	0.31	0.00	0.00	0.13	418	35	800	0.03
SB4RE-32-503-35 (#888-9)	SB4	Hist		0.78	0.31	0.00	0.00	0.13	503	35	800	0.03
SB4RE-32-P2-2-35 (#890-1)	SB4	Hist		0.78	0.31	0.00	0.00	0.13	p2-2	35	800	0.03
SB4RE-34-418-FA Only (#892-3)	SB4	Hist		1.09	0.27	0.00	0.00	0.11	418	35	800	0.03
SB4RE-34-503-FA Only (#894-5)	SB4	Hist		1.09	0.27	0.00	0.00	0.11	503	35	800	0.03
SB4RE-34-P2-2-FA Only (#896-7)	SB4	Hist		1.09	0.27	0.00	0.00	0.11	p2-2	35	800	0.03
SB4-41-418 no addition	SB4	Hist		0.98	0.40	0.00	0.00	0.11	418	35	800	0.03
SB4-41-P2-2 no addition	SB4	Hist		0.98	0.40	0.00	0.00	0.11	P2-2	35	800	0.03
SB4-41-418 full formic (50 gal)	SB4	Hist		0.98	0.40	0.00	0.00	0.11	418	35	800	0.03
SB4-41-418 half formic (25 gal)	SB4	Hist		0.98	0.40	0.00	0.00	0.11	418	35	800	0.03
SB4-49 (#961-962)	SB4	Hist		1.07	0.41	0.00	0.00	0.13	418	35	800	0.03
SB4-51 (#963-964)	SB4	Hist		1.05	0.40	0.00	0.00	0.13	425	35	800	0.03
SB4-49/50 MIX (SB4-0979)	SB4	Hist		1.06	0.40	0.00	0.00	0.13	418	35	800	0.03
SB4-51/52 MIX (SB4-0984)	SB4	Hist		0.93	0.37	0.00	0.00	0.13	425	35	800	0.03
SB4-61(#1145-1146)	SB4	Hist	N	1.35	0.38	0.00	0.00	0.15	503	35	800	0.03
SB4-62 (#1147-48)	SB4	Hist	N	1.42	0.54	0.00	0.00	0.14	503	35	800	0.03
SB4-63 (#1149-1150)	SB4	Hist	N	1.40	0.52	0.00	0.00	0.13	503	35	800	0.03
SB4-64 (#1151-52)	SB4	Hist	N	1.49	0.50	0.00	0.00	0.13	503	35	800	0.03
S9-L-F300	HISTORIC	Hist		1.56	0.24	0.00	0.00	0.09			800	0.03
S9-L-F800	HISTORIC	Hist		1.59	0.23	0.00	0.00	0.09			800	0.03
S9-L-F800	HISTORIC	Hist		1.63	0.23	0.00	0.00	0.09			800	0.03

Sample ID	Data Type	Data Subtype	Good Glass?	Any Formate mol/kg	Any Nitrate mol/kg	Any Oxalate mol/kg	Any Coal mol/kg	Any Mn mol/kg	Frit	Target Waste Loading	Total Antifoam (mg/kg)	Alt Total Antifoam Carbon from gal and mg/kg (mol/kg)
S9-L-N1000	HISTORIC	Hist		1.47	0.51	0.00	0.00	0.09			800	0.03
S9-L-N1000	HISTORIC	Hist		1.38	0.47	0.00	0.00	0.09			800	0.03
S9-L-N50	HISTORIC	Hist		1.39	0.24	0.00	0.00	0.09			800	0.03
S9-L-N50	HISTORIC	Hist		1.22	0.21	0.00	0.00	0.09			800	0.03
S9-L-N500	HISTORIC	Hist		1.52	0.37	0.00	0.00	0.09			800	0.03
S9-L-N500	HISTORIC	Hist		1.39	0.33	0.00	0.00	0.09			800	0.03
S9-L-P1500	HISTORIC	Hist		1.56	0.25	0.00	0.00	0.09			800	0.03
S9-L-P1500	HISTORIC	Hist		1.43	0.23	0.00	0.00	0.09			800	0.03
S9-L-P3000	HISTORIC	Hist		0.91	0.17	0.00	0.00	0.09			800	0.03
S9-L-P3000	HISTORIC	Hist		1.14	0.20	0.00	0.00	0.09			800	0.03
S9-L-P200	HISTORIC	Hist		1.28	0.23	0.00	0.00	0.09			800	0.03
S9-L-P200	HISTORIC	Hist		1.31	0.24	0.00	0.00	0.09			800	0.03
S10-L-F1500	HISTORIC	Hist		1.40	0.10	0.00	0.00	0.11			800	0.03
S10-L-F1500	HISTORIC	Hist		1.31	0.09	0.00	0.00	0.11			800	0.03
S10-L-F300	HISTORIC	Hist		1.11	0.11	0.00	0.00	0.11			800	0.03
S10-L-F300	HISTORIC	Hist		1.07	0.10	0.00	0.00	0.11			800	0.03
S10-L-F800	HISTORIC	Hist		1.13	0.09	0.00	0.00	0.11			800	0.03
S10-L-F800	HISTORIC	Hist		1.14	0.09	0.00	0.00	0.11			800	0.03
S10-L-N100	HISTORIC	Hist		0.99	0.13	0.00	0.00	0.11			800	0.03
S10-L-N100	HISTORIC	Hist		1.01	0.13	0.00	0.00	0.11			800	0.03
S10-L-N1000	HISTORIC	Hist		1.05	0.34	0.00	0.00	0.11			800	0.03
S10-L-N1000	HISTORIC	Hist		0.95	0.33	0.00	0.00	0.11			800	0.03
S10-L-N500	HISTORIC	Hist		1.00	0.24	0.00	0.00	0.11			800	0.03
S10-L-N500	HISTORIC	Hist		1.00	0.24	0.00	0.00	0.11			800	0.03
S10-L-P200	HISTORIC	Hist		1.01	0.11	0.00	0.00	0.11			800	0.03
S10-L-P200	HISTORIC	Hist		1.06	0.11	0.00	0.00	0.11			800	0.03
S10-L-N50	HISTORIC	Hist		0.86	0.09	0.00	0.00	0.11			800	0.03

Sample ID	Data Type	Data Subtype	Good Glass?	Any Formate mol/kg	Any Nitrate mol/kg	Any Oxalate mol/kg	Any Coal mol/kg	Any Mn mol/kg	Frit	Target Waste Loading	Total Antifoam (mg/kg)	Alt Total Antifoam Carbon from gal and mg/kg (mol/kg)
S10-L-P1500	HISTORIC	Hist		1.02	0.10	0.00	0.00	0.11			800	0.03
S10-L-P1500	HISTORIC	Hist		1.04	0.10	0.00	0.00	0.11			800	0.03
S10-L-P3000	HISTORIC	Hist		1.14	0.10	0.00	0.00	0.11			800	0.03
S10-L-P3000	HISTORIC	Hist		0.97	0.10	0.00	0.00	0.11			800	0.03
S10-L-P500	HISTORIC	Hist		0.98	0.10	0.00	0.00	0.11			800	0.03
S10-L-P500	HISTORIC	Hist		1.02	0.10	0.00	0.00	0.11			800	0.03
I-L-P1500	HISTORIC	Hist		1.01	0.55	0.00	0.00	0.08			800	0.03
I-L-P200	HISTORIC	Hist		0.98	0.52	0.00	0.00	0.08			800	0.03
I-L-P3000	HISTORIC	Hist		0.91	0.48	0.00	0.00	0.08			800	0.03
I-L-PF1500	HISTORIC	Hist		1.29	0.50	0.00	0.00	0.08			800	0.03
I-L-PF1500	HISTORIC	Hist		1.34	0.54	0.00	0.00	0.08			800	0.03
I-L-PF5/8	HISTORIC	Hist		1.29	0.55	0.00	0.00	0.08			800	0.03
I-L-PF5/8	HISTORIC	Hist		1.23	0.53	0.00	0.00	0.08			800	0.03
26-1000	HISTORIC	Hist		0.83	0.29	0.00	0.00	0.09			800	0.03
27-250	HISTORIC	Hist		0.41	0.26	0.00	0.00	0.09			800	0.03
27-750	HISTORIC	Hist		0.57	0.22	0.00	0.00	0.09			800	0.03
27-750	HISTORIC	Hist		0.50	0.19	0.00	0.00	0.09			800	0.03
DWPF-Batch1-9	HISTORIC	Hist		1.02	0.30	0.00	0.00	0.09			800	0.03
DWPF-Batch1-9	HISTORIC	Hist		0.94	0.30	0.00	0.00	0.09			800	0.03
DWPF-Batch1-10	HISTORIC	Hist		0.94	0.27	0.00	0.00	0.09			800	0.03
DWPF-Batch1-10	HISTORIC	Hist		0.91	0.32	0.00	0.00	0.09			800	0.03
DWPF-Batch1-12	HISTORIC	Hist		0.53	0.30	0.00	0.00	0.09			800	0.03
DWPF-Batch1-12	HISTORIC	Hist		0.52	0.32	0.00	0.00	0.09			800	0.03
DWPF-Batch1-13	HISTORIC	Hist		0.66	0.29	0.00	0.00	0.09			800	0.03
DWPF-Batch1-13	HISTORIC	Hist		0.68	0.32	0.00	0.00	0.09			800	0.03
DWPF-Batch1-14	HISTORIC	Hist		0.65	0.29	0.00	0.00	0.09			800	0.03
DWPF-Batch1-14	HISTORIC	Hist		0.61	0.29	0.00	0.00	0.09			800	0.03

Sample ID	Data Type	Data Subtype	Good Glass?	Any Formate mol/kg	Any Nitrate mol/kg	Any Oxalate mol/kg	Any Coal mol/kg	Any Mn mol/kg	Frit	Target Waste Loading	Total Antifoam (mg/kg)	Alt Total Antifoam Carbon from gal and mg/kg (mol/kg)
DWPF-Batch1-15	HISTORIC	Hist		0.64	0.29	0.00	0.00	0.09			800	0.03
DWPF-Batch1-15	HISTORIC	Hist		0.63	0.32	0.00	0.00	0.09			800	0.03
DWPF-Batch1-22	HISTORIC	Hist		0.56	0.32	0.00	0.00	0.09			800	0.03
DWPF-Batch1-16	HISTORIC	Hist		0.52	0.22	0.00	0.00	0.09			800	0.03
DWPF-Batch1-16	HISTORIC	Hist		0.46	0.24	0.00	0.00	0.09			800	0.03
DWPF-Batch1-21	HISTORIC	Hist		0.53	0.27	0.00	0.00	0.09			800	0.03
DWPF-Batch1-21	HISTORIC	Hist		0.60	0.33	0.00	0.00	0.09			800	0.03
DWPF-Batch1-22	HISTORIC	Hist		0.51	0.27	0.00	0.00	0.09			800	0.03
AFA-10000A	Antifoam	Hist		1.44	0.59	0.00	0.00	0.14	418	35.9	9040	0.37
AFA-10000B	Antifoam	Hist		1.44	0.59	0.00	0.00	0.14	418	35.9	9040	0.37
AFA-12000A	Antifoam	Hist		1.44	0.59	0.00	0.00	0.14	418	35.9	10920	0.45
AFA-12000B	Antifoam	Hist		1.44	0.59	0.00	0.00	0.14	418	35.9	10920	0.45
AFA-14000A	Antifoam	Hist		1.44	0.59	0.00	0.00	0.14	418	35.9	12600	0.51
AFA-14000B	Antifoam	Hist		1.44	0.59	0.00	0.00	0.14	418	35.9	12600	0.51
AFA-16000A	Antifoam	Hist		1.44	0.59	0.00	0.00	0.14	418	35.9	14500	0.59
AFA-16000B	Antifoam	Hist		1.44	0.59	0.00	0.00	0.14	418	35.9	14500	0.59
AFA-18000A	Antifoam	Hist		1.44	0.59	0.00	0.00	0.14	418	35.9	16310	0.67
AFA-18000B	Antifoam	Hist		1.44	0.59	0.00	0.00	0.14	418	35.9	16310	0.67
AFA-20000A	Antifoam	Hist		1.44	0.59	0.00	0.00	0.14	418	35.9	18240	0.74
AFA-20000B	Antifoam	Hist		1.44	0.59	0.00	0.00	0.14	418	35.9	18240	0.74
AFA-22000A	Antifoam	Hist		1.44	0.59	0.00	0.00	0.14	418	35.9	19930	0.81
AFA-22000B	Antifoam	Hist		1.44	0.59	0.00	0.00	0.14	418	35.9	19930	0.81
AFA-24000A	Antifoam	Hist		1.44	0.59	0.00	0.00	0.14	418	35.9	21820	0.89
AFA-24000B	Antifoam	Hist		1.44	0.59	0.00	0.00	0.14	418	35.9	21820	0.89
AFA-26000A	Antifoam	Hist		1.44	0.59	0.00	0.00	0.14	418	35.9	23550	0.96
AFA-26000B	Antifoam	Hist		1.44	0.59	0.00	0.00	0.14	418	35.9	23550	0.96
AFA-28000A	Antifoam	Hist		1.44	0.59	0.00	0.00	0.14	418	35.9	25410	1.04

Sample ID	Data Type	Data Subtype	Good Glass?	Any Formate mol/kg	Any Nitrate mol/kg	Any Oxalate mol/kg	Any Coal mol/kg	Any Mn mol/kg	Frit	Target Waste Loading	Total Antifoam (mg/kg)	Alt Total Antifoam Carbon from gal and mg/kg (mol/kg)
AFA-28000B	Antifoam	Hist		1.44	0.59	0.00	0.00	0.14	418	35.9	25410	1.04
AFA-30000A	Antifoam	Hist		1.44	0.59	0.00	0.00	0.14	418	35.9	27230	1.11
AFA-30000B	Antifoam	Hist		1.44	0.59	0.00	0.00	0.14	418	35.9	27230	1.11
AFA-32000A	Antifoam	Hist		1.44	0.59	0.00	0.00	0.14	418	35.9	28990	1.18
AFA-32000B	Antifoam	Hist		1.44	0.59	0.00	0.00	0.14	418	35.9	28990	1.18
AFA-13312A	Antifoam	Hist		1.44	0.59	0.00	0.00	0.14	418	35.9	12410	0.51
AFA-21166A	Antifoam	Hist		1.44	0.59	0.00	0.00	0.14	418	35.9	19580	0.80
AFA-25093A	Antifoam	Hist		1.44	0.59	0.00	0.00	0.14	418	35.9	23240	0.95
AFA-25093B	Antifoam	Hist		1.44	0.59	0.00	0.00	0.14	418	35.9	23210	0.95
AFA-25093C	Antifoam	Hist		1.44	0.59	0.00	0.00	0.14	418	35.9	23220	0.95
FCJ-HG-800A	Antifoam-II	Hist		0.84	0.27	0.00	0.00	0.08	418	35	800	0.03
FCJ-HG-800B	Antifoam-II	Hist		0.84	0.27	0.00	0.00	0.08	418	35	800	0.03
FCJ-HG-800C	Antifoam-II	Hist		0.84	0.27	0.00	0.00	0.08	418	35	800	0.03
FCJ-HG-3100A	Antifoam-II	Hist		0.83	0.27	0.00	0.00	0.08	418	35	3100	0.13
FCJ-HG-3100B	Antifoam-II	Hist		0.83	0.27	0.00	0.00	0.08	418	35	3100	0.13
FCJ-HG-3100C	Antifoam-II	Hist		0.83	0.27	0.00	0.00	0.08	418	35	3100	0.13
FCJ-HG-5400A	Antifoam-II	Hist		0.81	0.26	0.00	0.00	0.08	418	35	5400	0.22
FCJ-HG-5400B	Antifoam-II	Hist		0.81	0.26	0.00	0.00	0.08	418	35	5400	0.22
FCJ-HG-5400C	Antifoam-II	Hist		0.81	0.26	0.00	0.00	0.08	418	35	5400	0.22
FCJ-HG-7700A	Antifoam-II	Hist		0.80	0.26	0.00	0.00	0.08	418	35	7700	0.31
FCJ-HG-7700B	Antifoam-II	Hist		0.80	0.26	0.00	0.00	0.08	418	35	7700	0.31
FCJ-HG-10000A	Antifoam-II	Hist		0.79	0.26	0.00	0.00	0.08	418	35	10000	0.41
FCJ-HG-10000B	Antifoam-II	Hist		0.79	0.26	0.00	0.00	0.08	418	35	10000	0.41
FCJ-HG-10000C	Antifoam-II	Hist		0.79	0.26	0.00	0.00	0.08	418	35	10000	0.41

Appendix B. GLYCOL REDOX DATABASE

Table B1. GLYCOL REDOX DATABASE

Sample ID	Data Type	Data Subtype	Good Glass?	Formate mol/kg meas.	Oxalate mol/kg meas.	Coal mol/kg meas.	Nitrate (+nitrite) mol/kg meas.	Glycol Only mol/kg meas.	Any Mn mol/kg meas.	Frit	Target Waste Load	Total Anti-foam (mg/kg)	Anti-foam Carbon from gal and mg/kg (mol/kg)
GN34-11-2314-1	Newell	CChot	NO	0.031	0.019	0.000	0.704	0.496	0.101	418		801	0.033
GN34-11-2315-2	Newell	CChot	NO	0.031	0.019	0.000	0.704	0.496	0.101	418		801	0.033
GN34-11-2316-3	Newell	CChot	NO	0.031	0.019	0.000	0.704	0.496	0.101	418		801	0.033
GN34b-12-1122-1	Newell	CChot	NO	0.008	0.060	0.000	0.699	0.488	0.084	418		801	0.033
GN34b-12-1123-2	Newell	CChot	NO	0.008	0.060	0.000	0.699	0.488	0.084	418		801	0.033
GN34b-12-1124-3	Newell	CChot	NO	0.008	0.060	0.000	0.699	0.488	0.084	418		801	0.033
GN34c-12-1125-1	Newell	CChot	NO	0.005	0.067	0.000	0.686	0.530	0.083	418		801	0.033
GN34c-12-1126-2 (REDOX WAY OFF)	Newell	CChot	NO	0.005	0.067	0.000	0.686	0.530	0.083	418		801	0.033
GN34c-12-1127-3	Newell	CChot	NO	0.005	0.067	0.000	0.686	0.530	0.083	418		801	0.033
GN34b-12-1325-1R	Newell	CChot	NO	0.008	0.060	0.000	0.699	0.488	0.084	418		801	0.033
GN34b-12-1326-2R	Newell	CChot	NO	0.008	0.060	0.000	0.699	0.488	0.084	418		801	0.033
GN34b-12-1327-3R	Newell	CChot	NO	0.008	0.060	0.000	0.699	0.488	0.084	418		801	0.033
GN34c-12-1328-1R	Newell	CChot	NO	0.005	0.067	0.000	0.686	0.530	0.083	418		801	0.033
GN34c-12-1329-2R	Newell	CChot	NO	0.005	0.067	0.000	0.686	0.530	0.083	418		801	0.033
GN34c-12-1330-3R	Newell	CChot	NO	0.005	0.067	0.000	0.686	0.530	0.083	418		801	0.033
GN35-11-2317-1	Newell	CChot		0.052	0.037	0.000	0.734	0.548	0.123	418		801	0.033
GN35-11-2318-2	Newell	CChot		0.052	0.037	0.000	0.734	0.548	0.123	418		801	0.033
GN35-11-2319-3	Newell	CChot		0.052	0.037	0.000	0.734	0.548	0.123	418		801	0.033
GN36-11-2320-1	Newell	CChot		0.009	0.084	0.000	0.832	0.551	0.015	418		801	0.033
GN36-11-2321-2	Newell	CChot		0.009	0.084	0.000	0.832	0.551	0.015	418		801	0.033

Sample ID	Data Type	Data Subtype	Good Glass?	Formate mol/kg meas.	Oxalate mol/kg meas.	Coal mol/kg meas.	Nitrate (+nitrite) mol/kg meas.	Glycol Only mol/kg meas.	Any Mn mol/kg meas.	Frit	Target Waste Load	Total Anti-foam (mg/kg)	Anti-foam Carbon from gal and mg/kg (mol/kg)
GN36-11-2322-3	Newell	CChot		0.009	0.084	0.000	0.832	0.551	0.015	418		801	0.033
GN36b-12-0254-1	Newell	CChot		0.006	0.052	0.000	0.713	0.542	0.014	418		801	0.033
GN36b-12-0255-2	Newell	CChot		0.006	0.052	0.000	0.713	0.542	0.014	418		801	0.033
GN36b-12-0256-3	Newell	CChot		0.006	0.052	0.000	0.713	0.542	0.014	418		801	0.033
GN36b-12-0544-1R	Newell	CChot		0.006	0.052	0.000	0.713	0.542	0.014	418		801	0.033
GN36b-12-0545-2R	Newell	CChot		0.006	0.052	0.000	0.713	0.542	0.014	418		801	0.033
GN36b-12-0546-3R	Newell	CChot		0.006	0.052	0.000	0.713	0.542	0.014	418		801	0.033
GN36c-12-0257-1	Newell	CChot		0.005	0.054	0.000	0.707	0.560	0.014	418		801	0.033
GN36c-12-0258-2(broken lid)	Newell	CChot		0.005	0.054	0.000	0.707	0.560	0.014	418		801	0.033
GN36c-12-0259-3	Newell	CChot		0.005	0.054	0.000	0.707	0.560	0.014	418		801	0.033
GN36c-12-0546-1R	Newell	CChot		0.005	0.054	0.000	0.707	0.560	0.014	418		801	0.033
GN36c-12-0547-2R	Newell	CChot		0.005	0.054	0.000	0.707	0.560	0.014	418		801	0.033
GN36c-12-0548-3R	Newell	CChot		0.005	0.054	0.000	0.707	0.560	0.014	418		801	0.033
GN-37-11-2323-1	Newell	CChot		0.041	0.032	0.000	0.620	0.409	0.012	418		801	0.033
GN-37-11-2324-2	Newell	CChot		0.041	0.032	0.000	0.620	0.409	0.012	418		801	0.033
GN-37-11-2325-3	Newell	CChot		0.041	0.032	0.000	0.620	0.409	0.012	418		801	0.033
GN37b-12-0260-1	Newell	CChot		0.005	0.043	0.000	0.670	0.532	0.013	418		801	0.033
GN37b-12-0261-2	Newell	CChot		0.005	0.043	0.000	0.670	0.532	0.013	418		801	0.033
GN37b-12-0262-3	Newell	CChot		0.005	0.043	0.000	0.670	0.532	0.013	418		801	0.033
GN37b-12-0550-1R	Newell	CChot		0.005	0.043	0.000	0.670	0.532	0.013	418		801	0.033
GN37b-12-0551-2R	Newell	CChot		0.005	0.043	0.000	0.670	0.532	0.013	418		801	0.033
GN37b-12-0552-3R	Newell	CChot		0.005	0.043	0.000	0.670	0.532	0.013	418		801	0.033
GN37b-1Ramp	Johnson	CCramp		0.005	0.043	0.000	0.670	0.532	0.013	B12		801	0.033
GN37b-2Ramp	Johnson	CCramp		0.005	0.043	0.000	0.670	0.532	0.013	B12		801	0.033
GN37b-3Ramp	Johnson	CCramp		0.005	0.043	0.000	0.670	0.532	0.013	B12		801	0.033
GN38-12-0263-1	Newell	CChot	NO	0.008	0.044	0.000	0.765	0.612	0.012	418		801	0.033

Sample ID	Data Type	Data Subtype	Good Glass?	Formate mol/kg meas.	Oxalate mol/kg meas.	Coal mol/kg meas.	Nitrate (+nitrite) mol/kg meas.	Glycol Only mol/kg meas.	Any Mn mol/kg meas.	Frit	Target Waste Load	Total Anti-foam (mg/kg)	Anti-foam Carbon from gal and mg/kg (mol/kg)
GN38-12-0264-2	Newell	CChot	NO	0.008	0.044	0.000	0.765	0.612	0.012	418		801	0.033
GN38-12-0265-3	Newell	CChot	NO	0.008	0.044	0.000	0.765	0.612	0.012	418		801	0.033
GN38-12-0553-1	Newell	CChot	NO	0.008	0.044	0.000	0.765	0.612	0.012	418		801	0.033
GN38-12-0554-2	Newell	CChot	NO	0.008	0.044	0.000	0.765	0.612	0.012	418		801	0.033
GN38-12-0555-3	Newell	CChot	NO	0.008	0.044	0.000	0.765	0.612	0.012	418		801	0.033
GN38-1Ramp	Johnson	CCramp	NO	0.008	0.044	0.000	0.765	0.612	0.012	B12		801	0.033
GN38-2Ramp	Johnson	CCramp	NO	0.008	0.044	0.000	0.765	0.612	0.012	B12		801	0.033
GN38-3Ramp	Johnson	CCramp	NO	0.008	0.044	0.000	0.765	0.612	0.012	B12		801	0.033
GN38-1	Williams	CChot		0.008	0.044	0.000	0.765	0.612	0.012	B12		801	0.033
GN38-2	Williams	CChot		0.008	0.044	0.000	0.765	0.612	0.012	B12		801	0.033
GN38-3	Williams	CChot		0.008	0.044	0.000	0.765	0.612	0.012	B12		801	0.033
GN40-12-1128-1	Newell	CChot	NO	0.012	0.175	0.000	0.777	0.655	0.094	418		801	0.033
GN40-12-1129-2	Newell	CChot	NO	0.011	0.176	0.000	0.871	0.609	0.094	418		801	0.033
GN40-12-1130-3	Newell	CChot	NO	0.011	0.176	0.000	0.871	0.609	0.094	418		801	0.033
GN40-12-1331-1R	Newell	CChot	NO	0.011	0.176	0.000	0.871	0.609	0.094	418		801	0.033
GN40-12-1332-2R	Newell	CChot	NO	0.011	0.176	0.000	0.871	0.609	0.094	418		801	0.033
GN40-12-1333-3R	Newell	CChot	NO	0.011	0.176	0.000	0.871	0.609	0.094	418		801	0.033
GN41-11-1131-1	Newell	CChot	NO	0.027	0.151	0.000	0.673	0.648	0.088	418		801	0.033
GN41-11-1132-2	Newell	CChot	NO	0.007	0.200	0.000	0.782	0.603	0.088	418		801	0.033
GN41-11-1133-3	Newell	CChot	NO	0.007	0.200	0.000	0.782	0.603	0.088	418		801	0.033
GN41-12-1334-1	Newell	CChot	NO	0.007	0.200	0.000	0.782	0.603	0.088	418		801	0.033
GN41-12-1335-2	Newell	CChot	NO	0.007	0.200	0.000	0.782	0.603	0.088	418		801	0.033
GN41-12-1336-3	Newell	CChot	NO	0.007	0.200	0.000	0.782	0.603	0.088	418		801	0.033
GN43-12-2067-1	Johnson	CCramp		0.014	0.013	0.000	0.819	0.439	0.164	418		649	0.027
GN43-12-2068-2	Johnson	CCramp		0.014	0.013	0.000	0.819	0.439	0.164	418		649	0.027
GN43-12-2069-3	Johnson	CCramp		0.014	0.013	0.000	0.819	0.439	0.164	418		649	0.027

Sample ID	Data Type	Data Subtype	Good Glass?	Formate mol/kg meas.	Oxalate mol/kg meas.	Coal mol/kg meas.	Nitrate (+nitrite) mol/kg meas.	Glycol Only mol/kg meas.	Any Mn mol/kg meas.	Frit	Target Waste Load	Total Anti-foam (mg/kg)	Anti-foam Carbon from gal and mg/kg (mol/kg)
GN44-12-2070-1	Johnson	CCramp		0.039	0.149	0.000	0.673	0.363	0.164	418		649	0.027
GN44-12-2071-2	Johnson	CCramp		0.039	0.149	0.000	0.673	0.363	0.164	418		649	0.027
GN44-12-2072-3	Johnson	CCramp		0.039	0.149	0.000	0.673	0.363	0.164	418		649	0.027
GN45-13-0025-1	Johnson	CCramp		0.018	0.018	0.000	0.700	0.490	0.165	418		649	0.027
GN45-13-0026-2	Johnson	CCramp		0.018	0.018	0.000	0.700	0.490	0.165	418		649	0.027
GN45-13-0027-3	Johnson	CCramp		0.018	0.018	0.000	0.700	0.490	0.165	418		649	0.027
GN46-13-0028-1	Johnson	CCramp		0.010	0.053	0.000	0.668	0.457	0.164	418		649	0.027
GN46-13-0026-2	Johnson	CCramp		0.010	0.053	0.000	0.668	0.457	0.164	418		649	0.027
GN46-13-0027-3	Johnson	CCramp		0.010	0.053	0.000	0.668	0.457	0.164	418		649	0.027
GN47-13-0039-1	Lambert/John	CCramp		0.005	0.043	0.000	0.740	0.514	0.163	418		649	0.027
GN47-13-0040-2	Lambert/John	CCramp		0.005	0.043	0.000	0.740	0.514	0.163	418		649	0.027
GN47-13-0041-3	Lambert/John	CCramp		0.005	0.043	0.000	0.740	0.514	0.163	418		649	0.027
GN48-13-0042-1	Lambert/John	CCramp		0.004	0.050	0.000	0.647	0.567	0.166	418		649	0.027
GN48-13-0043-2	Lambert/John	CCramp		0.004	0.050	0.000	0.647	0.567	0.166	418		649	0.027
GN48-13-0044-3	Lambert/John	CCramp		0.004	0.050	0.000	0.647	0.567	0.166	418		649	0.027
GN49-13-0156-1	Johnson	CCramp		0.004	0.046	0.000	0.826	0.451	0.172	418		649	0.027
GN49-13-0157-2	Johnson	CCramp		0.004	0.046	0.000	0.826	0.451	0.172	418		649	0.027
GN49-13-0158-3	Johnson	CCramp		0.004	0.046	0.000	0.826	0.451	0.172	418		649	0.027
GN49-13-0301-1R	Johnson	CCramp		0.004	0.046	0.000	0.826	0.451	0.172	418		649	0.027
GN49-13-0302-2R	Johnson	CCramp		0.004	0.046	0.000	0.826	0.451	0.172	418		649	0.027
GN49-13-0303-3R	Johnson	CCramp		0.004	0.046	0.000	0.826	0.451	0.172	418		649	0.027
GN50-13-0159-1	Johnson	CCramp		0.002	0.040	0.000	0.925	0.438	0.170	418		649	0.027
GN50-13-0160-2	Johnson	CCramp		0.002	0.040	0.000	0.925	0.438	0.170	418		649	0.027
GN50-13-0161-3	Johnson	CCramp		0.002	0.040	0.000	0.925	0.438	0.170	418		649	0.027
25GN47:75GN49-13-0292-1	Johnson	CCramp		0.000	0.024	0.000	0.818	0.541	0.168	418		301	0.012
25GN47:75GN49-13-0292-2	Johnson	CCramp		0.000	0.024	0.000	0.818	0.541	0.168	418		301	0.012

Sample ID	Data Type	Data Subtype	Good Glass?	Formate mol/kg meas.	Oxalate mol/kg meas.	Coal mol/kg meas.	Nitrate (+nitrite) mol/kg meas.	Glycol Only mol/kg meas.	Any Mn mol/kg meas.	Frit	Target Waste Load	Total Anti-foam (mg/kg)	Anti-foam Carbon from gal and mg/kg (mol/kg)
25GN47:75GN49-13-0292-3	Johnson	CCramp		0.000	0.024	0.000	0.818	0.541	0.168	418		301	0.012
50GN47:50GN49-13-0295-1	Johnson	CCramp		0.000	0.027	0.000	0.802	0.558	0.168	418		301	0.012
50GN47:50GN49-13-0296-2	Johnson	CCramp		0.000	0.027	0.000	0.802	0.558	0.168	418		301	0.012
50GN47:50GN49-13-0297-3	Johnson	CCramp		0.000	0.027	0.000	0.802	0.558	0.168	418		301	0.012
75GN47:25GN49-13-0298-1	Johnson	CCramp		0.000	0.023	0.000	0.857	0.527	0.169	418		301	0.012
75GN47:25GN49-13-0299-2	Johnson	CCramp		0.000	0.023	0.000	0.857	0.527	0.169	418		301	0.012
75GN47:25GN49-13-0300-3	Johnson	CCramp		0.000	0.023	0.000	0.857	0.527	0.169	418		301	0.012
GN51-13-0262-1	Johnson	CCramp		0.086	0.014	0.000	0.738	0.462	0.174	418		3502	0.143
GN51-13-0263-2	Johnson	CCramp		0.086	0.014	0.000	0.738	0.462	0.174	418		3502	0.143
GN51-13-0264-3	Johnson	CCramp		0.086	0.014	0.000	0.738	0.462	0.174	418		3502	0.143
GN51-13-0265-4	Johnson	CCramp		0.086	0.014	0.000	0.738	0.462	0.174	418		3502	0.143
GN51-13-0266-5	Johnson	CCramp		0.086	0.014	0.000	0.738	0.462	0.174	418		3502	0.143
GN51-13-0267-6	Johnson	CCramp		0.086	0.014	0.000	0.738	0.462	0.174	418		3502	0.143
FN1-13-0267-1	Johnson	CCramp		0.906	0.000	0.000	0.311	0.000	0.046	418		801	0.033
FN1-13-0268-2	Johnson	CCramp		0.906	0.000	0.000	0.311	0.000	0.046	418		801	0.033
FN1-13-0269-3	Johnson	CCramp		0.906	0.000	0.000	0.311	0.000	0.046	418		801	0.033
FN1-13-0270-4	Johnson	CCramp		0.906	0.000	0.000	0.311	0.000	0.046	418		801	0.033
FN1-13-0271-5	Johnson	CCramp		0.906	0.000	0.000	0.311	0.000	0.046	418		801	0.033
FN1-13-0272-6	Johnson	CCramp		0.906	0.000	0.000	0.311	0.000	0.046	418		801	0.033
FN2-S51-13-0737-1	Johnson	CCramp		0.952	0.000	0.000	0.268	0.000	0.035	418		801	0.033
FN2-S51-13-0738-2	Johnson	CCramp		0.952	0.000	0.000	0.268	0.000	0.035	418		801	0.033
FN2-S51-13-0739-3	Johnson	CCramp		0.952	0.000	0.000	0.268	0.000	0.035	418		801	0.033
GN52-13-0274-1	Johnson	CCramp		0.086	0.012	0.000	0.777	0.473	0.173	418		3502	0.143
GN52-13-0275-2	Johnson	CCramp		0.086	0.012	0.000	0.777	0.473	0.173	418		3502	0.143
GN52-13-0276-3	Johnson	CCramp		0.086	0.012	0.000	0.777	0.473	0.173	418		3502	0.143
GN52-13-0277-4	Johnson	CCramp		0.086	0.012	0.000	0.777	0.473	0.173	418		3502	0.143

Sample ID	Data Type	Data Subtype	Good Glass?	Formate mol/kg meas.	Oxalate mol/kg meas.	Coal mol/kg meas.	Nitrate (+nitrite) mol/kg meas.	Glycol Only mol/kg meas.	Any Mn mol/kg meas.	Frit	Target Waste Load	Total Anti-foam (mg/kg)	Anti-foam Carbon from gal and mg/kg (mol/kg)
GN52-13-0278-5	Johnson	CCramp		0.086	0.012	0.000	0.777	0.473	0.173	418		3502	0.143
GN52-13-0279-6	Johnson	CCramp		0.086	0.012	0.000	0.777	0.473	0.173	418		3502	0.143
GN53-13-0280-1	Johnson	CCramp		0.046	0.014	0.000	0.940	0.604	0.177	418		3502	0.143
GN53-13-0281-2	Johnson	CCramp		0.046	0.014	0.000	0.940	0.604	0.177	418		3502	0.143
GN53-13-0282-3	Johnson	CCramp		0.046	0.014	0.000	0.940	0.604	0.177	418		3502	0.143
GN53-13-0283-4	Johnson	CCramp		0.046	0.014	0.000	0.940	0.604	0.177	418		3502	0.143
GN53-13-0284-5	Johnson	CCramp		0.046	0.014	0.000	0.940	0.604	0.177	418		3502	0.143
GN53-13-0285-6	Johnson	CCramp		0.046	0.014	0.000	0.940	0.604	0.177	418		3502	0.143
GN54-13-0320-1	Johnson	CCramp		0.094	0.013	0.000	0.772	0.418	0.173	418		3429	0.140
GN54-13-0321-2	Johnson	CCramp		0.094	0.013	0.000	0.772	0.418	0.173	418		3429	0.140
GN54-13-0322-3	Johnson	CCramp		0.094	0.013	0.000	0.772	0.418	0.173	418		3429	0.140
GN55-13-0323-1	Johnson	CCramp		0.101	0.014	0.000	0.897	0.183	0.183	418		3478	0.142
GN55-13-0324-2	Johnson	CCramp		0.101	0.014	0.000	0.897	0.183	0.183	418		3478	0.142
GN55-13-0325-3	Johnson	CCramp		0.101	0.014	0.000	0.897	0.183	0.183	418		3478	0.142
GN56-13-0733-1	Johnson	CCramp		0.156	0.009	0.000	0.935	0.442	0.183	418		3576	0.146
GN56-13-0734-2	Johnson	CCramp		0.156	0.009	0.000	0.935	0.442	0.183	418		3576	0.146
GN56-13-0735-3	Johnson	CCramp		0.156	0.009	0.000	0.935	0.442	0.183	418		3576	0.146
GN57-S93-1	Johnson	CCramp		0.004	0.041	0.000	0.935	0.478	0.171	418		367	0.015
GN57-S93-2	Johnson	CCramp		0.004	0.041	0.000	0.935	0.478	0.171	418		367	0.015
GN57-S93-3	Johnson	CCramp		0.004	0.041	0.000	0.935	0.478	0.171	418		367	0.015
GN58-1	Johnson	CCramp		0.000	0.012	0.000	1.087	0.550	0.163	418		3600	0.147
GN58-2	Johnson	CCramp		0.000	0.012	0.000	1.087	0.550	0.163	418		3600	0.147
GN58-3	Johnson	CCramp		0.000	0.012	0.000	1.087	0.550	0.163	418		3600	0.147
GN59-13-0758-1	Johnson	CCramp		0.010	0.013	0.000	1.106	0.506	0.156	418		3600	0.147
GN59-13-0759-2	Johnson	CCramp		0.010	0.013	0.000	1.106	0.506	0.156	418		3600	0.147
GN59-13-0760-3	Johnson	CCramp		0.010	0.013	0.000	1.106	0.506	0.156	418		3600	0.147

Sample ID	Data Type	Data Subtype	Good Glass?	Formate mol/kg meas.	Oxalate mol/kg meas.	Coal mol/kg meas.	Nitrate (+nitrite) mol/kg meas.	Glycol Only mol/kg meas.	Any Mn mol/kg meas.	Frit	Target Waste Load	Total Anti-foam (mg/kg)	Anti-foam Carbon from gal and mg/kg (mol/kg)
GN70-14-0066-1	Newell	CCramp		0.020	0.038	0.000	0.794	0.633	0.175	418		980	0.040
GN70-14-0066-2	Newell	CCramp		0.020	0.038	0.000	0.794	0.633	0.175	418		980	0.040
GN70-1	Hall?	CChot	Y	0.020	0.038	0.000	0.794	0.633	0.175	418		980	0.040
GN70-2	Hall?	CChot	Y	0.020	0.038	0.000	0.794	0.633	0.175	418		980	0.040
GN70-3	Hall?	CChot	Y	0.020	0.038	0.000	0.794	0.633	0.175	418		980	0.040
GN71-14-0066-1	Newell	CCramp		0.011	0.030	0.000	0.937	0.700	0.162	418		649	0.027
GN71-14-0066-2	Newell	CCramp		0.011	0.030	0.000	0.937	0.700	0.162	418		649	0.027
GN71-3460	Williams	CChot	N	0.011	0.030	0.000	0.937	0.700	0.162	418		649	0.027
GN71 purge 2-3353	Amoroso	CCOG	N-swirls	0.011	0.030	0.000	0.937	0.700	0.162	418		649	0.027
GN71-4467	Williams	CCAr	N-NiS	0.011	0.030	0.000	0.937	0.700	0.162	418		649	0.027
GN71-4468	Williams	CCAr	N-NiS	0.011	0.030	0.000	0.937	0.700	0.162	418		649	0.027
GN71 25-3731	Williams	MRF	N	0.011	0.030	0.000	0.937	0.700	0.162	418		649	0.027
GN72-14-0067-1	Newell	CCramp	Y	0.024	0.042	0.000	0.818	0.526	0.198	418		980	0.040
GN72-14-0068-2	Newell	CCramp	Y	0.024	0.042	0.000	0.818	0.526	0.198	418		980	0.040
GN72-14-0069-3	Newell	CCramp	Y	0.024	0.042	0.000	0.818	0.526	0.198	418		980	0.040
GN72-3461	Williams	CChot	Y	0.024	0.042	0.000	0.818	0.526	0.198	418		980	0.040
GN72-3462	Williams	CChot	Y	0.024	0.042	0.000	0.818	0.526	0.198	418		980	0.040
GN73-14-0070-1	Newell	CCramp	Y	0.008	0.030	0.000	0.816	0.537	0.173	418		1102	0.045
GN73-14-0071-2	Newell	CCramp	Y	0.008	0.030	0.000	0.816	0.537	0.173	418		1102	0.045
GN73-14-0072-3	Newell	CCramp	Y	0.008	0.030	0.000	0.816	0.537	0.173	418		1102	0.045
GN73	Hall	CChot	N	0.008	0.030	0.000	0.816	0.537	0.173			1102	0.045
GN73	Hall	CChot	N	0.008	0.030	0.000	0.816	0.537	0.173			1102	0.045
GN73	Hall	CChot	N	0.008	0.030	0.000	0.816	0.537	0.173			1102	0.045
GN74-14-0067-1	Newell	CCramp	Y	0.010	0.020	0.000	0.640	0.505	0.187	418		980	0.040
GN74-14-0068-2-bad rep	Newell	CCramp	Y	0.010	0.020	0.000	0.640	0.505	0.187	418		980	0.040
GN74-14-0069-3	Newell	CCramp	Y	0.010	0.020	0.000	0.640	0.505	0.187	418		980	0.040

Sample ID	Data Type	Data Subtype	Good Glass?	Formate mol/kg meas.	Oxalate mol/kg meas.	Coal mol/kg meas.	Nitrate (+nitrite) mol/kg meas.	Glycol Only mol/kg meas.	Any Mn mol/kg meas.	Frit	Target Waste Load	Total Anti-foam (mg/kg)	Anti-foam Carbon from gal and mg/kg (mol/kg)
GN74	Hall	CChot	N	0.010	0.020	0.000	0.640	0.505	0.187			980	0.040
GN74	Hall	CChot	N	0.010	0.020	0.000	0.640	0.505	0.187			980	0.040
GN74	Hall	CChot	N	0.010	0.020	0.000	0.640	0.505	0.187			980	0.040
GN75-14-0070-1	Newell	CCramp	N	0.007	0.030	0.000	0.868	0.564	0.176	418		872	0.036
GN75-14-0071-2	Newell	CCramp	N	0.007	0.030	0.000	0.868	0.564	0.176	418		872	0.036
GN75-14-0072-3	Newell	CCramp	N	0.007	0.030	0.000	0.868	0.564	0.176	418		872	0.036
GN75	Hall	CChot	N	0.007	0.030	0.000	0.868	0.564	0.176			872	0.036
GN75	Hall	CChot	N	0.007	0.030	0.000	0.868	0.564	0.176			872	0.036
GN75	Hall	CChot	N	0.007	0.030	0.000	0.868	0.564	0.176			872	0.036
GN76-1	Newell	CCramp	N	0.036	0.042	0.000	0.618	0.500	0.172	418		1011	0.041
GN76-1	Newell	CCramp	N	0.036	0.042	0.000	0.618	0.500	0.172	418		1011	0.041
GN76-1	Newell	CCramp	N	0.036	0.042	0.000	0.618	0.500	0.172	418		1011	0.041
GN76-4469	Williams	CChot	Y	0.036	0.042	0.000	0.618	0.500	0.172			1011	0.041
GN76-4470	Williams	CChot	Y	0.036	0.042	0.000	0.618	0.500	0.172			1011	0.041
GN76-4471	Williams	CChot	Y	0.036	0.042	0.000	0.618	0.500	0.172			1011	0.041
GN76-1-NO REDOX	Hall	CChot	Y	0.036	0.042	0.000	0.618	0.500	0.172			1011	0.041
GN76-1-NO REDOX	Hall	CChot	Y	0.036	0.042	0.000	0.618	0.500	0.172			1011	0.041
GN76-2-NO REDOX	Hall	CChot	Y	0.036	0.042	0.000	0.618	0.500	0.172			1011	0.041
GN76-2-NO REDOX	Hall	CChot	Y	0.036	0.042	0.000	0.618	0.500	0.172			1011	0.041
GN76-3-NO REDOX	Hall	CChot	Y	0.036	0.042	0.000	0.618	0.500	0.172			1011	0.041
GN76-3-NO REDOX	Hall	CChot	Y	0.036	0.042	0.000	0.618	0.500	0.172			1011	0.041
GN77-14-0123-1	Newell	CCramp	N	0.006	0.034	0.000	0.779	0.520	0.171	418		999	0.041
GN77-14-0124-2	Newell	CCramp	N	0.006	0.034	0.000	0.779	0.520	0.171	418		999	0.041
GN77-14-0125-3	Newell	CCramp	N	0.006	0.034	0.000	0.779	0.520	0.171	418		999	0.041
GN77-4521	Williams	CChot	Y	0.006	0.034	0.000	0.779	0.520	0.171			999	0.041
GN77-4522	Williams	CChot	Y	0.006	0.034	0.000	0.779	0.520	0.171			999	0.041

Sample ID	Data Type	Data Subtype	Good Glass?	Formate mol/kg meas.	Oxalate mol/kg meas.	Coal mol/kg meas.	Nitrate (+nitrite) mol/kg meas.	Glycol Only mol/kg meas.	Any Mn mol/kg meas.	Frit	Target Waste Load	Total Anti-foam (mg/kg)	Anti-foam Carbon from gal and mg/kg (mol/kg)
GN77-4523	Williams	CChot	N	0.006	0.034	0.000	0.779	0.520	0.171			999	0.041
GN77-1	Hall	CChot	N	0.006	0.034	0.000	0.779	0.520	0.171			999	0.041
GN77-2	Hall	CChot	N	0.006	0.034	0.000	0.779	0.520	0.171			999	0.041
GN77-3	Hall	CChot	N	0.006	0.034	0.000	0.779	0.520	0.171			999	0.041
GN78-1-N	Newell	CCramp	N	0.002	0.032	0.000	0.837	0.577	0.162	418		982	0.040
GN78-2-N	Newell	CCramp	N	0.002	0.032	0.000	0.837	0.577	0.162	418		982	0.040
GN78-3-N	Newell	CCramp	N	0.002	0.032	0.000	0.837	0.577	0.162	418		982	0.040
GN78-3501	Williams	CChot	Y	0.002	0.032	0.000	0.837	0.577	0.162	418		982	0.040
GN78-3502	Williams	CChot	Y	0.002	0.032	0.000	0.837	0.577	0.162	418		982	0.040
GN78-1-H	Hall	CChot		0.002	0.032	0.000	0.837	0.577	0.162	418		982	0.040
GN78-2-H	Hall	CChot		0.002	0.032	0.000	0.837	0.577	0.162	418		982	0.040
GN78-3-H	Hall	CChot		0.002	0.032	0.000	0.837	0.577	0.162	418		982	0.040
GN78-3087	Williams	CChot	N	0.002	0.032	0.000	0.837	0.577	0.162	418		982	0.040
GN78-3088	Williams	CChot	Y	0.002	0.032	0.000	0.837	0.577	0.162	418		982	0.040
GN78-3874	Williams	CChot	Y	0.002	0.032	0.000	0.837	0.577	0.162	418		982	0.040
GN78-3875	Williams	CChot	N	0.002	0.032	0.000	0.837	0.577	0.162	418		982	0.040
GN78-3876	Williams	CChot	Y	0.002	0.032	0.000	0.837	0.577	0.162	418		982	0.040
GN78 purge 1-2881	Williams	CCOG	Y	0.002	0.032	0.000	0.837	0.577	0.162	418		982	0.040
GN78 purge 1-2881	Williams	CCOG	Y	0.002	0.032	0.000	0.837	0.577	0.162	418		982	0.040
GN78 purge 3-3352	Williams	CCOG	N	0.002	0.032	0.000	0.837	0.577	0.162	418		982	0.040
GN78-25-3498	Williams	CChot	Y	0.002	0.032	0.000	0.837	0.577	0.162	418		982	0.040
GN78-3081	Williams	CCAr	N	0.002	0.032	0.000	0.837	0.577	0.162	418		982	0.040
GN78-3082	Williams	CCAr	N	0.002	0.032	0.000	0.837	0.577	0.162	418		982	0.040
GN79-1-N	Newell	CCramp	N	0.007	0.035	0.000	0.674	0.516	0.171	418		1244	0.051
GN79-2-N	Newell	CCramp	N	0.007	0.035	0.000	0.674	0.516	0.171	418		1244	0.051
GN79-3-N	Newell	CCramp	N	0.007	0.035	0.000	0.674	0.516	0.171	418		1244	0.051

Sample ID	Data Type	Data Subtype	Good Glass?	Formate mol/kg meas.	Oxalate mol/kg meas.	Coal mol/kg meas.	Nitrate (+nitrite) mol/kg meas.	Glycol Only mol/kg meas.	Any Mn mol/kg meas.	Frit	Target Waste Load	Total Anti-foam (mg/kg)	Anti-foam Carbon from gal and mg/kg (mol/kg)
GN79-1-H	Hall	CChot		0.007	0.035	0.000	0.674	0.516	0.171	418		1244	0.051
GN79-2-H	Hall	CChot		0.007	0.035	0.000	0.674	0.516	0.171	418		1244	0.051
GN79-3-H	Hall	CChot		0.007	0.035	0.000	0.674	0.516	0.171	418		1244	0.051
GN79-3089	Williams	CChot	N	0.007	0.035	0.000	0.674	0.516	0.171	418		1244	0.051
GN79-3090	Williams	CChot	N	0.007	0.035	0.000	0.674	0.516	0.171	418		1244	0.051
GN79-3499	Williams	CChot	Y	0.007	0.035	0.000	0.674	0.516	0.171	418		1244	0.051
GN79-3500	Williams	CChot	Y	0.007	0.035	0.000	0.674	0.516	0.171	418		1244	0.051
GN79 purge 2-3351	Williams	CCOG	N	0.007	0.035	0.000	0.674	0.516	0.171	418		1244	0.051
GN79 purge 1-2942	Williams	CCOG	Y	0.007	0.035	0.000	0.674	0.516	0.171	418		1244	0.051
GN79 purge 1-2942	Williams	CCOG		0.007	0.035	0.000	0.674	0.516	0.171	418		1244	0.051
GN79 purge 1-2942	Williams	CCOG		0.007	0.035	0.000	0.674	0.516	0.171	418		1244	0.051
GN79 purge 1-2942	Williams	CCOG		0.007	0.035	0.000	0.674	0.516	0.171	418		1244	0.051
GN79-3083	Williams	CCAr	Y	0.007	0.035	0.000	0.674	0.516	0.171	418		1244	0.051
GN79-3084	Williams	CCAr	Y	0.007	0.035	0.000	0.674	0.516	0.171	418		1244	0.051
GN80-2975-1	Hall	CChot		0.007	0.031	0.000	0.859	0.570	0.163	418		1101	0.045
GN80-2975-2-BAD REDOX	Hall	CChot		0.007	0.031	0.000	0.859	0.570	0.163			1101	0.045
GN80-2982-1	Hall	CChot		0.007	0.031	0.000	0.859	0.570	0.163			1101	0.045
GN80-2982-2-BAD REDOX	Hall	CChot		0.007	0.031	0.000	0.859	0.570	0.163			1101	0.045
GN80-2982-3-BAD REDOX	Hall	CChot		0.007	0.031	0.000	0.859	0.570	0.163			1101	0.045
GN81-3022-1-BAD REDOX	Hall	CChot		0.007	0.033	0.000	0.884	0.583	0.177	418		1101	0.045
GN81-3022-2	Hall	CChot		0.007	0.033	0.000	0.884	0.583	0.177			1101	0.045
GN81-3029-1-BAD REDOX	Hall	CChot		0.007	0.033	0.000	0.884	0.583	0.177			1101	0.045
GN81-3029-2-BAD REDOX	Hall	CChot		0.007	0.033	0.000	0.884	0.583	0.177			1101	0.045
GN81-3029-3-BAD REDOX	Hall	CChot		0.007	0.033	0.000	0.884	0.583	0.177			1101	0.045
GN82-1	Hall	CChot		0.007	0.035	0.000	0.827	0.551	0.162	418		1101	0.045
GN82-2	Hall	CChot		0.007	0.035	0.000	0.827	0.551	0.162			1101	0.045

Sample ID	Data Type	Data Subtype	Good Glass?	Formate mol/kg meas.	Oxalate mol/kg meas.	Coal mol/kg meas.	Nitrate (+nitrite) mol/kg meas.	Glycol Only mol/kg meas.	Any Mn mol/kg meas.	Frit	Target Waste Load	Total Anti-foam (mg/kg)	Anti-foam Carbon from gal and mg/kg (mol/kg)
GN82-3	Hall	CChot		0.007	0.035	0.000	0.827	0.551	0.162			1101	0.045
GN83-1	Hall	CChot		0.008	0.036	0.000	0.856	0.564	0.164	418		1101	0.045
GN83-2	Hall	CChot		0.008	0.036	0.000	0.856	0.564	0.164			1101	0.045
GN83-3	Hall	CChot		0.008	0.036	0.000	0.856	0.564	0.164			1101	0.045
CEF P2 100 composite	SRAT (SME)	CCramp		0.054	0.013	0.000	0.934	0.461	0.171	418		4384	0.179
CEF P2 100 composite	SRAT (SME)	CCramp		0.054	0.013	0.000	0.934	0.461	0.171	418		4384	0.179
CEF P2 100 composite	SRAT (SME)	CCramp		0.054	0.013	0.000	0.934	0.461	0.171	418		4384	0.179
100 CEF2-F-013 AD	SRAT (SME)	CCramp		0.055	0.013	0.000	0.954	0.466	0.162	418		4384	0.179
100 CEF2-F-013 AD	SRAT (SME)	CCramp		0.055	0.013	0.000	0.954	0.466	0.162	418		4384	0.179
100 CEF2-F-013 AD	SRAT (SME)	CCramp		0.055	0.013	0.000	0.954	0.466	0.162	418		4384	0.179
100 CEF2-F-015 AD	SRAT (SME)	CCramp		0.056	0.017	0.000	0.947	0.473	0.165	418		4384	0.179
100 CEF2-F-015 AD	SRAT (SME)	CCramp		0.056	0.017	0.000	0.947	0.473	0.165	418		4384	0.179
100 CEF2-F-015 AD	SRAT (SME)	CCramp		0.056	0.017	0.000	0.947	0.473	0.165	418		4384	0.179
100 CEF2-F-041 AD	SRAT (SME)	CCramp		0.041	0.013	0.000	1.017	0.490	0.147	418		8865	0.362
100 CEF2-F-041 AD	SRAT (SME)	CCramp		0.041	0.013	0.000	1.017	0.490	0.147	418		8865	0.362
100 CEF2-F-042 AD	SRAT (SME)	CCramp		0.052	0.016	0.000	0.914	0.475	0.150	418		8865	0.362
100 CEF2-F-042 AD	SRAT (SME)	CCramp		0.052	0.016	0.000	0.914	0.475	0.150	418		8865	0.362
125 CEF2-F-008 IC PSAL CQ	SRAT (SME)	CCramp		0.032	0.018	0.000	1.011	0.629	0.148	418		4384	0.179
125 CEF2-F-008 IC PSAL CQ	SRAT (SME)	CCramp		0.032	0.018	0.000	1.011	0.629	0.148	418		4384	0.179
125 CEF2-F-008 IC PSAL CQ	SRAT (SME)	CCramp		0.032	0.018	0.000	1.011	0.629	0.148	418		4384	0.179
125 CEF2-F-008 IC AD-0990	SRAT (SME)	CCramp		0.032	0.018	0.000	1.011	0.629	0.148	418		4384	0.179
125 CEF2-F-008 IC AD-0991	SRAT (SME)	CCramp		0.032	0.018	0.000	1.011	0.629	0.148	418		4384	0.179
125 CEF2-F-008 IC AD-0992	SRAT (SME)	CCramp		0.032	0.018	0.000	1.011	0.629	0.148	418		4384	0.179
125 CEF2-F-009 IC AD-0993	SRAT (SME)	CCramp		0.036	0.016	0.000	0.863	0.583	0.083	418		4384	0.179
CEF-2A-3091-SME A		CChot	Y	0.051	0.011	0.000	0.971	0.461	0.167	418		4384	0.179

Sample ID	Data Type	Data Subtype	Good Glass?	Formate mol/kg meas.	Oxalate mol/kg meas.	Coal mol/kg meas.	Nitrate (+nitrite) mol/kg meas.	Glycol Only mol/kg meas.	Any Mn mol/kg meas.	Frit	Target Waste Load	Total Anti-foam (mg/kg)	Anti-foam Carbon from gal and mg/kg (mol/kg)
CEF-2A-3092 SME B		CChot	Y	0.051	0.011	0.000	0.971	0.461	0.167	418		4384	0.179
CEF-2 SRAT A		CChot	Y	0.053	0.017	0.000	1.104	0.443	0.167	418		4384	0.179
CEF-2 SRAT B		CChot	Y	0.053	0.017	0.000	1.104	0.443	0.167	418		4384	0.179
CEF1 061-1-33		CCramp		1.016	0.000	0.000	0.289	0.000	0.043	418		2226	0.091
CEF1 061-1-34		CCramp		1.016	0.000	0.000	0.289	0.000	0.043	418		2226	0.091
CEF1 065-1-35		CCramp	N	1.049	0.000	0.000	0.276	0.000	0.041	418		2226	0.091
CEF1 065-1-36		CCramp	N	1.049	0.000	0.000	0.276	0.000	0.041	418		2226	0.091
CEF1-065 Baseline	Amaroso	CCOG		1.049	0.000	0.000	0.276	0.000	0.041	418		2226	0.091
CEF1-065 Baseline	Amaroso	CCOG		1.049	0.000	0.000	0.276	0.000	0.041	418		2226	0.091
CEF1-065 Baseline	Amaroso	CCOG		1.049	0.000	0.000	0.276	0.000	0.041	418		2226	0.091
CEF2-F-019-1-0997		CCramp	N	0.054	0.013	0.000	0.971	0.461	0.171	418		4384	0.179
CEF2-F-014-1-0994		CCramp		0.056	0.017	0.000	0.947	0.473	0.165	418		4384	0.179
CEF2-F-014-1-0995		CCramp		0.056	0.017	0.000	0.947	0.473	0.165	418		4384	0.179
CEF2-F-014-1-0996		CCramp		0.056	0.017	0.000	0.947	0.473	0.165	418		4384	0.179
CEF2-F-014-1289		CCOG		0.056	0.017	0.000	0.947	0.473	0.165	418		4384	0.179
CEF2-F-014-1290		CCOG		0.056	0.017	0.000	0.947	0.473	0.165	418		4384	0.179
CEF2-F-041-1291		CCOG		0.041	0.013	0.000	1.017	0.490	0.147	418		8865	0.362
CEF2-F-041-1292		CCOG		0.041	0.013	0.000	1.017	0.490	0.147	418		8865	0.362
CEF-2 purge 1-3067		CCOG	Y	0.051	0.011	0.000	0.971	0.461	0.171	418		4384	0.179
CEF-2 purge 1-3067		CCOG	Y	0.051	0.011	0.000	0.971	0.461	0.171	418		4384	0.179
CEF-2 purge 1-3067		CCOG	Y	0.051	0.011	0.000	0.971	0.461	0.171	418		4384	0.179
CEF-2 purge 1-3067		CCOG	Y	0.051	0.011	0.000	0.971	0.461	0.171	418		4384	0.179
CEF-2-3085		CCAr	Y	0.051	0.011	0.000	0.971	0.461	0.171	418		4384	0.179
CEF-2-3086		CCAr	Y	0.051	0.011	0.000	0.971	0.461	0.171	418		4384	0.179
CEF-2 SRAT 20-4524		MRF	Y	0.003	0.001	0.000	0.066	0.027	0.167	418		263	0.011
CEF-2 SRAT 20-4525		MRF	Y	0.003	0.001	0.000	0.066	0.027	0.167	418		263	0.011

Sample ID	Data Type	Data Subtype	Good Glass?	Formate mol/kg meas.	Oxalate mol/kg meas.	Coal mol/kg meas.	Nitrate (+nitrite) mol/kg meas.	Glycol Only mol/kg meas.	Any Mn mol/kg meas.	Frit	Target Waste Load	Total Anti-foam (mg/kg)	Anti-foam Carbon from gal and mg/kg (mol/kg)
CEF-2 SRAT 25-4526		MRF	Y	0.003	0.001	0.000	0.066	0.027	0.167	418		263	0.011
CEF-2 SRAT 25-4527		MRF	Y	0.003	0.001	0.000	0.066	0.027	0.167	418		263	0.011
CEF-2 comp 20-3496		MRF	Y	0.054	0.011	0.000	0.971	0.461	0.171	418		4384	0.179
CEF-2 comp 20-3497		MRF	Y	0.054	0.011	0.000	0.971	0.461	0.171	418		4384	0.179
CEF-2 SRAT 20-3494		MRF	Y	0.054	0.013	0.000	0.971	0.461	0.010	418		4384	0.179
CEF-2 SRAT 20-3495		MRF	Y	0.054	0.013	0.000	0.971	0.461	0.010	418		4384	0.179
CEF-2 comp 25-4325		MRF	Y	0.054	0.011	0.000	0.971	0.461	0.010	418		4384	0.179
CEF-2 comp 25-4325		MRF	Y	0.054	0.011	0.000	0.971	0.461	0.010	418		4384	0.179
CEF-2-27 25-4326		MRF	Y	0.054	0.011	0.000	0.787	0.372	0.171	418		4384	0.179
CEF-2-27 25-4326		MRF	Y	0.054	0.011	0.000	0.787	0.372	0.171	418		4384	0.179
SB8-D3 BL		CCAr	N	1.255	0.034	0.000	0.487	0.000	0.196	418		513	0.021
SB8-D3AF		CCAr	Y	1.255	0.034	0.000	0.487	0.000	0.196	418		1646	0.067
SB8-D3 bAF		CCAr	Y	1.255	0.034	0.000	0.487	0.000	0.196	418		1644	0.067
SB8-D3 PEG		CCAr	N	1.255	0.034	0.000	0.487	0.000	0.196	418		1371	0.056
SB8-D3 BL-1		CCOG	N	1.255	0.034	0.000	0.487	0.000	0.196	418		513	0.021
SB8-D3 BL-2		CCOG	N	1.255	0.034	0.000	0.487	0.000	0.196	418		513	0.021
SB8-D3 BL-3		CCOG	N	1.255	0.034	0.000	0.487	0.000	0.196	418		513	0.021
SB8-D3AF-1		CCOG	Y	1.255	0.034	0.000	0.487	0.000	0.196	418		1646	0.067
SB8-D3AF-2		CCOG	Y	1.255	0.034	0.000	0.487	0.000	0.196	418		1646	0.067
SB8-D3AF-3		CCOG	Y	1.255	0.034	0.000	0.487	0.000	0.196	418		1646	0.067
SB8-D3 bAF-1		CCOG	Y	1.255	0.034	0.000	0.487	0.000	0.196	418		1644	0.067
SB8-D3 bAF-2		CCOG	Y	1.255	0.034	0.000	0.487	0.000	0.196	418		1644	0.067
SB8-D3 bAF-3		CCOG	Y	1.255	0.034	0.000	0.487	0.000	0.196	418		1644	0.067
SB8-D3 PEG-1		CCOG		1.255	0.034	0.000	0.487	0.000	0.196	418		1371	0.056
SB8-D3 PEG-2		CCOG		1.255	0.034	0.000	0.487	0.000	0.196	418		1371	0.056
SB8-D3 PEG-3		CCOG		1.255	0.034	0.000	0.487	0.000	0.196	418		1371	0.056

Sample ID	Data Type	Data Subtype	Good Glass?	Formate mol/kg meas.	Oxalate mol/kg meas.	Coal mol/kg meas.	Nitrate (+nitrite) mol/kg meas.	Glycol Only mol/kg meas.	Any Mn mol/kg meas.	Frit	Target Waste Load	Total Anti-foam (mg/kg)	Anti-foam Carbon from gal and mg/kg (mol/kg)
12-SB8-A1-6792-A	SB8-with ox	CCramp		1.077	0.065	0.000	0.394	0.000	0.172		34.8	867	0.035
12-SB8-A1-6792-B	SB8-with ox	CCramp		1.077	0.065	0.000	0.394	0.000	0.172		34.8	867	0.035
12-SB8-A1-6792-C	SB8-with ox	CCramp		1.077	0.065	0.000	0.394	0.000	0.172		34.8	867	0.035
12-SB8-A2-6824-A	SB8-with ox	CCramp		1.407	0.063	0.000	0.367	0.000	0.186		36	747	0.031
12-SB8-A2-6824-B	SB8-with ox	CCramp		1.407	0.063	0.000	0.367	0.000	0.186		36	747	0.031
12-SB8-A2-6824-C	SB8-with ox	CCramp		1.407	0.063	0.000	0.367	0.000	0.186		36	747	0.031
12-SB8-A3-6857-A	SB8-with ox	CCramp		1.093	0.064	0.000	0.406	0.000	0.176		35.2	862	0.035
12-SB8-A3-6857-B	SB8-with ox	CCramp		1.093	0.064	0.000	0.406	0.000	0.176		35.2	862	0.035
12-SB8-A3-6857-C	SB8-with ox	CCramp		1.093	0.064	0.000	0.406	0.000	0.176		35.2	862	0.035
12-SB8-A4-6890-A	SB8-with ox	CCramp		1.526	0.067	0.000	0.373	0.000	0.179		37.9	911	0.037
12-SB8-A4-6890-B	SB8-with ox	CCramp		1.526	0.067	0.000	0.373	0.000	0.179		37.9	911	0.037
12-SB8-A4-6890-C	SB8-with ox	CCramp		1.526	0.067	0.000	0.373	0.000	0.179		37.9	911	0.037
12-SB8-B1-6934-A	SB8-with ox	CCramp		1.274	0.055	0.000	0.478	0.000	0.247		35.7	750	0.031
12-SB8-B1-6934-B	SB8-with ox	CCramp		1.274	0.055	0.000	0.478	0.000	0.247		35.7	750	0.031
12-SB8-B2-6967-A	SB8-with ox	CCramp		1.670	0.053	0.000	0.443	0.000	0.219		33.8	718	0.029
12-SB8-A1-6792-AVG	SB8-with ox	CCramp		1.077	0.065	0.000	0.394	0.000	0.172		34.8	867	0.035
12-SB8-A2-6824-AVG	SB8-with ox	CCramp		1.407	0.063	0.000	0.367	0.000	0.186		36	747	0.031
12-SB8-A3-6857-AVG	SB8-with ox	CCramp		1.093	0.064	0.000	0.406	0.000	0.176		35.2	862	0.035
12-SB8-A4-6890-AVG	SB8-with ox	CCramp		1.526	0.067	0.000	0.373	0.000	0.179		37.9	911	0.037
12-SB8-B1-6934-AVG	SB8-with ox	CCramp		1.274	0.055	0.000	0.478	0.000	0.247		35.7	750	0.031
12-SB8-B2-6967-AVG (1)	SB8-with ox	CCramp		1.670	0.053	0.000	0.443	0.000	0.219		33.8	718	0.029
12-SB8-D1-7253-A	SB8-no ox	CCramp		1.221	0.034	0.000	0.452	0.000	0.189		35.9	994	0.041
12-SB8-D1-7253-B-No LID	SB8-no ox	CCramp		1.221	0.034	0.000	0.452	0.000	0.189		35.9	994	0.041
12-SB8-D1-7253-C	SB8-no ox	CCramp		1.221	0.034	0.000	0.452	0.000	0.189		35.9	994	0.041
12-SB8-D2-7224-A	SB8-no ox	CCramp		1.333	0.033	0.000	0.509	0.000	0.182		36.2	869	0.035
12-SB8-D2-7224-B	SB8-no ox	CCramp		1.333	0.033	0.000	0.509	0.000	0.182		36.2	869	0.035

Sample ID	Data Type	Data Subtype	Good Glass?	Formate mol/kg meas.	Oxalate mol/kg meas.	Coal mol/kg meas.	Nitrate (+nitrite) mol/kg meas.	Glycol Only mol/kg meas.	Any Mn mol/kg meas.	Frit	Target Waste Load	Total Anti-foam (mg/kg)	Anti-foam Carbon from gal and mg/kg (mol/kg)
12-SB8-D2-7224-C	SB8-no ox	CCramp		1.333	0.033	0.000	0.509	0.000	0.182		36.2	869	0.035
12-SB8-D3-7293-A	SB8-no ox	CCramp		1.255	0.034	0.000	0.487	0.000	0.196		36.2	901	0.037
12-SB8-D3-7293-B	SB8-no ox	CCramp		1.255	0.034	0.000	0.487	0.000	0.196		36.2	901	0.037
12-SB8-D3-7293-C	SB8-no ox	CCramp		1.255	0.034	0.000	0.487	0.000	0.196		36.2	901	0.037
12-SB8-D4-7322-A	SB8-no ox	CCramp		1.338	0.033	0.000	0.492	0.000	0.192		36	958	0.039
12-SB8-D4-7322-B	SB8-no ox	CCramp		1.338	0.033	0.000	0.492	0.000	0.192		36	958	0.039
12-SB8-D4-7322-C	SB8-no ox	CCramp		1.338	0.033	0.000	0.492	0.000	0.192		36	958	0.039
12-SB8-D5-7401-A	SB8-no ox-MCU/ARP	CCramp		1.526	0.045	0.000	0.560	0.000	0.197		35.5	1080	0.044
12-SB8-D5-7401-B	SB8-no ox-MCU/ARP	CCramp		1.526	0.045	0.000	0.560	0.000	0.197		35.5	1080	0.044
12-SB8-D5-7401-C	SB8-no ox-MCU/ARP	CCramp		1.526	0.045	0.000	0.560	0.000	0.197		35.5	1080	0.044
12-SB8-D1-7253-AVGR	SB8-no ox	CCramp		1.221	0.034	0.000	0.452	0.000	0.189		35.9	994	0.041
12-SB8-D2-7224-AVGR	SB8-no ox	CCramp		1.333	0.033	0.000	0.509	0.000	0.182		36.2	869	0.035
12-SB8-D3-7293-AVGR	SB8-no ox	CCramp		1.255	0.034	0.000	0.487	0.000	0.196		36.2	901	0.037
12-SB8-D4-7322-AVGR	SB8-no ox	CCramp		1.338	0.033	0.000	0.492	0.000	0.192		36	958	0.039
12-SB8-D5-7401-AVGR	SB8-no ox-MCU/ARP	CCramp		1.526	0.045	0.000	0.560	0.000	0.197		35.5	1080	0.044
12-SB8-D1-1-7253R	SB8-no ox	CCramp		1.221	0.034	0.000	0.452	0.000	0.189		35.9	994	0.041
12-SB8-D1-2-7253R	SB8-no ox	CCramp		1.221	0.034	0.000	0.452	0.000	0.189		35.9	994	0.041
12-SB8-D1-3-7253R	SB8-no ox	CCramp		1.221	0.034	0.000	0.452	0.000	0.189		35.9	994	0.041
12-SB8-D2-1-7224R	SB8-no ox	CCramp		1.333	0.033	0.000	0.509	0.000	0.182		36.2	869	0.035
12-SB8-D2-2-7224R	SB8-no ox	CCramp		1.333	0.033	0.000	0.509	0.000	0.182		36.2	869	0.035
12-SB8-D2-3-7224R	SB8-no ox	CCramp		1.333	0.033	0.000	0.509	0.000	0.182		36.2	869	0.035
12-SB8-D3-1-7293R	SB8-no ox	CCramp		1.255	0.034	0.000	0.487	0.000	0.196		36.2	901	0.037
12-SB8-D3-2-7293R	SB8-no ox	CCramp		1.255	0.034	0.000	0.487	0.000	0.196		36.2	901	0.037
12-SB8-D3-3-7293R	SB8-no ox	CCramp		1.255	0.034	0.000	0.487	0.000	0.196		36.2	901	0.037
12-SB8-D4-1-7322R	SB8-no ox	CCramp		1.338	0.033	0.000	0.492	0.000	0.192		36	958	0.039

Sample ID	Data Type	Data Subtype	Good Glass?	Formate mol/kg meas.	Oxalate mol/kg meas.	Coal mol/kg meas.	Nitrate (+nitrite) mol/kg meas.	Glycol Only mol/kg meas.	Any Mn mol/kg meas.	Frit	Target Waste Load	Total Anti-foam (mg/kg)	Anti-foam Carbon from gal and mg/kg (mol/kg)
12-SB8-D4-2-7322R	SB8-no ox	CCramp		1.338	0.033	0.000	0.492	0.000	0.192		36	958	0.039
12-SB8-D4-3-7322R	SB8-no ox	CCramp		1.338	0.033	0.000	0.492	0.000	0.192		36	958	0.039
12-SB8-D5-2-7401-R	SB8-no ox	CCramp		1.526	0.045	0.000	0.560	0.000	0.197		35.5	1080	0.044
12-SB8-D5-3-7401-R	SB8-no ox	CCramp		1.526	0.045	0.000	0.560	0.000	0.197		35.5	1080	0.044

D.E. Dooley, 773-A
T. B. Brown, 773-A
M. E. Cercy, 773-42A
D. A. Crowley, 773-43A
A. P. Fellinger. 773-42A
S. D. Fink, 773-A
C. C. Herman, 773-A
D. T. Hobbs, 773-A
E. N. Hoffman, 999-W
J. E. Hyatt, 773-A
K. M. Kostelnik, 773-42A
B. B. Looney, 773-42A
D. A. McGuire, 773-42A
T. O. Oliver, 773-42A
F. M. Pennebaker, 773-42A
G. N. Smoland, 773-42A
B. J. Weidemann, 773-42a
W. R. Wilmarth, 773-A
Records Administration (EDWS)

H. P. Boyd, 704-27S
J. M. Bricker, 704-S
J. S. Contardi, 704-56H
T. L. Fellinger, 766-H
E. J. Freed, 704-S
J. M. Gillam, 766-H
B. A. Hamm, 766-H
E. W. Holtzscheiter, 766-H
J. F. Iaukea, 704-27S
V. Jain, 766-H
C. J. Martino, 999-W
J. W. Ray, 704-27S
P. J. Ryan, 704-26S
M. A. Rios-Armstrong, 766-H
H. B. Shah, 766-H
D. C. Sherburne, 249-8H
C. Sudduth, 707-7E
D. P. Lambert, 999-W
M. E. Stone, 999-W
R. E. Edwards, 766-H
J. D. Newell, 999-W
F. C. Johnson, 999-W
C.L. Trivelpiece, 999-W
S.T. Isom, 773-67A
T.E. Colleran, 773-67A

P. R. Jackson, DOE-SR, 703-46A
J. A. Crenshaw, 703-46A

V. Jain, 766-H
R. T. McNew, 766-H
M. A. Rios-Armstrong, 766-H
J. R Vitali, 704-30S
A. W. Wiggins, 241-168H

M. A. Broome, 704-29S
W. A. Drown, 773-41A